

CHAPTER 3. REACTOR

3.1 DESIGN BASES

The initial reactor core rating has been established as 3025 MW thermal. The reactor core is a three-region cycled core consisting of 193 fuel assemblies. The core is controlled by 53 rod cluster control (RCC) assemblies duplicating those used in the Indian Point Unit #2 for reactor control. In addition to these, a soluble neutron poison in the form of boric acid is employed for long term reactivity control augmenting the RCC assemblies.

The fuel rods are cold worked Zircaloy tubes containing slightly enriched uranium dioxide fuel. These tubes are designed to be free standing under reactor operating conditions. The fuel assembly is of the canless type with the basic assembly consisting of the RCC guide thimbles welded to the grids and the top and bottom nozzles. The fuel rods are held by the spring clip grids in this assembly which provides rigid support for the fuel rods.

The 53 rod cluster control assemblies are inserted into the guide thimbles of the fuel assemblies. The absorber sections of the control rods are fabricated of silver-indium-cadmium alloy sealed in stainless steel tubes. The control rods, being long and slender, are relatively free to conform to any small misalignments. Tests have shown that the rods are very easily inserted and not subject to binding even under conditions of severe misalignments.

The control rod drive mechanisms are of the magnetic latch type and are the same as used in the Brookwood and Indian Point #2 Plants. The latches are controlled by three magnetic coils, and are so designed that the rod cluster control assembly is released upon a loss of power to the coils and falls by gravity to shut down the reactor.

Preliminary design core characteristics are reported in Table 3-1. Experimental measurements from critical experiments, operating reactors, or both, are used to validate the methods to be employed in the final design. During

8110300226 670426
PDR ADOCK 05000286
B PDR

final design, nuclear parameters will be calculated for every phase of operation of the first core cycle and, where applicable, will be compared with design limits to show that an adequate margin of safety exists.

In the thermal-hydraulic design of the core, the maximum fuel and clad temperatures during normal reactor operation and at the maximum overpower are conservatively evaluated and are consistent with safe operating limitations.

A design safety margin, expressed as the minimum ratio between the Departure-from-Nucleate-Boiling (DNB) heat flux at a given point and the local heat flux, or a minimum Departure-from-Nucleate-Boiling Ratio (DNBR) of 1.30 is established. The Reactor Control and Protection System for design transients, will prevent the reactor from reaching conditions corresponding to a margin smaller than the design margin.

3.2 REACTOR DESIGN

3.2.1 NUCLEAR DESIGN AND EVALUATION

The nuclear parameters which contribute to the safety of the reactor are presented in this section. In evaluating the nuclear characteristics of the core to demonstrate its safety, a two-step approach is taken. First, detailed description of the methods used in the calculation of the nuclear parameters is presented. Second, a justification is given for the methods of calculation employed. Experimental measurements from critical facilities or operating reactors or both are used to validate the methods employed for design calculations. In this manner, it is shown that the calculations can accurately predict core operational conditions, and that a high confidence level is attained in achieving the design nuclear characteristics.

A general description of the core with the method of operation and types of control is given in Section 3.2.1.1. Section 3.2.1.2 contains a description of the calculational methods and justification of methods for neutron

multiplication, power distribution and depletion. Data from more than 100 critical experiments have been used to test the calculation of neutron multiplication and power distributions. Data from an extensive analysis of the depleted Yankee Core I have been used to validate the depletion calculations.

Section 3.2.1.2 also describes the important reactivity control aspects of the nuclear design. The description of control by chemical shim and control rods with the methods of analysis is included.

The methods of calculating the moderator temperature and pressure coefficients, the void coefficients and the Doppler and power coefficients are illustrated with an expected range of variation included. Finally, a justification is given for the calculated control rod worths and reactivity coefficients. Calculated rod worths are compared to measured values from critical experiments forming a mockup of the rod cluster control (RCC) assemblies. Data from operating power reactors indicate that the methods used to calculate reactivity coefficients are valid.

3.2.1.1 Nuclear Characteristics of the Design

a) Core Description

The core is arranged to form a unit that is roughly cylindrical in shape. The active fuel length of the core is 144 inches and the equivalent diameter is 133.7 inches, which result in a length to diameter ratio of 1.08. The core, containing 193 fuel assemblies, employs non-uniform, multiregion loading and fuel cycling with shim control by soluble chemical absorber.

The fuel loading scheme of the first core is based upon a division of the core into three approximately equal-volume regions with higher enrichment fuel located on the outside periphery of the core.

Reactivity control is provided by neutron absorbing control rods and by a soluble chemical neutron absorber (boric acid) in the reactor coolant. The concentration of boric acid is varied as necessary during the life of the core to compensate for: (1) changes in reactivity which occur with change in temperature of the primary coolant from cold shutdown to the hot operating, zero power conditions; (2) changes in reactivity associated with changes in the fission product poisons xenon and samarium; and (3) reactivity losses associated with the depletion of fissile inventory and buildup of long-lived fission product poisons (other than xenon and samarium).

The RCC assemblies provide reactivity control for: (1) fast shutdown; (2) reactivity changes associated with changes in the average coolant temperature above hot zero power (core average coolant temperature is increased with power level); (3) reactivity associated with any void formation; (4) reactivity changes associated with the power coefficient of reactivity.

In a core in which all of the control is supplied by control rods, the maximum burnup is limited by the maximum number of rods that can be inserted in the core. However, when chemical shim is used to control the installed excess reactivity necessary for burnup, this limitation no longer exists. For increased burnup in a chemical shim core, the extra control is achieved by the addition of more boron and the number of control rods is not affected except for the compensation of a small decrease in rod worth with increasing boron concentration. In any event, the control rods will always provide the minimum shutdown margin of one per cent reactivity following trip to hot, zero power conditions with the most reactive RCC assembly stuck in the fully withdrawn position.

The first core average burnup will be about 22,800 MWD/MTU. In order to achieve this burnup, the fuel enrichments in the first core are approximately 2.1 w/o, 2.6 w/o and 3.2 w/o. The fuel loading arrangements for the first cycle loading are shown in Figure 3-32.

An initial effective multiplication for this core is estimated to be 1.293 in the cold, clean core at beginning of life. Of the total excess reactivity, 0.045 is allotted for the increment from cold to hot zero power conditions, 0.024 for the change from zero to full power and 0.041 for equilibrium poisons. The remaining 0.181 is provided for long term depletion of reactivity with burnup.

To a large degree, the power capability of a reactor core is established by the ratio of the peak-to-average power density in the core. The local power density in the core is limited by; (1) the lineal power density, (2) the fuel cladding surface heat flux, and (3) the enthalpy rise of the coolant.

Because the first two of these are local power density limitations for a given fuel rod size, a limitation is imposed upon the maximum-to-average ratio of the distribution of power density to achieve a given core power capability, which is related to the average power density. This ratio, F_q^N , is known as the heat flux nuclear hot channel factor. The third limit, rather than being a limit to local power density is a limit to the line integral of the power density along a vertical trace through a coolant channel from bottom to top of the core. A limitation to the maximum-to-average ratio of this line integral is imposed to achieve a given power capability. This ratio, $F_{\Delta H}^N$, is known as the enthalpy rise nuclear hot channel factor. In the simplified situation where the radial and axial power distributions are assumed to be separable, F_q^N and $F_{\Delta H}^N$ are related by the maximum-to-average power density ratio along the core axis, the ratio of F_q^N and $F_{\Delta H}^N$ being F_Z^N .

The design nuclear hot channel factors for F_q^N and $F_{\Delta H}^N$ are 2.71 and 1.58, respectively, for the core capability of 3025 MWt. In the final design, power distribution analysis of the first core will be made to verify the hot channel factors.

A summary of the principal nuclear design data is given in the Table 3-1.

b) Reactivity Control

The concept of chemical shim in a water moderated reactor permits a significant reduction in the amount of reactivity which must be controlled by movable control rods. Since the soluble absorber concentration requires a significant time for adjustment, it cannot be employed for compensation of rapid reactivity variations, and some control rods are required. The reactivity requirements which are controlled by rods include the variation with power resulting from both Doppler broadening in U-238 resonances and changes in the core average coolant temperature, as well as the shutdown margin of 1 per cent reactivity at hot conditions with the assumption of a stuck RCC assembly. Boric acid addition supplements rod cluster control for xenon decay and plant cooldown. Fundamentally, the reactivity control by rods is based upon the requirements for rapid shutdown or trip. These requirements are in excess of any operational control band requirements.

1. Control by Chemical Shim

Control to render the reactor subcritical at temperatures below operating range is provided by chemical absorber (boron) in the coolant. The boron concentration necessary to provide adequate shutdown ($k_{eff} \leq .90$ with all rods in) for the initial fueling of the core at room temperature is estimated to be about 2100 ppm. This concentration is well within the solubility limits of boric acid at ambient temperature. The boron concentration to insure the minimum shutdown margin at ambient and operating temperature will also be verified.

Table 3-1

Preliminary Nuclear Design Data

(A) STRUCTURAL CHARACTERISTICS

1.	Fuel Weight (as UO_2), lbs.	218,530
	Zircaloy Weight, lbs.	41,993
2.	Core Diameter, inches	133.7
	Core Height, inches	144
	Reflector Thickness & Composition	
	Top - Water plus steel	~10 in.
	Bottom - Water plus steel	~10 in.
	Side - Water plus steel	~15 in.
3.	$\text{H}_2\text{O}/\text{U}$, unit cell (cold)	3.48
4.	Number of Fuel Assemblies	193
5.	UO_2 Rods per Assembly	204

(B) PERFORMANCE CHARACTERISTICS

1.	Heat Output, MWt	3025
2.	Loading Technique	3 region, non-uniform
3.	Fuel Discharge Burnup, MWD/MTU	
	Average First Cycle	13,600
	Average First Core	22,800
	Equilibrium Core Average	33,000
4.	Feed Enrichments, w/o	
	Region 1	2.1
	Region 2	2.6
	Region 3	3.2

(C) CONTROL CHARACTERISTICS (Beginning of Life)

1.	Effective Multiplication	
	Cold, No Power, Clean	1.293
	Hot, No Power, Clean	1.248
	Hot, Full Power, Clean ($T_{\text{mod}} = 582.1^\circ\text{F}$)	1.222
	Hot, Full Power, Xe and Sm Equilibrium ($T_{\text{mod}} = 573^\circ\text{F}$)	1.181
2.	Rod Cluster Control Assemblies	
	Material	5% Cd-15% In-80% Ag
	Number of RCC Assemblies	53
	Number of Absorber Rods per RCC Assembly	20
	Total Rod Worth	7%

Table 3-1 (Continued)

3.	Boron Concentrations To shut reactor down with no rods inserted, clean Cold/Hot	1700 ppm/2100 ppm
	To control at power with no rods inserted, clean/equilibrium xenon and samarium	1800 ppm/1500 ppm
4.	Boron Worth Hot Cold	1% $\delta k/k$ / 85 ppm 1% $\delta k/k$ / 70 ppm
(D) KINETIC CHARACTERISTICS		
1.	Moderator Temperature Coefficient	$+1 \times 10^{-4}$ to -3×10^{-4} $\delta k/k$ / °F
2.	Moderator Pressure Coefficient	-1×10^{-6} to $+3 \times 10^{-6}$ $\delta k/k$ / psi
3.	Moderator Void Coefficient	$+1 \times 10^{-3}$ to -3×10^{-3} $\delta k/k$ / % void
4.	Doppler Coefficient	-1×10^{-5} to -2×10^{-5} $\delta k/k$ / °F

The boron worth (W_B), defined as the fractional change in effective multiplication factor (K) per ppm of boron (C_B) added to the moderator,

$$W_B = 1/K (\delta K / \delta C_B)$$

will be calculated at different temperatures from ambient to the operating conditions, for boron concentrations up to the maximum expected during operation.

2. Control by RCC Assemblies

Neutron absorbing control RCC assemblies provide reactivity control to compensate for rapid variations in reactivity. The RCC assemblies are divided into two categories according to the function performed by each group. Control rod group assemblies are used to compensate for changes in reactivity due to variations in operating conditions of the reactor such as power or temperature. The remaining assemblies are those which provide shutdown reactivity and are termed shutdown rods. Enough shutdown rods are supplied to provide adequate shutdown with the most reactive RCC assembly stuck in the fully withdrawn position. To specify the number of control rods required for the core, design criteria are established to determine the control requirements. These criteria are summarized below.

Reactivity Control Requirements of Control Groups:

The requirements for control rods in the chemically shimmed core are discussed in the following paragraphs along with the reasons for each requirement.

Control rod insertion necessary to maintain a minimum incremental worth is known as control rod "bite". This incremental worth will be large enough to compensate for the reactivity variation

due to changes in power and temperature caused by a ramp load change of five per cent per minute, a step load change of ten per cent, and a loss of 40% load, from full power without reactor trip by steam dump to the condensers.

The value of the minimum available reactivity insertion rate and consequently, the value of the minimum insertion with the selected speed, will be established so as to be adequate for the most adverse combinations of power and moderator coefficients.

Operational Maneuvering Band:

At full power, the control group operates within a prescribed band of travel in the core to compensate for periodic changes in boron concentration, temperature or xenon. This band has been defined as the operational maneuvering band. When the control rods reach either limit of this band, a change in boron concentration will be made to compensate for any additional change in reactivity.

Hot Zero Power to Hot Full Power Reactivity Variation due to the Doppler Effect:

RCC assemblies compensate for the reactivity change incurred with a change in power level due to the Doppler effect. The expected change in reactivity from zero to full power due to the Doppler effect is about 1.4% $\Delta k/k$. The computation for this is based on a method developed by a correlation of experimental results of the Yankee, Saxton, BR-3 and SELNI cores.

Void Content:

The reactivity associated with the void fraction in the core at full power is very small. At end-of-life with the most negative temperature coefficient it is expected that voids will amount to approximately 0.1% reactivity.

Variable Average Coolant Temperature:

The average temperature of the coolant is varied with power level in the core. This change is actually a part of the power dependent reactivity change, and along with the Doppler effect and void formation, the total associated reactivity change must be controlled by rods. The largest amount of reactivity associated with the moderator coefficient that must be controlled is 1.0% at the end of life when the moderator temperature coefficient is the most negative. At beginning of life, when the moderator coefficient is close to zero, this requirement becomes minimal.

Shutdown Margin:

The RCC assembly worth specification will be based upon making the core subcritical by at least one per cent following trip at hot, zero power conditions with the most reactive RCC assembly stuck in its fully withdrawn position. Boric acid addition is to be used to supplement rod control for xenon decay or plant cooldown.

Summary of Control Rod Requirements:

The requirements will be separated into those which must be supplied during power operation and are included in the control groups, and those which furnish the excess reactivity insertion for shutdown and are included in the shutdown group.

Calculations will be performed to determine the net effect of burnup on rod worth. A gain will occur due to boron removal and possibly gross power redistribution. A loss in worth will arise from increase in core blackness and local power redistribution adjacent to the rods. Additional effects such as the loss of rod worth because of the change in core spectrum with lifetime and depletion of the poison material in the rods are also included in the overall control specification.

Xenon Induced Spatial Instability:

A preliminary evaluation⁽¹⁾ of the spatial stability of the power density distribution has been performed for the proposed core design. The following conclusions have been drawn:

- a) It is our "best estimate" that only damped radial and azimuthal xenon induced (i.e., not free running) oscillations can occur in a core of this length and operating at its rated power density.
- b) There exists, at present, sufficient uncertainty in the above statement concerning azimuth oscillations that one must admit to the possibility of under-damped oscillations and therefore control strategies will be developed.
- c) Similarly it is assumed that an axial xenon induced oscillation is possible. Instrumentation and equipment will be provided to detect and correct a free running oscillation and, thus, prevent subsequent core damage. Sufficient time exists (the order of hours) to take such corrective action due to the long period with which xenon oscillations would proceed. Engineering design work for Indian Point Unit #2 will provide the information necessary to design the instrumentation and control system for this plant.

3.2.1.2 Nuclear Evaluation Methods

a) Neutron Multiplication Calculations

The basic methods of computation employed in the nuclear design of the core are based upon multigroup neutron diffusion theory. The design assumes the separability of the spatial and energy dependence of the neutron flux. A series of computer codes has been employed to develop the computational method summarized below which has been verified by comparison of analysis with numerous experimental critical configurations (2), (3).

1. Fast Neutron Constants

Initially, a set of spatially independent spectral calculations is performed to obtain the energy dependent neutron flux distribution. This is done in two parts. A "fast" neutron calculation⁽⁴⁾ is performed in which the thermal motion of the material constituents of the reactor core is ignored. All neutrons which have an energy well above the thermal energy of the core are treated in this calculation. A standard break point or lower energy limit for fast neutrons is taken to be 0.625 ev. This particular value is selected specifically to avoid absorption resonances as well as to be substantially above the thermal energy to assure an "asymptotic" spectrum for the transition from the fast to the slow neutron calculations.

The fast neutron spectrum is computed by means of an approximation to the Boltzman transport equation which is correct in angular dependence to the first moment or P_1 term in the notation of spherical harmonics. The spatial dependence is suppressed through the technique of spatial Fourier transforms⁽⁵⁾ which, for reasonably large systems (i.e., 10 mean free paths), is equivalent to the assumption that the neutron leakage is related to the flux level by a geometric buckling. Specifically, an effective neutron removal cross section for leakage of $D B_G^2$ results. The energy dependence is based upon an approximation of the energy variation by means of moments⁽⁶⁾ in the logarithm of energy (lethargy). By a particular grouping of terms in the series expansion in moments, an equation is obtained which is exact for hydrogen and is accurate to the order of the fourth moment for heavy moderating materials. It, therefore, is significantly better for heavy moderators than age theory which is accurate to the order of the first moment. This approximation is applied consistently to both the flux and current equations in the P_1 approximation. A computer calculation based upon this approximation, MUFT⁽⁴⁾,

has been programmed by Bettis Atomic Power Laboratory. The version of MUFT used contains the library published in WAPD-TM-224⁽⁷⁾ with the exception that the capture to fission ratio for U-235 in the resonance range is set equal to 0.5. Resonance absorption is not computed directly by the fast neutron spectrum code, MUFT. This is primarily because the spectral analysis is by finite difference techniques and the characteristic energy range over which a resonance applies is so small that the mesh spacing would be unreasonably small. To avoid this situation, the analytic solution to the slowing down approximation employed in MUFT is found for an isolated Breit-Wigner resonance and then used to find the rate of neutron capture. This solution is inserted into the MUFT calculation in the appropriate mesh interval in the calculation.

The major approximation in the MUFT calculation is the assumption that a homogenized mixture of materials will yield the same results as the usual heterogeneity encountered in a reactor core. In general, this is a valid assumption because of the fact that cross sections tend to be low at higher energies; thus, the "optical thickness" of an individual material region in a nominal PWR lattice tends to be quite low. There are two situations for which the approximation of homogenization may not be valid. First, because all neutrons are formed in the fuel region and not uniformly throughout the core material, there may be a "first flight" type of correction which accentuates the high energy absorption and fission interaction with the fuel. Detailed analysis demonstrates that although this effect is detectable, it is relatively small in normal PWR lattices⁽²⁾. Second, the important instance in which the assumption of homogenization fails is in the consideration of resonance absorption. Although this absorption is not evaluated directly by MUFT, it is possible to apply a correction to the analytic solution to account for the heterogeneity of core lattice. This correction, or "L" factor, is an input to the calculation. A semi-empirical technique

of evaluating the "L" factor for U-238 (the most prominent resonance absorbing material in this PWR core) has been developed which has been demonstrated⁽²⁾ to correlate UO₂ rod, U metal rod, and homogeneous mixtures of scattering material and U-238. With one exception, all other resonance bearing materials are sufficiently dilute that the approximation of homogeneity appears to be adequate and the "L" factors are generally set equal to unity. In high burnup calculations, however, the Pu-240 concentrations becomes too large to ignore self-shielding. In these cases an "L" factor equal to that used for U-238 is applied to Pu-240 resonances.

Another approximation is that involved with the assumption that the core material has no thermal motion. This is certainly a valid assumption as far as scattering kinetics considerations are concerned; however, the effect of thermal motion on the resonance absorption is not insignificant. The thermal agitation results in a neutron of given energy relative to the resonance absorber and, therefore, under certain circumstances having an increased probability of being absorbed. This is the well-known Doppler broadening effect. This is incorporated in the MUFT through the same "L" factor used for the spatial effects.

A final consideration is the matter of inelastic scattering. The MUFT calculation considers this as an effective absorption with concurrent neutron emission in the appropriate mesh interval. An inelastic scattering matrix is used for each element, where appropriate, to account for all possible energy transitions.

2. Thermal Neutron Constants

The thermal neutron spectrum is computed on the basis of inconsistent P₁ theory in which only the zeroth energy moment in current is retained and up to the second energy moment in flux

is employed. Spatial effects are suppressed by means of a Fourier transform as in MUFT. The scattering transfer function is taken to be that for a unit mass scatterer. The motion of this scattering kernel is incorporated in the evaluation of the scattering kernel, after the method of Wigner and Wilkins. This calculation has been programmed⁽⁸⁾ and the BAPL library⁽⁹⁾ is used with the exception of data for Pu-239 which is based on Leonard's results⁽¹⁰⁾.

Because of the bound states of vibration and rotation of the water molecules, the water molecule in a PWR core exhibits an apparent scattering mass in the range of unity rather than 10 as the chemical formula would predict so that the assumption of unit mass scattering by the water is reasonable. A comparison of experimental data⁽¹¹⁾ has demonstrated that SOFOCATE⁽⁸⁾ (the code which performs the Wigner-Wilkins scattering calculation) is reasonably accurate although more refined analysis⁽¹²⁾ can lead to perceptible changes.

The SOFOCATE code calculation uses a homogeneous mixture assumption with a flux weighting correction⁽¹³⁾ applied as a function of energy in SOFOCATE. This correction, a mono-energetic calculation applied pointwise in an energy dependent solution, does appear to agree with more exact analyses^{(14), (15)} although its derivation is not completely rigorous.

3. Spatial Distributions and Neutron Multiplication

Having obtained the neutron spectrum for a reactor core (assumed constant over a large region) effective, few-group constants are determined by flux weighting. If an experimental material buckling is known for a given core configuration, the analysis can be checked by using the B_m^2 with the few group constants to evaluate the predicted neutron multiplication which, of course, should be unity.

A large number of experiments have been examined with the technique⁽²⁾ described above and the agreement is found to be good (standard deviation equal to 0.32%) for criticals performed at Westinghouse for the slightly enriched, oxide lattice PWR.

For non-uniform cores, however, a more complete analysis is required and a distribution code is employed in either one⁽¹⁶⁾ or two⁽¹⁷⁾ dimensions. This analysis is based upon a few neutron groups, usually either one or three fast groups plus one thermal group. The group boundaries are selected to collect significant physical processes together. That is, group 1 may include all energy from 0.821 Mev to above the source range for fission neutrons. This is the U-238 fast fission group. Group 2 may be from 5.500 kev to 0.821 Mev. There is little significant absorption in this range, and it may be termed the slowing-down group. Group 3 may be from 0.625 ev to 5.500 kev. This is the range where resonances are predominant and it may be termed the resonance group. Finally, group 4 is for all energy below 0.625 ev and is termed the thermal group.

Few group constants are obtained using the calculational scheme described above with the following exception. For the averaged thermal macroscopic data, the Mixed Number Density thermal activation model⁽¹⁸⁾ is used as input to a distribution calculation. The MND model is used because it gives considerably better agreement with experiment⁽¹⁹⁾ when the effects of water slots or water holes are being evaluated. The neutron distribution analysis in each group is based upon P_1 theory in which the energy variation is suppressed (zero lethargy moment). The source term in each group is either slowing down from the next higher group, fission, or both. An iterative process is employed in which the value of the total integrated source of neutrons is maintained at unity by dividing ν (neutrons per fission) in each group by the static neutron multiplication λ .

Burnup, conversion, fission product production and decay can be studied by coupling material conservation equations to the distribution calculations to obtain depletion characteristics in either one⁽²⁰⁾ or two⁽²¹⁾ dimensions. These codes retain few group microscopic cross sections which are assumed to be independent of burnup. A code has been developed which evaluates the effect of burnup on neutron spectrum but suppresses spatial effects⁽²²⁾. This code called LEOPARD is employed in selecting the constants to be used in spatial calculations to account in an average fashion for the depletion effects on spectrum.

The effective fission product cross section in LEOPARD has been adjusted to predict the observed Yankee core lifetime performance and is assumed to vary according to the results of time dependent analysis performed at BAPL⁽²³⁾. The energy per fission is based upon direct fission yield as well as concurrent neutron capture energy release.

The above methods for the evaluation of water reactor lattices involve the replacement of a typical unit cell which includes uranium dioxide, clad and coolant associated with a fuel rod by a set of homogenized few-group constants. Inhomogeneities in the uniform lattice require separate treatment to evaluate their effect on power distribution and eigenvalue. In the core, two design features lead to such lattice distortions. These are water slots between fuel assemblies, and water holes within fuel assemblies to accommodate absorber rods required in the core.

The approach adopted in LEOPARD to evaluate the distortion in the uniform lattice is the treatment of material outside the homogenized unit cell as a separate region. A prescription

for the determination of constants in a consistent fashion is employed on the basis that it reproduces the results of a series of critical experiments designed to test the analysis⁽²⁴⁾. This prescription involves the use of "soft spectrum" macroscopic constants from a non-fuel spectrum as opposed to those from the harder fuel spectrum.

The two-dimensional depletion code TURBO⁽²¹⁾ with LEOPARD microscopic library constants, MND thermal constants and "soft spectrum" water hole, water slot and reflector constants will be used to evaluate the burnup performance of the first cycle. The boron concentration will be varied throughout the core lifetime so that the core will always be just critical in the calculation.

In performing the depletion analysis in TURBO, the non-uniform burnup in the axial dimension is treated in the following manner. An effective axial buckling, B_{eff}^2 , is that value of B^2 in a uniform axial calculation which gives the same neutron multiplication as a non-uniform axial calculation.

Axial hot channel factors are obtained for RCC group withdrawal using a modified version of the few-group neutron diffusion code FOG⁽²⁵⁾ which is similar to the AIM-5⁽¹⁶⁾ code. This is a one-dimensional analysis. The modifications allow the code to incorporate the effects of non-uniform Doppler broadening as well as the non-uniform distribution of equilibrium xenon. In order to account for the transverse leakage in these axial problems, a constant radial buckling is used as input to the code. Representation of the group of RCC assemblies as a radially uniformly dispersion of absorber is accomplished by increasing the few group macroscopic absorption cross sections in that portion of the core height which contains rods.

The modified FOG code simulates the non-uniform effect of Doppler broadening of U-238 resonances by varying the core fast absorption macroscopic cross section as a function of the power density distribution.

The modification to the code that permits the non-uniform equilibrium xenon to be calculated is such that the homogenized Xe-135 number density is computed at each mesh point of the fuel bearing regions with the standard relationship. It is not possible to find the distribution as a result of non-equilibrium xenon with this code.

4. Basis for Confidence

The calculational scheme described has been tested on a wide range of experimental lattices. A summary of the results and discussion of the agreement with measured values is given in the following paragraphs.

Reactivity Analysis:

Data from 55 oxide and 56 metal lattice critical and exponential experiments have been evaluated⁽¹²⁾. The results of these studies are summarized in Table 3-2. The values of neutron multiplication k are computed using experimentally measured material bucklings, and should equal unity. Table 3-2 demonstrates that much of the scatter can be attributed to variations in results from one experimental laboratory to another, whereas the evaluation demonstrated that errors do not develop with variations of certain significant parameters. As the calculational accuracy is independent of variations in hydrogen to uranium ratio, uranium enrichment, pellet diameter and buckling, extrapolation from experiments to operating cores or extrapolation from one operating core to another should not lead to any significant error.

It can be seen from Table 3-2 that if only WAPD experimental results are considered, the computational method predicts k to a standard deviation of 0.36 per cent which is a better estimate of the accuracy of the method because of the more detailed information available. Much of the additional scatter in the standard deviation for the other cases can be attributed to insufficient information on the dimensions and results of many of the cases published.

Table 3-2
Results of Calculations as a Function of
Laboratory Providing Experimental Data⁽⁵⁾

Laboratory	Type of Experiment	No. of Experiments	Calculated $k + \sigma$
Westinghouse Atomic Power Division (WAPD)	Critical	16	0.9968 \pm 0.0036
Bettis Atomic Power Laboratory	Critical	14	0.9940 \pm 0.0022
Brookhaven National Laboratory	Exponential	35	0.9964 \pm 0.0051
Hanford Atomic Products Operation	Exponential	20	0.9953 \pm 0.0105
Babcock and Wilcox	Critical	<u>26</u>	0.9885 \pm 0.0094
		111	

Data from the Yankee spent core analysis have been compared with calculated data using the design techniques. The results are summarized in Figure 3-1 through 3-3. Uranium depletion and net plutonium production have a direct bearing on the core lifetime. The figures show the comparison between calculations (solid lines) and measured concentrations of the various isotopes. Although some small deviations can be observed between analysis and experiment, they are not considered serious.

Power Peaking Analysis:

A series of critical experiments were carried out at the Westinghouse Reactor Evaluation Center (WREC) to determine the power peaking in fuel rods adjacent to water holes and to determine the effects of voids on power distribution.

The power peaking experiment was performed in a 30 x 30 array of 2.72 per cent enriched fuel with a water-to-uranium ratio of 3.5 with and without boron in the moderator. The pattern of 16 water holes was symmetrical about the center of the core. The core arrangement and pattern of fuel rods scanned are shown in Figure 3-4 for the unborated core and Figure 3-5 for the same core with 479 ppm boron in the water.

The analysis consisted of PDQ calculations using two-group constants obtained from LEOPARD. Mixed Number Density thermal constants were used, and "soft spectrum" microscopic constants were used in the reflector and water holes. In the PDQ analysis, two mesh spacings per fuel rod were used. Also, in the unborated core a calculation was performed for one mesh space per fuel rod. The experimental data were normalized to the PDQ results using the average of the four central rods. The experimental and calculated results for the borated and unborated cores with two mesh spacers per fuel rod are shown in Figures 3-6 and 3-7, respectively, and in Figure 3-8 for the unborated core calculated with one mesh spacer per fuel rod. The data are presented numerically using 1/8 core symmetry. Each block in the figures represents a fuel rod. The experimental values correspond to the average values of counts taken at five positions on the fuel rod.

The agreement between analysis and experiment is within 2 to 3 per cent and is of the same order as the scatter in the experimental data. There is no consistent difference in over-estimating or underestimating peaking using the one mesh per fuel rod or two mesh per fuel rod representation.

The void experiments were performed for two different core configurations. The first series of experiments was carried out in a 47 x 47 square core of 2.7% enriched fuel with a W/U of 2.9, with no boron. The second series was performed using a 53 x 53 square core of 3.7% enriched fuel with a W/U of 2.9, and with 1046 ppm boron in the water. In both cores voids were simulated by empty 0.1875 inch O.D., 0.022 inch wall aluminum tubes inserted between fuel rods. The moderator in the voided region consisted of 11.52% aluminum, 16.29% void and 72.19% water. Data were taken for the following cases:

1. No void tubes
2. Four void tubes (2x2) located around the central fuel rod
3. Sixteen void tubes (4x4) at core center
4. One hundred ninety-six void tubes (14x14) at core center

The analysis again consisted of PDQ using two-group constants from LEOPARD, with MND thermal constants and "soft spectrum" water hole and reflector constants. The calculated power distribution is compared with the experimental power scans in Figure 3-9 and 3-10 for the unborated and borated cores for the four cases examined. The agreement between experiment and calculation is good except at the transition region between voided and non-voided regions. Here the calculated peaks are higher than those obtained by experimental measurements.

The reactivity effects of the void tubes were calculated assuming a constant axial reflector savings. Calculation and experiment for each case examined are compared in Table 3-3. Calculations overestimate the reactivity effect of the voids by approximately 10%, which is good agreement in view of the small magnitude of the effects being studied.

Table 3-3

Calculated and Measured Reactivity Effects of Void Tubes

<u>Type of Core</u>	<u>No. of Tubes</u>	<u>Reactivity Change %$\Delta k/k$</u>	
		<u>Measured</u>	<u>Calculated</u>
Unborated Core	0		
	4	-0.03	-0.034
	16	-0.11	-0.125
	196	-1.33	-1.416
Borated Core	0		
	4	-0.017	-0.020
	16	-0.076	-0.085
	196	-0.850	-0.942

Gross Power Distribution Analysis:

The ability to evaluate power distributions in multiregion critical cores with no burnup has been evaluated in detail⁽¹⁹⁾. Agreement for all situations, including those with large enrichment variation and small regions, is found to be good as is illustrated in Figure 3-11. The ability to evaluate power distributions in depleted cores at power has been demonstrated by core evaluation programs using in-core instrumentation data from Yankee and Saxton. Other pertinent data will be obtained in the future from other Westinghouse reactors including large PWR cores controlled by chemical shim and will be factored into the final design.

As an example of such a comparison, a power distribution is shown in Figure 3-12 for the end of life in Yankee Core I, which was not controlled by chemical shim. A comparison of the burnup distribution is also presented in Figure 3-13.

In both cases two calculated values are given which show the effect of a rod program interchange during life. These results have been taken from Reference 26.

b) RCC Assembly Worth Calculation

The RCC assembly worth necessary to satisfy the requirements pointed out in the preceding paragraphs will be calculated⁽²⁷⁾ using the two-dimensional PDQ code for both the beginning and end of core life. In both of these situations, the rod cluster control (RCC) rods, water slots and water holes in assemblies which do not contain RCC rods will be represented as explicit regions, with one exception. In the stuck rod analyses, a full core geometric representation is necessary, as opposed to 1/4 core representation for all other calculations. Because of mesh point limitations, it will be necessary to homogenize the RCC rods and the unrodded water holes with some of the fuel. The homogenization scheme that has proven the most successful is a ring homogenization in which the 20 RCC rods (or water holes) are homogenized with the fuel constants in a ring within the fuel assembly by volume weighting and choosing values of Σ_p such that the controlled multiplication equals that of the discrete representation. The control rods in the discrete geometry will be represented by diffusion constants in the fast energy group and as a black region with an extrapolation distance in the thermal energy group. This method of RCC rod representation, as well as the ring homogenization, is discussed in Reference 28.

1. Maximum RCC Assembly Worth Calculation

As outlined in Section 12.1, an analysis will be made of the hypothetical situation in which one of the rod cluster assemblies is ejected from the core during power operation. The most reactive situation that could occur is when the most reactive RCC assembly is ejected from the full inserted position. Therefore, the worth of the most reactive RCC assembly will be calculated when completely removed from the core.

2. Differential and Cumulative RCC Assembly Worths

Differential worths will be obtained for various RCC assembly group worths under hot zero power and hot full power core conditions. The hot full power calculations include the effects of

the pointwise variation of Doppler broadening and equilibrium xenon. These effects will be calculated in the same manner that was described for neutron multiplication calculations. In the full power calculations, the xenon and Doppler effects will be assumed to have time to redistribute to the rod position after the incremental rod movement.

3. Effect of Control Group Insertion on Nuclear Hot Channel Factor

The effects of RCC assembly insertion will be considered in determining the total nuclear hot channel factor of the core.

An estimate of the behavior of $F_{\Delta H}^N$ as the control groups are inserted can be made in the following manner: it will be assumed that the enthalpy rise along a channel can be obtained by weighing the local to average ratio of enthalpy rise in the unrodded and rodded portion of the core by the fraction of energy generated in each portion. This analysis is performed for the channels containing the peak in the rodded (upper) and unrodded (lower) portions of the core, and also for other channels which in one cross section of the core may not be limiting, but which may be limiting in combination.

The behavior of the axial power distribution with burnup depends on the position of the RCC assemblies. The same is true for differential RCC assembly worths and fractional power below the RCC assemblies. The axial power distribution will be measured at intervals throughout the life of the core, so that these quantities will be known as a function of core burnup. Therefore, the in-core instrumentation will be employed to determine the nuclear hot channel factors over the life of the core.

c) Reactivity Coefficients

The response of the reactor core to plant conditions or operator adjustments during normal operation, as well as the response during abnormal or accident transients, is evaluated by means of analog computations. In these calculations, reactivity coefficients are required to couple the response of the core neutron multiplication to the variables which are set in part by conditions external to the core. The discussion in this section pertains to these coefficients. This includes the moderator temperature and pressure coefficients, moderator void coefficient, and Doppler and power coefficients of reactivity.

1. Moderator Temperature Coefficient

The moderator temperature coefficient in a core controlled by chemical shim is less negative than the coefficient in an equivalent rodged core. One reason for this difference is that control rods contribute a negative increment to the coefficient and, in a chemical shim core, the rods are only partially inserted. Of greater importance, however, is the fact that the chemical poison density is decreased along with the water density upon an increase in temperature. This gives rise to a positive component of the moderator temperature coefficient due to the reduction in absorber density in the core. This latter effect is directly proportional to the amount of reactivity controlled by dissolved absorber.

The moderator temperature coefficient is defined as the fractional change in effective multiplication factor per degree change in moderator temperature.

$$\alpha_m = 1/k \delta k / \Delta T_m$$

This coefficient will be obtained by calculating the neutron multiplication for a series of moderator temperatures from ambient conditions to 600°F (315°C) with a temperature

increment of 10°F (5.5°C) at each temperature studied. Only the moderator temperature and density will be changed in the calculations, so that the coefficient calculated will be a true moderator temperature coefficient. The values of neutron multiplication for the various cases will be determined using the one-dimensional AIM-5 code. These calculations will be performed for a cylindrical geometry representing the three region core. Fast and thermal macroscopic constants used as input to AIM-5 will be calculated by LEOPARD.

The moderator temperature coefficient becomes more negative with increasing burnup. This is due to the buildup of plutonium and fission products with burnup and the decrease of boron concentration required in the coolant.

The consequences of a positive moderator coefficient in a pressurized water reactor core have been examined⁽²⁹⁾ in detail. The positive coefficient results from the use of chemical shim control with high burnup cycles. The various effects on system performance have been determined and it has been concluded that the positive coefficient within relatively broad limitations on the magnitude does not present a safety problem in the operation of the PWR core.

Specifically, the study and calculations show that:

1. The slightly enriched PWR core requires control rod action (either manual or automatic) to change power level regardless of the sign or magnitude of the moderator coefficient.
2. The Doppler coefficient represents the primary terminating mechanism for power transients in PWR cores regardless of the sign or magnitude of the moderator coefficient.

3. The detailed balance of neutron conservation in PWR cores results in a local decrease in power at the point of temperature rise in spite of the fact that total core reactivity is increasing.
4. Although there is a theoretical possibility of spatial instability as a result of the positive moderator coefficient, the boron concentration is far below the value for which concern arises.
5. Normal operation of the PWR core with a positive moderator coefficient results in no deleterious effects in the controlled response of the plant.
6. The existence of a positive moderator coefficient does not reduce the safety margin in the design of PWR cores because its effect is included in accident evaluation through detailed spatial and time dependent calculations.

The expected range of variation of the moderator temperature coefficient is reported in Table 3-1.

Hydrodynamic and Flow Power Coupled Instability

The interaction of hydrodynamic and spatial effects have been considered and it is concluded that a large margin exists between the design conditions and those for which an instability is possible.

It has been known for some time that heated channels in parallel can lead to flow instability. If substantial boiling takes place, periodic flow instabilities have been observed and, as long ago as 1938, Ledinegg⁽³⁰⁾ proposed a stability criterion on the basis of which the concept of inlet orificing has been developed to stabilize flow. More recent work⁽³¹⁾⁽³²⁾⁽³³⁾ has demonstrated that periodic instabilities are possible which violate the Ledinegg criterion.

In normal flow channels with little or no boiling, the type of instability proposed by Ledinegg is not possible since it results primarily from the large changes in water density along the channel due to boiling. Moreover, the periodic instabilities examined by Quandt⁽³¹⁾⁽³²⁾ and Meyer⁽³³⁾ are not exhibited in non-boiling channels of the type found in PWR cores.⁽³⁴⁾

In the presence of a positive moderator coefficient, it has been determined that a combination of spatial and hydrodynamic interaction can lead to a less stable situation since there will be a tendency for the power to rise as the flow is reduced. This problem has been under study in a Westinghouse funded program and preliminary results indicate that the combined effects do, in fact, decrease stability.

The interactions are similar to that in a published spatial stability analysis⁽²⁹⁾ with the exception of a multiplier on the reactivity held in the coolant; i.e.:

$$C \rho_c + \rho_f < M^2 \Delta B^2 \text{ for stability}$$

ρ_c = reactivity in coolant

ρ_f = reactivity in the power coefficient

$M^2 \Delta B^2$ = leakage increase in first overtone

C = hydrodynamic multiplier

C is found to be very sensitive to local boiling void. At this time, all channels must be treated as having the same hydrodynamic characteristics. For any channel which has no local void, $C \approx 1.03$ constituting a trivial effect.

A few per cent of the channels in the core which are clustered around the hottest channel have significant local boiling void. If all channels are assumed to have the peak local void content an upper bound to C is found to be 2.0. Now, the concern is for excitation of the first overtone which is smooth over many channels and it is appropriate to use some average hydrodynamic

properties. It is reasonable to expect that the correct value of C is closer to 1.03 than 2.0. Work on this particular aspect of the problem is continuing under Westinghouse development programs.

2. Moderator Pressure Coefficient

Under any given set of reactor conditions, the moderator pressure coefficient has an opposite sign to the moderator temperature coefficient and, therefore, tends to oppose it. The effect of the pressure on the total coefficient will be small because the pressure coefficient has been found to be about 100 times smaller in reactivity worth per change in psi as compared to reactivity worth per °F.

3. Moderator Void Coefficient

A uniform void coefficient will be calculated by assuming that a uniform change in the moderator atom density corresponds to a direct change in the amount of void present in the core. The expected range for this coefficient is reported in Table 3-1 page 3-7.

4. Doppler and Power Coefficients

The Doppler coefficient is defined as the change in neutron multiplication per degree change in fuel temperature. This coefficient will be obtained by calculating multiplication as a function of fuel temperature by LEOPARD. The expected range of Doppler coefficient is reported in Table 3-1.

In order to know the change in reactivity with power, it is necessary to know the change in effective fuel temperature with power as well as the Doppler coefficient. An empirical approach will

be taken to calculate the power coefficient, based on operating experience of existing cores. This method will be discussed in some detail later in this section.

d) Reactivity Control Analysis

The calculations described below for reactivity control have been formulated and tested by comparing them with many experimental results. These experiments include criticals performed at the Westinghouse Reactor Evaluation Center (WREC) and other facilities, and also measured data from operating power reactors.

1. RCC Assembly Worth Analysis

In the control rod calculations performed by the PDQ computer code, the RCC rods are represented by internal boundary conditions (α 's) in the fast and thermal groups. These boundary conditions applied to the unit cell in which the absorber rod, its clad and the associated water are homogenized. The values of these α 's will be determined to make the calculated rod worth of a single fuel assembly equal to that calculated by a more refined model. The better model represents each absorber rod explicitly and is used to analyze an extensive set of critical measurements. Approximately 30 different critical measurements were made for uniform and cluster arrays of absorber rods with different enrichments, rod diameters, water-to-uranium ratios and boron concentrations.

In the analysis of these measurements, the rods were represented by a theoretically determined thermal boundary condition and by a diffusion region in the single fast group. The fast absorption cross section was empirically determined from the measured rod worth to give agreement between analytical and experimental.

results. The development of this calculation scheme for RCC rod worth and a description of the measurements is given in Reference 27. Figures 3-14 and 3-15 are reproduced from this reference to show the fast absorption cross section as a function of the radius of the absorber which fits the experimental measurements for cluster and uniform cases, respectively. The solid lines were obtained by a least square fitting of the experimental data.

2. Moderator Coefficient Analysis

Inasmuch as the safe operation of any plant is closely associated with the ability to predict the behavior of that plant, correlation of analysis with experiment will be presented to show that the moderator temperature coefficient is quite predictable. Measurements were made during the startup and operation of the SELNI core to get data for a core operated entirely by chemical shim. During the startup, the core was heated from room to operating temperature at a constant boron concentration of 1600 ppm. Figure 3-16 shows the results of the moderator coefficient measurements taken during this core heatup, and also the comparable calculated values. The calculations were performed with the one-dimensional AIM-5 code with LEOPARD input constants as described for neutron multiplication calculations. The agreement between calculation and experiment is good over the entire temperature range.

In order to measure the moderator coefficient at different boron concentrations, control rods were traded for boron during the hot, no power startup tests. This procedure permitted moderator coefficient measurements to be made over a range of boron concentrations from 1300 to 1800 ppm. The method of analysis for the case of trading rods for boron is, of necessity, different

from the method discussed above. The AIM-5 code was again used, but an axial calculation was performed with an homogenized bank of absorber used to represent the moving control rods. The results of analysis and measurement are shown in Figure 3-17. The calculations were performed in the same manner as the measurements; i.e., the control group was inserted as boron was removed. When the control group was fully inserted, further boron removal was compensated for by insertion of all rods banked. PDQ analyses were also performed for the all rods in and all rods out end points and the results are given in Figure 3-17. It can be seen that the one-dimensional calculations in which rods are represented by an homogenized absorber predicts the measured data very well.

The effect of burnup on the moderator coefficient has been measured in the core evaluation program performed on Yankee Core I⁽³⁵⁾. Yankee Core I was controlled by cruciform blade rods, and so it was necessary to separate the effect of control rods from the effect of burnup on the moderator coefficient. Figure 3-18 illustrates these components and the agreement between analysis and measurement. The effect of rods was evaluated by treating the rods as an equivalent absorption area (approximation 1 in Figure 3-18) with a correlation for the effects of resonance absorption (approximation 2 in Figure 3-18). The results of the analysis lie within the experimental uncertainty and the burnup effect on the moderator coefficient results in a more negative coefficient with increasing burnup.

3. Doppler and Power Coefficient Analysis

As the fuel pellet temperature increases with power, the resonance absorption in U-238 increases due to Doppler broadening of the resonances. In order to predict the reduction in reactivity

caused by this effect, it is necessary to know the temperature of the fuel as a function of power level, the position and burnup of fuel in the core, as well as the radial distribution of temperature within the individual fuel rods. However, uncertainties arise during operation at power which make it difficult to predict accurately the temperature of the fuel pellet. For example, pellets do not remain intact (i.e., uncracked) and in a concentric relationship with the clad, as has been observed from the Yankee spent fuel analysis⁽³⁶⁾. In addition, the composition of gases in the gap changes with burnup because of diffusion of fission product gases to the gap. This generally results in an uncertainty in the temperature drop across the gap as a function of power level and burnup.

A semi-empirical model has been developed for calculating the effective fuel temperature (T_{eff}) based on fitting the measured power coefficients of the Yankee, Saxton, BR-3 and SELNI reactor cores. The measured power coefficient $1/k \delta k / \delta P$ can be written

$$\frac{1}{K} \frac{\delta k}{\delta P} = \frac{1}{k} \frac{\delta k}{\delta T_{eff}} \cdot \frac{\delta T_{eff}}{\delta P} \quad (1)$$

The first term in the product on the right side of Equation (1) is the Doppler coefficient which can be computed without knowing the heat transfer behavior of the fuel pellet or the relationship of T_{eff} and power. The second term on the right side of Equation (1) can then be related to the measured values of power coefficients. In this manner an empirical expression for the effective fuel temperature is obtained which makes it possible to relate T_{eff} to power, and thus calculate the power coefficient.

The method of analysis described in the preceding paragraph assumes accuracy of prediction of the Doppler coefficient as a function of the effective fuel temperature. This assumption

indicates that the behavior of the U-238 resonance integral with a change in the fuel temperature is well known. Data is presented here to support this assumption. A correlation has been developed for the U-238 resonance integral which is known as the metal-oxide correlation⁽²⁾. This correlation has been found to agree with Hellstrand's uranium metal⁽³⁷⁾ and uranium dioxide⁽³⁸⁾ correlations for isolated rods. The correlation is also consistent with Hellstrand's temperature correlations⁽³⁹⁾. Thus, a single correlation replaces the four Hellstrand correlations. The metal-oxide correlation is

$$R.I.^{28} = 2.16X + 1.48 + (0.0279X - 0.0536) T_{eff}^{1/2}$$

where T_{eff} is in degrees Kelvin and

$$X = \left[\frac{\Sigma_{so}}{N_o^{28}} P_o + \frac{D}{l_o N_o^{28}} \right]^{1/2}$$

Σ_{so} = scattering cross section of the fuel (10.7 barns for uranium and 3.8 barns for oxygen)

N_o^{28} = U-238 number density in the fuel region

l_o = mean chord length in the fuel

D = shielding factor (calculated by Sauer's Method⁽⁴⁰⁾)

$P_o = 1 - P_c$ (P_c is tabulated in Reference 41)

This form of the resonance integral is not strictly rigorous, but its validity is demonstrated in Figure 3-19 (taken from Reference 2) where it is compared with Hellstrand's results for different temperatures.

An extensive evaluation of power coefficient measurements has been made for the Yankee, Saxton, BR-3 and SELNI cores. The results of these measurements are given in Figure 3-20 which shows the change in the effective fuel temperature per kw/ft as a function

of core average kw/ft. From these data an empirical equation for T_{eff} has been developed which will predict T_{eff} as a function of power level⁽⁴²⁾. This equation for T_{eff} is given below.

$$T_{\text{eff}}(P/P_o) = 0.55 \Delta T_{\text{fuel}} + \alpha(\bar{q}'') \delta \bar{q}'' + 1.571 P/P_o \Delta T_o(\text{clad} + \text{film}) + T_{\text{coolant}}$$

where

P/P_o	= fraction of full power
ΔT_{fuel}	= difference between maximum and surface fuel pellet temperature (function of power)
$\alpha(\bar{q}'')$	= Empirical parameter dependent upon average heat flux
δ	= ratio of the cold diametral gap to the inner diameter of the clad
\bar{q}''	= average surface heat flux to the pellet
$\Delta T_o(\text{clad} + \text{film})$	= temperature drop across clad and film (function of power)
T_{coolant}	= average temperature of the coolant (function of power)

The empirically determined α is given in Figure 3-21 as a function of pellet surface heat flux. The difference in the effective temperature obtained from the experimental data of Figure 3-20 and from the correlation employing Figure 3-21 is shown in Figure 3-22 as a function of surface heat flux. It can be seen that even though there is some scatter in the experimental data (Figure 3-20), all the experimental points fall into a small band when the T_{eff} correlation is used. The most scattered experimental data points deviate from the predicted value (solid line) by no more than $\pm 80^\circ\text{F}$. It is concluded that the T_{eff} correlation can predict T_{eff} at any power level to within $\pm 80^\circ\text{F}$ which constitutes less than $\pm 5\%$ of the effective fuel temperature at full power.

REFERENCES, Section 3.2.1

- (1) McGaugh, J. D., "The Effects of Xenon Spatial Variations and the Moderator Coefficient on Core Stability," WCAP 2983, August, 1966.
- (2) Strawbridge, L. E., "Calculations of Lattice Parameters and Criticality for Uniform Water Moderated Lattices," WCAP-3269-25 (1964).
- (3) Strawbridge., L. E., Barry, R. F., "Criticality Calculations for Uniform Water Moderated Lattices," Nuclear Science and Engineering 23 (58-73) 1965.
- (4) Bohl, R., Gelbard, E.; and Ryan, G., "MUFT-4 Fast Neutron Spectrum Code for the IBM-704," WAPD-TM-72 (July 1957).
- (5) Hellens, R. L. "Neutron Slowing Down in Group Diffusion Theory," WAPD-114 (1956).
- (6) Greuling, E., Clark, F., and Goertzer, G., "A Multigroup Approximation to the Boltzman Equation," NDA-10-96.
- (7) Henry, A. F., "54 Group Library for P₁ Program," WAPD-TM-224.
- (8) Amster, H. J., and Saurez, R., "The Calculation of Thermal Constants Averaged Over a Wigner-Wilkins Flux Spectrum: Description of the SOFOCATE Code," WAPD-TM-39 (1957).
- (9) Amster, H. J., et al, "KATE-1, A Program for Calculating Wigner-Wilkins and Maxwellian Averaged Thermal Constants," WAPD-TM-232.
- (10) Sher, R., et al, "Least Square Analysis of 2200 m/sec Parameters of U-233, U-235 and Pu-239," BNL-722.
- (11) Amster, H. J., "The Wigner-Wilkins Calculated Thermal Neutron Spectra Compared with Measurements in a Water Moderator," Nuclear Science and Engineering 2, 394-404 (1957).
- (12) Honeck, H. C., "The Calculation of the Thermal Utilization and Disadvantage Factor in U-Water Lattices," Nuclear Science and Engineering 1, 49 (1964).
- (13) Amouyal, A., and Benoist, P., J. Nuclear Engineering 6, 79 (1957).
- (14) Poncelet, C. G., "Burnup Physics of Heterogeneous Reactor Lattices," WCAP-6069 (1965).
- (15) Rist, H. A., and Krug, H. E., "Results of Comparisons of Thermal Calculational Models for Heterogeneous Light-Water Moderated PuO₂ - UO₂ Reactor Systems," ANS Transactions, Vol. 8, No. 1 (1965).

- (16) Flatt, H. P., and Baller, D. G., "AIM-5 - A Multigroup, One Dimensional Diffusion Equation Code," NAA-SR-4694 (March 1960).
- (17) Bilodeau, G., Cadwell, W., Dorsey, J., Fairey, J., Varga, R., "PDQ - An IBM-704 Code to Solve the Two-Dimensional Few-Group Neutron Diffusion Equation," WAPD-TM-70 (1957).
- (18) Breen, R. J., "A One Group Model for Thermal Activation Calculations," Nuclear Science and Engineering 9 (1961).
- (19) Eich, W. J., and Kovacic, W. P., "Reactivity and Neutron Flux Studies in Multiregion Loaded Core," WCAP-1433 (1961).
- (20) Marlow, O. J., and Ombrellaro, P. A., "CANDLE, A One-Dimensional Few Group Depletion Code for the IBM-704," WAPD-TM-53 (1957).
- (21) Marlow, O. J., "Neutron Reactor Depletion Programs for the Philco-2000 Computer," WAPD-TM-221 (1961).
- (22) Barry, R. F., "LEOPARD - A Spectrum Dependent Non-Spatial Depletion Code for the IBM-7094," WAPD-3741 (September 1963).
- (23) England, T. R., "Time Dependent Fission Product Thermal and Resonance Absorption Cross Sections," WAPD-TM-333.
- (24) Lacey, P. G., "Fine Structure Power Peaking in a Critical Experiment Mockup of a Chemical Shim Core," WCAP-3723 (1963).
- (25) Flatt, H. P., "The FOG One-Dimensional Neutron Diffusion Equation Codes," NAA-SR-6104 (1960).
- (26) McGaugh, J. D., and Chastain, R. H., "Power Density vs Burnup Distribution in Yankee Core I," WCAP-6051 (1963).
- (27) Sha, W. T., "An Analysis of Reactivity Worth of the Rod Cluster Control (RCC) Elements and Local Water Hole Power Density Peaking," WCAP-3269-47 (1965).
- (28) Miller, D. L., "Control Rod Requirements in a Chemical Shim Core," WCAP-3727 (1963).
- (29) French, R. J., Moore, J. S., and Wiesemann, R. A., "Reactivity Coefficients in Westinghouse Pressurized Water Reactors," WCAP-2585, 1965.
- (30) Ledinegg, M., "Die Warme," 61 (48), (1938), 891-8.
- (31) Quandt, E. R., "Analysis of Parallel Channel Transient Response and Flow Oscillations," WAPD-AD-TH-489, (1959).
- (32) Quandt, E. R., "Analysis and Measurement of Flow Oscillations," Chemical Engineering Progress Symposium Series, Vol. 57, 32, (1961) 111.

- (33) Meyer, J. E., Rose, R. P., Journal of Heat Transfer, Vol. 85, 1 (1963) 1.
- (34) Tong, L. S. et. al., "HYDNA Digital Computer Program for Hydrodynamic Transient," CVNA-77, 1961.
- (35) Poncelet, C. G., "Effects of Fuel Burnup on Reactivity and Reactivity Coefficients in Yankee Core I," WCAP-6076 (1965).
- (36) "Yankee Core Evaluation Program Quarterly Progress Report for the Period Ending June 30, 1963," WCAP-6055 (1963).
- (37) Hellstrand, E., and Lundgren, G., "The Resonance Integral for Uranium Metal and Oxide," Nuclear Science and Engineering 12, 435 (1962).
- (38) Hellstrand, E., J. Applied Physics 28, 1493 (1957).
- (39) Hellstrand, E., Blomberg, P., and Horner, S., "The Temperature Coefficient of the Resonance Integral for Uranium Metal and Oxide," Nuclear Science and Engineering 8, 497 (1960).
- (40) Sauer, A., "Approximate Escape Probabilities," Nuclear Science and Engineering 16, 329 (1963).
- (41) Case, K. M., de Hoffman, F., and Placzek, G., "Introduction to the Theory of Neutron Diffusion," (1953).
- (42) Sha, W. T., "An Experimental Evaluation of the Power Coefficient in Slightly Enriched PWR Cores," WCAP-3269-40 (1965).

3.2.2 THERMAL AND HYDRAULIC DESIGN AND EVALUATION

3.2.2.1 Thermal and Hydraulic Criteria

The main thermal-hydraulic criterion for core design is to prevent departure from nucleate boiling (DNB) during normal operation. Normal operation includes conditions that may occur as a result of normal system perturbations. A safety margin from DNB during normal operation is maintained by setting a minimum allowable DNB ratio. The Reactor Control and Protection System is designed to provide actuation of automatic reactor trip to prevent expected plant transients from producing core conditions which would give a DNB ratio lower than 1.30.

A second criterion is that there shall be no melting of the uranium dioxide fuel during any anticipated operating conditions.

3.2.2.2 Thermal and Hydraulic Characteristics of the Design

a) Departure from Nucleate Boiling (DNB)

DNB is a combination of hydrodynamic and heat transfer phenomena and is affected by the local and upstream conditions including the flux distribution.

In the reactor design, it is not only the power associated with DNB, but also the location of DNB that is important. The DNB location affects the magnitude of the local fuel rod temperature after DNB. The W-3 DNB correlation includes both local and system parameters for predicting the local DNB heat flux ratio. This correlation includes the non-uniform flux effect and the upstream effect (inlet enthalpy or length). The local DNB heat flux ratio indicates the actual allowable uncertainty of heat flux without reaching DNB.

Explained in the paragraphs that follow are details of the local DNB heat flux prediction for a non-uniform flux distribution when the W-3 correlation is employed.

1. Objective of this Correlation

The W-3 DNB correlation ⁽¹⁾ has been developed to predict the DNB flux and the location of DNB equally well for a uniform and an axially non-uniform heat flux distribution. This correlation replaces the preceding WAPD q" and H DNB correlations published in Nucleonics ⁽²⁾ May 1963, in order to eliminate the discontinuity of the latter at the saturation temperature, and to provide a single unambiguous criterion of the design margin.

The sources of the data used in developing this correlation are:

WAPD-188	(1958)	CU-TR-No. 1 (NW-208)	(1964)
ASME Paper 62-WA-297	(1962)	CISE-R-90	(1964)
CISE-R-63	(1962)	DP-895	(1964)
ANL-6675	(1962)	AEW-R-356	(1964)
GEAP-3766	(1962)	BAW-3238-7	(1965)
AEW-R-213 and 309	(1963)	AE-RTL-778	(1965)
CISE-R-74	(1963)	AEW-355	(1965)
CU-MPR-XIII	(1963)		

The comparison of the measured to predicted DNB flux of this correlation is given in Figure 3-23. The local flux DNB ratio versus the probability of not reaching DNB is plotted in Figure 3-24.

It should be emphasized that the inlet subcooling effect of this correlation was obtained from both uniform and non-uniform data. The existence of an inlet subcooling effect is demonstrated

to be real and hence the actual subcooling should be used in the calculations. The W-3 correlation was developed from tests with flow in tubes and rectangular channels. Good agreement is obtained when the correlation is applied to test data for rod bundles.

2. Local Non-Uniform DNB Flux

The W-3 correlation gives the equivalent uniform DNB heat flux, $q''_{\text{DNB,EU}}$. The heat distribution upstream of the DNB point affects the value of the DNB flux. This influence is accounted for by the F-factor, described in Reference (3) and in Section 3.2.2.3. The non-uniform DNB heat flux, $q''_{\text{DNB,N}}$, is given by

$$q''_{\text{DNB,N}} = q''_{\text{DNB,EU}}/F \quad (1)$$

3. Definition of DNB Ratio (DNBR)

The DNB heat flux ratio is defined as

$$\text{DNBR} = q''_{\text{DNB,N}}/q''_{\text{loc}} = q''_{\text{DNB,EU}}/F q''_{\text{loc}} \quad (2)$$

The F-factor may be considered as a DNB hot spot factor due to the axial heat flux distribution. An alternate, although improper, DNB ratio could be defined as $q''_{\text{DNB,EU}}/q''_{\text{loc}}$ instead of $q''_{\text{DNB,EU}}/F q''_{\text{loc}}$. Since the F-factor at the minimum DNBR location is generally greater than unity, this alternate DNBR would be greater than the proper DNBR as defined by equation (2). Because this alternate DNBR does not consider the effects of the non-uniform flux distribution, it does not give the correct physical meaning to DNB and is therefore not used in the evaluation of DNB ratios.

4. Procedure for Using W-3 Correlation

In predicting the local DNB flux in a non-uniform heat flux channel, the following two steps are required:

- i) The uniform DNB heat flux, $q''_{\text{DNB,EU}}$, is computed with the W-3 correlations using the local reactor conditions.
- ii) This equivalent uniform heat flux is converted into corresponding non-uniform DNB heat flux, $q''_{\text{DNB,N}}$, for the non-uniform flux distribution in the reactor. This is accomplished by dividing the uniform DNB flux by the F-factor described in Reference (3). Since F is generally greater than unity $q''_{\text{DNB,N}}$ will be smaller than $q''_{\text{DNB,EU}}$.

To calculate the DNBR of a reactor channel, one may evaluate the values of $q''_{\text{DNB,N}}/q''_{\text{local}}$ along the channel and take the minimum value as the minimum DNBR of the channel.

The W-3 correlation depends on both local and inlet enthalpies of the actual system, and the upstream conditions are included through the F-factor. Hence, it gives a realistic safety margin on heat flux.

b) Film Boiling Heat Transfer Coefficient

Heat transfer after departure from nucleate boiling is conservatively assumed to be limited by film boiling immediately, and the period of transition boiling is neglected. The heat transfer coefficient in film boiling was obtained by correlating the existing data as shown in Figure 3-25.

c) Central Temperature of the Hot Pellet

The temperature distribution in the pellet is mainly a function of the uranium dioxide thermal conductivity and the local power density. The absolute value of the temperature distribution is affected by the cladding temperature and the thermal conductance of the gap between the pellet and the cladding.

The occurrence of nucleate boiling maintains maximum cladding surface temperature below about 657 F at nominal system pressure. The contact conductance between the fuel pellet and cladding is a function of the contact pressure and the composition of the gas in the gap⁽⁴⁾⁽⁵⁾ and may be calculated by the following equation::

$$h = 0.6 P + \frac{k}{f(14.4 \times 10^{-6})}$$

where

h is conductance in Btu/hr ft² °F

P is contact pressure in psi

k is the thermal conductivity of the gas mixture in the rod

f is the correction factor for the accommodation coefficient

This calculational procedure yields a conductance of approximately 1000 Btu/hr ft² °F when the pellet contacts the clad with zero contact pressure and gas composition is 75% fission gas and 25% air.

The thermal conductivity of uranium dioxide was evaluated from published results of recent work at ORNL⁽⁶⁾, Chalk River⁽⁷⁾, and WAPD⁽⁸⁾⁽⁹⁾. The design curve for thermal conductivity is given in Figure 3-26. The section of the curve at temperatures between 0°F and 3000°F is based on the data of Godfrey, et al⁽⁶⁾.

The section of the curve between 3000°F and 5000°F was based on two factors:

- i) In-pile observations of fuel melting dictate a positive temperature coefficient for conductivity above approximately 3000°F. The temperature dependence in this range should conform to an exponential curve since this reflects the most credible physical interpretation of the high temperature conductivity increase.

- ii) The area under the recommended curve is such that the integral $\int k dt$ is equal to approximately 97 w/cm as given by Robertson, et al⁽¹⁰⁾ and Duncan⁽¹¹⁾. This value is based upon the interpretation of fuel melt radius as determined at Hanford⁽¹²⁾ and Chalk River⁽¹³⁾.

Thermal conductivity can be represented best by the following equations:

$$\text{Temperature Range - } 0 \leq T \leq 1650^{\circ}\text{C}$$
$$k = \frac{40.4}{464 + T} + 1.32 \times 10^{-4} e^{1.88 \times 10^{-3} T}$$

$$\text{Temperature Range - } 1650^{\circ}\text{C} \leq T \leq 2800^{\circ}\text{C}$$
$$k = 0.019 + 1.32 \times 10^{-4} e^{1.88 \times 10^{-3} T}$$

with k in w/cm°C for 95 per cent dense UO₂ and T in °C.

Based upon the above considerations, the maximum central temperature of the hot pellet at steady state is 4000°F for the conditions shown in Table 3-5. This temperature is well below the melting temperatures of the irradiated UO₂ which is assumed to be about 4800°F⁽¹³⁾. The central temperature is about 4250°F during the maximum overpower transient of 112%.

d) Hot Channel Factors

The total hot channel factors for heat flux and enthalpy rise are defined as the maximum-to-core-average ratios of these quantities. The heat flux factors consider the local maximum at a point (the "hot spot"), and the enthalpy rise factors involve the maximum integrated value along a channel (the "hot channel").

1. Definition of Engineering Hot Channel Factor

Each of the total hot channel factors is the product of a nuclear hot channel factor describing the neutron flux distribution and an engineering hot channel factor to allow for variations

from design conditions. The engineering hot channel factors account for the effects of flow conditions and fabrication tolerances and are made up of subfactors accounting for the influence of the variations of fuel pellet diameter, density and enrichment; fuel rod diameter; pitch and bowing; inlet flow distribution; flow redistribution; and flow mixing.

The engineering hot channel factors for the 3025 Mwt design are 1.04 for F_q^E and 1.075 for $F_{\Delta H}^E$. The subfactors used in obtaining these values are described in the following paragraph.

2. Heat Flux Engineering Subfactor, F_q^E

This subfactor, determined by statistically combining the tolerances for the fuel diameter, density, enrichment and the fuel rod diameter, pitch and bowing is 1.04. Measured manufacturing data from the first three Yankee cores, the SELNI core and Indian Point Core B show this factor is conservative on comparison to the value obtained for the probability limit of three standard deviations. Thus, it is expected that a statistical sampling of the fuel assemblies of this plant will also show this subfactor is conservative..

3. Enthalpy Rise Engineering Subfactors, $F_{\Delta H}^E$

Pellet Diameter, Density Enrichment and Fuel Rod Diameter, Pitch and Bowing:

Based on the applicable tolerances and consistent with the probability limit of three standard deviations for the measured Yankee, SELNI and Indian Point data, a value of 1.08 was selected for this subfactor.

Inlet Flow Maldistribution:

The inlet flow maldistribution was studied in a one-seventh scale hydraulic model of a typical pressurized water reactor⁽²⁰⁾⁽²¹⁾. Combining the flow distribution with the power distribution in the core indicated that an inlet plenum hot channel factor of 1.03 is reasonable.

Flow Redistribution:

Differences in the hydraulic resistance in the local boiling region and adjacent regions in the core which are not in local boiling cause a flow redistribution.

The amount of flow redistribution due to local boiling between the neighboring channels has been calculated with the CAT⁽¹⁴⁾ code. This code computes the flow in the hot channel by equating the pressure gradient in the hot channel to the pressure gradient in the average channel. The code results indicated the effect of flow redistribution due to local boiling in the hot channel enthalpy rise could be accounted for by using a hot channel subfactor of 1.05.

Flow Mixing:

Mixing vanes have been incorporated into the spacer grid design for this core. These vanes induce flow mixing between the various flow channels in a fuel assembly and also between adjacent assemblies. This mixing reduces the enthalpy rise in the hot channel resulting from local power peaking or unfavorable mechanical tolerances.

Flow mixing studies have been performed on fuel assemblies with mixing vanes at Westinghouse APD⁽¹⁵⁾. These tests were performed in a single fuel assembly and indicated mixing reduced the enthalpy

rise hot channel factor by 8%. Thus, a mixing factor of 0.92 is used for the flow mixing hot channel subfactor. Since mixing between fuel assemblies was not included, this value is conservative.

The above subfactors are combined to obtain the total engineering hot channel factor for enthalpy rise of 1.075. Table 3-4 is a tabulation of the design engineering hot channel factors.

4. Basis for Confidence.

Generally, in the early stages of design the engineering hot channel factors are estimated using the allowable manufacturing deviations to determine each engineering hot channel subfactor. These subfactors are combined by multiplication which gives a resulting engineering hot channel factor with the maximum deviations occurring simultaneously at the hot spot or hot channel. These estimated engineering hot channel factors are combined with the nuclear hot channel factors to establish the design objective.

After the core fabrication tolerances have been established by measurements, the engineering hot channel subfactors are re-evaluated as a check on the estimated numbers used in design.

One would expect deviations in fabrication to occur in a statistical manner⁽¹⁸⁾, and sample measurements taken during fabrication of the first three Yankee cores, the SELNI core, and Indian Point Core B, show that variations in the fuel rod fabrication tolerances are, in fact, normally distributed. As a result, the subfactors related to these variations can be treated statistically⁽¹⁹⁾. The subfactors related to flow distribution, redistribution, and mixing, however, do not lend themselves readily to a statistical prediction, but are determined from flow tests and computer studies.

TABLE 3-4
ENGINEERING HOT CHANNEL FACTORS
3025 MWt

$F_{\Delta H}^E$	Pellet Diameter, Density, Enrichment, and Eccentricity	1.04
	Rod Diameter, Pitch and Bowing	
<hr/>		
$F_{\Delta H}^E$	Pellet Diameter, Density, Enrichment	1.08
	Rod Diameter, Pitch and Bowing	
	Inlet Flow Maldistribution	1.03
	Flow Redistribution	1.05
	Flow Mixing	<u>0.92</u>
	Resulting $F_{\Delta H}^E$	1.075
<hr/>		

e) Bulk Boiling

During normal operating transients, bulk boiling is permitted in the hot region of the core. In order to avoid premature DNB possibly caused by flow pattern instability, the local void fraction at the exit region of the non-statistical hot channel of this reactor will be limited to 32%. (Equivalent to about 7% quality by weight at 2250 psia.) Experimental evidence has shown that bubbly flow is stable at this void fraction^(22,23). Bulk boiling in the hot channels causes additional flow redistribution which is not accounted for by the 1.05 hot channel subfactor. Under these conditions this subfactor is recalculated and the DNB ratios are determined using this greater adverse flow distribution.

f) Total Coolant Flow Rate and Bypass Flow

The total coolant flow rate at operating temperature and pressure is 133.1×10^6 lb/hr. This flow enters through four inlet nozzles, is deflected downward through the annulus formed by the core barrel and the vessel wall. The thermal shield divides this flow into two paths. At the bottom of the vessel the direction of the coolant flow is changed 180° . The coolant then flows upward through the core and exits through four outlet nozzles located at the same elevation as the inlet nozzles.

Ninety-one per cent of the total coolant flow rate is effective for heat removal from the core. The remaining nine per cent is considered as bypass flow as it is not fully effective for removing heat generated in the core. This bypass flow includes the flow through the RCC guide thimbles, the flow between the core baffle and barrel, the leakage across the outlet nozzles, the flow deflected into the head of the vessel for cooling the upper flange, and the excess flow in the flow cells surrounding the RCC guide thimbles. The hydraulic forces are not sufficient to lift a rod control cluster during normal operation even if the rod cluster is detached from its coupling.

The total pressure loss across the reactor vessel, including the inlet and outlet nozzles, is about 51 psi; this value includes a 10% uncertainty factor. The pressure drop across the core is about 32 psi which also includes 10% for uncertainties.

g) Variation of Reactor Coolant System Temperature and Pressure

1. Pressure

The maximum steady state primary system pressure variation, including instrument errors and deadband, is ± 30 psi.

2. Temperature

The maximum steady state temperature variation from the reference temperature, including temperature control deadband and instrument errors, is $\pm 4^\circ\text{F}$.

h) Hydraulic and Thermal Design Parameters

The preliminary hydraulic and thermal design parameters are given below in Table 3-5 for operation at 3025 MWt.

TABLE 3-5
HYDRAULIC AND THERMAL DESIGN PARAMETERS

Total Heat Output, MWt	3025
Total Heat Output, Btu/hr	$10,324 \times 10^6$
Heat Generated in Fuel, %	97.4
Maximum Overpower	12%
System Pressure, Nominal, psia	2250
System Pressure, Minimum Steady State, psia	2220
Hot Channel Factors	
Heat Flux, F	2.82
Enthalpy Rise, F ^q	1.70
DNB Ratio (W-3) at Nominal Conditions	1.82
Coolant Flow	
Total Flow Rate, lbs/hr	133.1×10^6
Effective Flow Rate for Heat Transfer, lbs/hr	121.2×10^6
Effective Flow Area for Heat Transfer, ft ²	47.9
Average Velocity along Fuel Rods, ft/sec	15.7
Average Mass Velocity, lb/hr-ft ²	2.53×10^6
Coolant Temperatures, °F	
Nominal Inlet	549.7
Maximum Inlet due to Instrumentation	
Error and Deadband, °F	553.7
Average Rise in Vessel, °F	58.0
Average Rise in Core	63.2
Average in Core	582.7
Average in Vessel	578.8
Nominal Outlet of Hot Channel	648.3
Average Film Coefficient, Btu/hr-ft ² -F	5920
Average Film Temperature Difference, °F	33
Heat Transfer at 100% Power	
Active Heat Transfer Surface Area, ft ²	52,200
Average Heat Flux, Btu/hr-ft ²	193,000
Maximum Heat Flux, Btu/hr-ft ²	543,000
Average Thermal Output, kw/ft	6.24
Maximum Thermal Output, kw/ft	17.6
Maximum Clad Surface Temperature at Nominal Pressure, °F	657
Fuel Central Temperature, °F	
Maximum at 100% over	4000
Maximum at 112% Power	4250
Thermal Output, kw/ft	
Maximum at 112% Power	19.7

3.2.2.3 Thermal and Hydraulic Evaluation

a) W-3 Equivalent Uniform Flux DNB Correlation

The equivalent uniform DNB flux $q''_{\text{DNB,EU}}$ is calculated from the W-3 equivalent uniform flux DNB correlation as follows:

$$\frac{q''_{\text{DNB,EU}}}{10^6} = [(2.022 - 0.0004302p) + (0.1722 - 0.0000984p) e^{(18.177 - 0.004129p)\chi}] \times [(0.1484 - 1.596\chi + 0.1729|\chi|) G/10^6 + 1.037] \times [1.157 - 0.869\chi] \times [0.2664 + 0.8357e^{-3.151D}] \times [0.8258 + 0.000794 (H_{\text{sat}} - H_{\text{in}})] \quad (3)$$

The heat flux is in Btu/hr ft² and the units of the parameters are as listed below. The ranges of parameters of the data used in developing this correlation are:

System pressure, $p = 800$ to 2300 psia

Mass velocity, $G = 0.5 \times 10^6$ to 5.0×10^6 lb/hr ft²

Equivalent diameter, $D_e = 0.2$ to 0.7 inches

Quality, $\chi_{\text{loc}} = -0.15$ to $+0.15$

Inlet enthalpy, $H_{\text{in}} \geq 400$ Btu/lb

Length, $L = 10$ to 144 inches

Heated perimeter = 0.88 to 1.00

Wetted perimeter

Geometries = circular tube and rectangular channel

Flux = Uniform and equivalent uniform flux converted from non-uniform data by using F-factor of Reference (3).

b) Local Non-Uniform DNB Flux

The local non-uniform $q''_{\text{DNB,N}}$ is calculated as follows:

$$q''_{\text{DNB,N}} = q''_{\text{DNB,EU}}/F \quad (4)$$

where

$$F = \frac{C}{q''_{\text{local}} \text{ at } l_{\text{DNB}} \times (1 - e^{-Cl_{\text{DNB}}})} \int_0^{l_{\text{DNB}}} q''(z) e^{-C(l_{\text{DNB}} - z)} dz \quad (5)$$

$$C = 0.44 \frac{(1 - \chi_{\text{DNB}}) 7.9}{(G/10^6) 1.72} \text{ inch}^{-1}$$

In determining the F-factor, the value of q''_{local} at $z = z_{\text{DNB}}$ in equation (5) was measured at $z = z_{\text{DNB}}$. For a uniform flux, F becomes unity so that $q''_{\text{DNB,N}}$ reduces to $q''_{\text{DNB, uniform}}$ as expected. The comparisons of predictions by using W-3 correlations and the non-uniform DNB data obtained at B&W⁽¹⁶⁾, Winfrith⁽¹⁷⁾ and Fiat are given in Figures 3-27, -28, -29, and -30. The criterion for determining the predicted location of DNB is to evaluate the ratio of the predicted DNB flux to the local heat flux along the length of the channel. The location of the minimum DNB ratio is considered to be location of DNB. It can be seen from the above figures that the agreement in DNB flux is excellent and the prediction of location is conservative.

c) Application of the W-3 Correlation in Design

During steady state operation at the nominal design conditions the DNB ratios are determined. Under other operating conditions, particularly overpower transients, more limiting conditions develop than those existing during steady state operation. The DNB correlations are sensitive to several parameters. In addition, thermal flux generated under transient conditions is also sensitive to many parameters. Therefore, for each case studied, the most adverse combination of the following factors was used.

1. Calorimetric Error

This is always assumed to be negative: that is, the indicated heat balance data are assumed to be less than the actual reactor thermal power output. An error of 2 per cent is assumed although experience in the operation of Yankee, SELNI and Indian Point indicates that less than one per cent will be demonstrated in actual operation.

2. Maximum Overpower

Maximum errors are assigned to the nuclear instrumentation due to drift and reactor trip set point reproducibility. The trip setting selected is such that the maximum thermal overpower

level, including the effects of calorimetric, drift and set point errors, will be 112 per cent. For operation at 3025 MWt, a 112 per cent maximum thermal overpower level includes a conservative allowance for errors due to control rod motion.

3. Axial Flux Distribution

This plant will operate with chemical shim and the axial flux distribution was calculated on the basis of a modified cosine function with a maximum to average value of 1.72.

4. Hot Channel Factors at 3025 MWt

The design hot channel factors are:

$$\begin{array}{ll} \text{Nuclear} & F_q^N = 2.71 \qquad F_{\Delta H}^N = 1.58 \end{array}$$

$$\begin{array}{ll} \text{Engineering} & F_q^E = 1.04 \qquad F_{\Delta H}^E = 1.075 \end{array}$$

$$F_q = 2.82 \qquad F_{\Delta H} = 1.70$$

$F_{\Delta H}^N$ is determined as stated in Section 3.2.1. F_q^N is the product of the maximum to average value of the flux distribution and the nuclear factor, $F_{\Delta H}^N$.

For transient accident conditions where the power level, system pressure and core temperatures may increase, the DNBR is limited to a minimum value = 1.30. The Reactor Control and Protection System is designed to prevent any credible combination of conditions from occurring which would result in a lower DNB ratio.

5. DNB Evaluation

An evaluation was made to predict the number of fuel rods in the core that might reach DNB, both under normal operating conditions and under assumed overpower conditions. For this calculation, a convolution procedure was used in which the product of the number of fuel rods experiencing a given DNB ratio and the probability of DNB was summed over the entire core.

The results are tabulated as follows:

<u>Case</u>	<u>Power MWT</u>	<u>Pressure Psia</u>	<u>Tin °F</u>	<u>Statistical Number* of Fuel Rods Which Could Experience DNB</u>
Nominal	3025	2250	549.7	0.4
112% Over- Power (DNBR= 1.30)	3388	2200	555	21

The power distributions used in the analysis were based on the beginning of life core conditions when the worst power distribution is expected. A conservative design power distribution having a peak radial factor of 1.58 was used. This distribution was obtained by statistically combining uncertainties with the best estimate radial power distribution whose peak radial factor is 1.38.

To demonstrate the sensitivity of the above approach to various parameters, a study was made to study the effect of varying: (a) Power Distributions, (b) Power Levels, and (c) Flow Rates. Nominal conditions were used for pressure and inlet temperature.

* The maximum number of rods which could experience DNB taking into account the distribution of the experimental data from which the W-3 DNB correlation was developed, and the distribution of the power in the core.

(a) Effect of Varying the Power Distribution

<u>Power Distribution</u>	<u>Power % of Nominal</u>	<u>Maximum Statistical* Number of Fuel Rods Which May Experience DNB</u>
Design	112	5.52
Best Estimate	112	0.59
Design	100	0.34
Best Estimate	100	0.04

(b) Effect of Varying Power Levels

<u>Power Distribution</u>	<u>Power % of Nominal</u>	<u>Maximum Statistical* Number of Fuel Rods Which May Experience DNB</u>
Best Estimate	100	0.04
Best Estimate	112	0.6

(c) Effect of Varying Flow Rate at 112% Power

<u>Power Distribution</u>	<u>Flow % of Nominal</u>	<u>Maximum Statistical* Number of Fuel Rods Which May Experience DNB</u>
Best Estimate	100	0.6
Best Estimate	95	1.2
Best Estimate	90	2.9

* The maximum number of rods which could experience DNB taking into account the distribution of the experimental data from which the W-3 DNB correlation was developed, and the distribution of the power in the core.

REFERENCES, SECTION 3.2.2

- (1) L. S. Tong, "DNB Prediction for an Axially Non-Uniform Heat Flux Distribution", WCAP-5584, Revision 1, 1966.
- (2) L. S. Tong, H. B. Currin and A. G. Thorp II, "New Correlations Predict DNB Conditions", Nucleonics, May 1963. Also WCAP-1997 (1963).
- (3) L. S. Tong, H. B. Currin, P. S. Larsen, and O. B. Smith, "Influence of Axially Non-Uniform Heat Flux on DNB", AIChE Preprint 17, Eighth National Heat Transfer Conference, Los Angeles 1965.
- (4) R. A. Dean, "Thermal Contact Conductance Between UO_2 and Zircaloy-2," CVNA-127, May 1962.
- (5) A. M. Ross and Stoute, R. L., "Heat Transfer Coefficient Between UO_2 and Zircaloy-2," AECL-1552, June 1962.
- (6) T. G. Godfrey, et al, "Thermal Conductivity of Uranium Dioxide and Armco Iron by an Improved Radial Heat Flow Technique", ORNL-3556, June 1964.
- (7) J. A. L. Robertson, et al, "Temperature Distribution of UO_2 Fuel Elements", Journal of Nuclear Materials 7, No. 3, 1962, pp. 225-262.
- (8) R. N. Duncan, "Rabbit Irradiation of UO_2 ", CVNA-142, June 1962.
- (9) J. A. Christensen, "Thermal Conductivity of Nearly Stoichiometric UO_2 - Temperature and Composition Effects", WCAP-2531, November 1963.
- (10) J. A. L. Robertson, et al, "Temperature Distribution in UO_2 Fuel Elements", Journal of Nuclear Materials 7, No. 3, 1962, pp. 225-262.
- (11) R. N. Duncan, "Rabbit Irradiation of UO_2 ", CVNA-142, June 1962.
- (12) G. R. Horn and J. A. Christensen, "Identification of the Molten Zone In Irradiated UO_2 ", ANS Winter Meeting Transactions, 1963, p. 348, No. 5.
- (13) J. A. Christensen, R. J. Allio and A. Biancheria, "Melting Point of Irradiated Uranium Dioxide", WCAP-6065, February 1965.
- (14) R. O. Sandberg, "CAT-II - An IBM 7090 Code for Predicting Thermal and Hydraulic Transients in an Open-Lattice Core", WCAP-2059.
- (15) R. A. Dean, "SENA Mixing Vane Effectiveness", WCAP-2678, September 1964.
- (16) D. F. Judd, et al, "Non-Uniform Heat Generation Experimental Program", BAW-3238-7 (1965).
- (17) D. H. Lee, J. D. Obertelli, "An Experimental Investigation of Forced Convection Burnout in High Pressure Water, Part II, Preliminary Results for Round Tubes with Non-Uniform Axial Heat Flux Distribution", AEEW-R-309, Winfrith, England (1963).

- (18) Nucleonics, Vol. 20, No. 9, September 1962, "Engineering Hot Channel Factors for Open-Lattice Core", H. Chelemer, L. S. Tong.
- (19) WCAP-1594, "Statistically Determined Engineering Hot Channel Factors of a Parallel Rod Bundle Core", H. Chelemer, L. S. Tong, 1960.
- 209) G. Hetsroni, "Hydraulic Tests of the San Onofre Reactor Model", WCAP-3269-8, 1964.
- (21) G. Hetsroni, "Studies of the Connecticut-Yankee Hydraulic Model", WCAP-2761, 1965.
- (22) Rose, S.C., Jr., and Griffith, P., "Some Hydrodynamic Characteristics of Bubbly Mixtures Flowing Vertically Upward in Tubes", MIT T. R. No. 5003-30 (1964).
- (23) Snyder, G. A., and Griffith, P., "The Bubbly-Slug Transition in a High Velocity Two-Phase Flow", TID-20947 (1964).

3.2.3 MECHANICAL DESIGN AND EVALUATION

The reactor core, shown in cross-section in Figure 3-31, consists of 193 fuel assemblies containing slightly enriched uranium dioxide pellets clad in Zircaloy tubes to form a lattice, roughly cylindrical in shape. The overall active height is 144 inches and the equivalent diameter is 133.7 inches. Demineralized light water flows upward through the lattice and acts as both moderator and coolant.

The core is divided into three regions of different enrichments. The outer region contains 64 fuel assemblies with the central region containing 129 fuel assemblies in a checkerboard array. The loading arrangement for the initial cycle is indicated on Figure 3-32. Refueling takes place generally in accordance with an inward loading schedule. Sixty-four spent fuel assemblies are removed and sixty-four new fuel assemblies are loaded at each refueling. The sixty-fifth element in the central region will be in the core for four cycles.

The control elements, designated as Rod Cluster Control (RCC) assemblies, are clusters of cylindrical absorber rods which insert directly into guide thimbles which form an integral part of the fuel assemblies. Figure 3-33 shows a typical schematic of these assemblies.

The 193 fuel assemblies will be held in position between a lower core plate and an upper core plate. The core is surrounded by a form-fitting baffle which confines the upward flow of coolant within the fuel bearing zone. Outside the baffle and surrounding it, there is a core barrel. A small amount of coolant is allowed to flow between the barrel and the baffle for cooling. Table 3-6 is a tabulation of the basic core mechanical design parameters.

TABLE 3-6
CORE MECHANICAL DESIGN PARAMETERS⁽¹⁾

Active Portion of the Core

Equivalent Diameter, in.	133.7
Active Fuel Height, in.	144.0
Length-to-Diameter Ratio	1.08
Total Cross-Section Area, ft ²	97.4

Fuel Assemblies

Number	193
Rod Array	15 x 15
Rods per Assembly	204 ⁽²⁾
Rod Pitch, in.	0.563
Overall Dimensions, in.	8.426 x 8.426
Fuel Weight (as UO ₂), pounds	218,530
Total Weight, pounds	279,631
Number of Grids per Assembly	9

Fuel Rods

Number	39,372
Outside Diameter, in.	0.422
Diametral Gap, in.	0.0065
Clad Thickness, in.	0.0243
Clad Material	Zircaloy

Fuel Pellets

Material	UO ₂ sintered
Density (% of Theoretical)	94 ² -93
Feed Enrichments, w/o	
Region 1	2.1
Region 2	2.6
Region 3	3.2
Diameter, in.	0.3669
Length, in.	0.600

Rod Cluster Control Assemblies

Neutron Absorber	5% Cd-15% In-80% Ag
Cladding Material	Type 304 SS - Cold Worked
Clad Thickness, in.	0.019
Number of Clusters	53
Number of Control Rods per Cluster	20

Core Structure

Core Barrel I.D./O.D., in.	148.5/152.5
Thermal Shield I.D./O.D., in.	158.5/164

- (1) All dimensions are for cold conditions.
 (2) Twenty-one rods are omitted: twenty to provide passage for control rods and one to contain in-core instrumentation.

3.2.3.1 Internal Layout

The reactor internals are designed to support and orient the reactor core fuel assemblies and control rod assemblies, absorb the control rod dynamic loads and transmit these and other loads to the reactor vessel flange, provide a passageway for the reactor coolant, and support in-core instrumentation. A cutaway schematic of the reactor internals is shown in Figure 3-34.

The internals are designed to withstand the forces due to weight, preload of fuel assemblies, control rod dynamic loading, vibration, and earthquake acceleration. These internals will be analyzed in a manner similar to Indian Point Unit No. 2, Connecticut Yankee, SCE, and SELNI. Where applicable, Section III, ASME Nuclear Vessel Code will be used as a guide. The dynamic criteria for design and the stress levels of the internals in this plant will be the same as those in Indian Point Unit #2.

The reactor internals will be equipped with bottom-mounted in-core instrumentation supports. These supports will be designed to sustain the applicable loads outlined above.

The downward vertical displacement of the internals will be limited by a special structure and energy absorbing devices attached to the bottom support casting. An outline of this device is shown on Figure 3-35. In the event of the postulated failure of the primary core support, the energy absorbers would contact the vessel bottom head. The load would transfer through the bottom support casting to the energy absorber devices to the vessel. The guide tubes, bolted to the instrumentation tie plate at their lower end, are supported from the underside of the core support forging at their upper end.

The energy absorbers, cylindrical in shape, will be attached to a plate which approximates the contour of the bottom surface of the reactor vessel bottom head. Their number and design will be determined so as to limit

the forces imposed to a safe value. Assuming a downward vertical displacement, the potential energy of the system is absorbed mostly by the strain energy of the energy absorbing device.

The free fall in the hot condition will be on the order of 1/2 inch, and there will be an additional strain displacement in the energy absorbing devices of approximately 3/4 inch.

Alignment features in the internals along with the instrumentation column stability will prevent cocking of the internals structure during this postulated drop. The control system as designed provides assurance of control rod insertion capabilities under these assumed drop conditions. The drop distance of about 1-1/4 inch is not enough to cause the tips of the shutdown group of RCC assemblies to come out of the guide tubes in the fuel assemblies. Also, the drop of 1-1/4 inch is not enough to cause a reactivity transient beyond the capability of the control system for either the hot full power or the hot, zero power just critical condition.

The components of the reactor internals are divided into three parts consisting of the lower core support structure (including the entire core barrel and thermal shield), the upper core support structure and the in-core instrumentation support structure.

a) Lower Core Support Structure

The major containment and support member of the reactor internals is the lower core support structure, shown in Figure 3-35. This completely assembled structure consists of the core barrel, the core baffle, the lower core plate and support columns, thermal shield, intermediate diffuser plate and the bottom support casting which is welded to the core barrel. All the major material for this structure is Type 304 stainless steel. The core support structure is supported at its upper flange from a ledge in the reactor vessel head flange and its lower end is restrained in its transverse movement by a radial support system attached to the vessel wall. Within the core barrel are axial baffle and former plates which are attached to the core

barrel wall and form the enclosure periphery of the assembled core. The lower core plate is positioned at the bottom level of the core below the baffle plates and provides support and orientation for the fuel assemblies.

It also has flow distributor holes for each fuel assembly. Fuel assembly locating pins are also inserted into this plate. Columns are placed between this plate and the bottom support casting of the core barrel in order to provide stiffness to this plate and transmit the core load to the bottom support plate. Intermediate between the support casting and lower core support plate is positioned a perforated plate to diffuse and mix the coolant flowing into the core.

The one piece thermal shield is supported from the core barrel by lugs positioned at the bottom of the shield and by a separate radial support system between the thermal shield and the core barrel. This thermal shield radial support consists of a key and keyway joint just below the top of the thermal shield. The upper end of the thermal shield is keyed to the core barrel in much the same arrangement as the main core barrel radial support system.

The lower core support structure and principally the core barrel serve to provide passageways and control for the coolant flow. Inlet coolant flow from the vessel inlet nozzles proceeds down the annulus between the core barrel and the vessel wall, flows on both sides of the thermal shield, and then into a plenum at the bottom of the vessel. It then turns and flows up through the bottom support casting, passes through the intermediate diffuser plate and then through the lower core plate. The flow holes in the diffuser plate and the lower core plate are arranged to give a very uniform entrance flow distribution to the core. After passing through the core, the coolant enters the area of the upper support structure and then flows generally radially to the core barrel outlet nozzles and directly through the vessel outlet nozzles.

A small amount of water also flows between the baffle plates and core barrel to provide additional cooling of the barrel. Similarly, a small amount of the entering flow is directed into the vessel head plenum and exits through the vessel outlet nozzles.

Vertically downward loads from weight, fuel assembly preload, control rod dynamic loading and earthquake acceleration are carried by the lower core plate partially into the lower core plate support flange on the core barrel shell and partially through the lower support columns to the bottom support casting and thence through the core barrel shell to the core barrel flange supported by the vessel head flange. Transverse loads from earthquake acceleration, coolant cross flow, and vibration are carried by the core barrel shell to be shared by the lower radial support to the vessel wall and the core barrel flange held at the vessel head flange. Transverse acceleration of the fuel assemblies is transmitted to the core barrel shell by direct connection of the lower core plate to the barrel wall and by a radial support type connection of the upper core plate to four slab sided pins pressed into the core barrel.

The main radial support system of the core barrel is one of supporting the core barrel by a key and keyway joint to the reactor vessel wall. At each of the support positions on the circumference, an Inconel block is welded to the vessel I.D. The item, referred to as the keyway, is attached to each of these blocks. Opposite each of these is a "key" which is attached to the internals. At assembly, as the internals are lowered into the vessel, the keys engage the keyways in the axial direction. With this design, the internals are provided with a support at the furthest extremity, and may be viewed as a beam fixed at the top and simply supported at the bottom.

Radial and axial expansions of the core barrel are accommodated but transverse movement of the core barrel is restricted by this design. With this system, cycle stresses in the internal structures are within the ASME Section III limits.

b) Upper Core Support Assembly

The upper core support assembly, shown in Figure 3-36, consists of the top support plate, deep beam sections, and upper core plate between which are contained support columns and guide tube assemblies. The support columns establish the spacing between the top support plate, deep beam sections, and the upper core plate and are fastened at top and bottom to these plates and beams. The support columns transmit the mechanical loadings between the two plates and serve the supplementary function of supporting thermocouple guide tubes. The guide tube assemblies, shown in Figure 3-37, sheath and guide the control rod drive shafts and control rods and provide no other mechanical functions. They are fastened to the top support plate and are guided by pins in the upper core plate for proper orientation and support. Additional guidance for the control rod drive shafts is provided by the control rod shroud tube which is attached to the upper support plate and guide tube.

The upper core support assembly, which is removed as a unit during refueling operations, is positioned in its proper orientation with respect to the lower support structure by flat-sided pins pressed into the core barrel which in turn engage in slots in the upper core plate. The flat-sided pins are located in the core barrel at the upper core plate elevation. Slots are milled into the core plate at the same angular position as the pins. As the upper support structure is lowered into the main internals, the slots in the plate engage the flat-sided pins in the axial direction. Lateral displacement of the plate and hence the upper support assembly is restricted by this design. Fuel assembly locating pins protrude from the bottom of the upper core plate and engage each fuel assembly as the upper assembly is lowered into place. Proper alignment of the lower core support structure, the upper core support assembly, the fuel assemblies and control rods is thereby assured by this system of locating pins and guidance arrangement. The upper core support assembly is restrained from any axial movements by a large circumferential spring which is compressed between the reactor vessel head and the internals.

Vertical loads from weight and fuel assembly preload are transmitted through the upper core plate via the support columns to the deep beams and top support plate through the circumferential spring to the reactor vessel head. Transverse loads from coolant cross flow, earthquake acceleration, and possible vibrations are distributed by the support columns to the top support plate and upper core plate. The top support plate is particularly stiff to minimize deflection.

c) In-Core Instrumentation Support Structures

The in-core instrumentation support structure consists of an upper system to convey and support thermocouples penetrating the vessel through the head and a lower system to convey and support flux detectors penetrating the vessel through the bottom.

The top entry thermocouple in core instrumentation system will utilize several of the reactor vessel head penetrations. A port column assembly will be attached to the top support plate and extend up through a penetration. A group of sheath tubes will be passed through the bore of a port column. An individual sheath tube on one end will pass through the port column, be routed across the top support plate to a position above a designated fuel assembly location and then pass vertically downward through and be supported by the support columns, terminating at the upper core plate. The other end of the sheath tube will run up through a plug at the top of the port column, where it will be brazed, and continue on up through a vessel head penetration. The brazed plug will have a conoseal joint which will seal the system pressure at the vessel head penetration. A stainless steel clad thermocouple will be inserted through the sheath tube to the extent that its hot junction will stop at the upper core plate elevation. An additional seal will be made between the sheath tube and the thermocouple at a point above the reactor head by the use of commercial tube fittings.

In addition to the upper in-core instrumentation, there will be reactor vessel bottom penetrations which will carry the retractable, cold worked stainless steel flux thimbles that are pushed upward into the reactor core. Heavy walled thimble guide tubes will extend from the bottom of the reactor vessel down through the concrete shield area and up to a thimble seal line as schematically shown in Figure 3-38. The trailing ends of the thimbles will be withdrawn to the seal line during refueling of the reactor to avoid interference within the core. The thimbles will be closed at the leading ends and serves as the pressure barrier between the reactor pressurized water and the containment atmosphere. Mechanical seals between the retractable thimbles and the thimble guide tubes will be provided at the seal line. During normal operation, the retractable thimbles will be stationary within the in-core guide tube of the fuel assembly and they will be withdrawn only during refueling, or for maintenance, at which time a space must be cleared for the retraction operation. Section 7.5 contains further information on the in-core instrumentation system.

The in-core instrumentation support structure will be designed to support the instrumentation during reactor operation and to resist damage or distortion under the conditions imposed by handling during the refueling sequence.

3.2.3.2 Fuel

a) Fuel Assembly

The fuel assembly shown on Figure 3-39 and 3-40 is of the "canless" type. The RCC guide thimbles and grids form the basic assembly.

The 15 x 15 array of fuel rods is located on a square pitch and supported axially at nine locations along the length by Inconel spring clip grid assemblies. Six of the grids are mixing grids which increase the

degree of inter-mixing flow within an assembly and also between adjacent assemblies. The mixing action of these grids reduces the temperature gradient within an assembly.

At the grid locations, each fuel rod is supported in two perpendicular directions by formed spring clips whose forces are opposed by two rigid support dimples as shown in Figure 3-41. This method provides a rigid support for the fuel rod and restrains flow induced vibration of the fuel rods. Since the spring fingers are not physically bound to the fuel rods, the rods are free to expand axially reducing undesirable reactivity effects due to thermal bowing. The main support structure of the assembly is formed by welding the twenty control rod guide thimbles to the grids and to the top and bottom nozzles.

The fuel rods are conservatively restrained from axial motion due to hydraulic forces by the spring loads of the grids and are limited from gross movement by the top and bottom nozzles. The possibility of any lifting of the entire fuel assembly due to abnormal hydraulic forces has also been eliminated by providing hold-down leaf springs in the top nozzle assembly which bear against the upper core support plate. The top and bottom grids are spaced so that the unsupported overhang of the fuel rod will be small, thus fixing the ends of the rods and severely restricting vibration.

All fuel assemblies of the core are of the same basic mechanical design. In locations where RCC assemblies will not be used, a plugging device will be installed in the upper nozzle to restrict the flow through the unused control rod guide thimbles. Each fuel assembly has an identifying number on the top nozzle so that fuel elements of the proper enrichment are loaded into their proper position in the core.

1. Bottom Nozzle

The bottom nozzle assembly is a box-like structure forming a plenum to distribute the flow through the fuel lattice. "Cut-outs" along the bottom and on the face of the sideplates permit

part of the flow to be directed to the sides and then upwards between adjacent fuel assemblies. The main portion of the flow is directed upward through the interior of the assembly.

The weight of the fuel assembly is supported by the bottom nozzle and distributed through four corner "feet" to the lower core plate. The individual fuel rods are bottomed on the cross bars which are joined to the sideplates. These cross bars are also the structural members to which the control rod guide thimbles are fastened.

The spacing between cross bars is less than the fuel tube diameter making it impossible for a fuel rod to pass the lower nozzle. Two holes are provided in diagonally opposite corners on the bottom of the nozzle, which mate with the locating pins in the lower core plate for positioning the fuel assembly. The entire lower nozzle assembly is fabricated from Type 304 stainless steel.

2. Top Nozzle

The top nozzle is also a box-like structure forming a plenum space where the heated coolant mixes and is directed toward the flow holes of the upper core plate. It also serves as the upper structural member of the fuel assembly, tying the control rod guide thimbles together, and locating the upper end of the fuel assembly relative to the upper core plate. As in the lower nozzle, two holes are located in diagonally opposite corners of the top plate which mate with the locating pins on the upper core plate. A third smaller hole is provided for orienting and handling the assembly.

The bottom component of the nozzle is a relatively heavy structure to which the control guide thimbles are welded. This structure also serves as a stop for the control rod cluster.

Leaf springs are fastened to the upper plate, parallel to the sides, to provide hold down forces to oppose upward hydraulic forces. The springs are clamped by bolts which are later lock-welded to prevent loosening in service. The ends of the spring are bent downward and captured in slots in the plate. To insure that the capture is permanent, even in the event of spring fracture, welded-in lock pins are used to close the slots after the springs have been installed. Rotation of the free end is prevented by the closeness of fit of the spring in the slot. Rotation at the clamp end is prevented by the fit of the spring in the undercut on the bottom of the clamp. The clamp cannot rotate since it is bolted and welded..

The springs are made from Inconel 718 and the bolts from Inconel 600. All other components of the upper nozzle are made from Type 304 stainless steel.

The selection of Inconel 600 as the bolt material precludes the possibility of loosening of the clamp due to thermal expansion. Since the clamp is stainless steel, which has a higher coefficient of thermal expansion than Inconel, the tendency is to increase bolt tension with temperature.

3. Grids

The spring clip grid is made by stacking individual slotted straps, much like an "egg-crate" and furnace brazing them to permanently join the individual straps at their points of intersection. Details, such as spring fingers, support dimples and mixing vanes, are punched and formed integral to the individual straps.

The mixing vanes on the outside strap, aside from performing their mixing function, guide adjacent assemblies during loading and unloading of the core. The small tabs on the underside

and the irregular contour of the outside straps are also for this purpose.

The grid material is Inconel 718 which has been selected for its mechanical properties in order to provide the necessary spring forces on the fuel rods. After the grids are brazed together they are solution heat treated to obtain the desired properties.

A mixing vane grid can be seen in Figure 3-42. Small vanes are positioned on the edges of the grid straps to provide the desired mixing action. The grids without the mixing vanes are similar with the exception that there are no mixing vanes on the internal straps. Mixing vanes are retained on the outer straps for guidance purposes.

b) Fuel Rods

Each fuel rod consists of a Zircaloy tube, containing the uranium dioxide pellets, sealed at each end by means of an end plug welded to the tube. Sufficient void volume is provided at the top end of the assembled fuel rods to accommodate fission product buildup and axial thermal expansion of the fuel column relative to the tube. Before the top end plug is installed, a compression spring is inserted into the void volume to prevent shifting of the fuel column during shipment. The spring is preloaded during installation to a load of approximately six times the fuel weight.

The fuel rods of each enrichment are identified by a marking on the top end plugs to provide an indication of the fuel enrichment within the fuel rods and insure proper insertion into the correct fuel assembly.

The cladding material is Zircaloy which has been slightly cold worked to improve its mechanical properties.

The cold diametral clearance between the pellet and tube wall is reduced by the relative thermal expansion of the pellet, thereby providing good heat transfer at operating temperatures. At the hot spot, the clearance is computed to be essentially zero for beginning of life conditions.

The fission gas release and the associated buildup of internal gas pressure is calculated by the FIGHT code based on experimentally determined rates. The increase of internal pressure in the fuel rod due to this phenomena is included in the determination of the maximum cladding stresses at the end of core life when the fission product gas inventory is a maximum. The internal gas pressure will always be less than the external coolant pressure under normal operating conditions.

The maximum allowable strain in the cladding, considering the combined effects of internal fission gas pressure, external coolant pressure, fuel pellet swelling and clad creep will be limited to about 1/2 to 1 per cent throughout core life. The associated stresses will be below the yield strength of the material under all normal operating conditions.

To assure that manufactured fuel rods meet a high standard of excellence from the standpoint of functional requirements, many inspections and tests are performed both on the raw material and the finished product. These tests and inspections include chemical analysis, tensile testing of fuel tubes, dimensional inspection, X-ray of both end plug welds, ultrasonic testing and helium leak tests.

c) Fuel Pellets

The basic component of the core is the fuel pellet which is manufactured by sintering slightly enriched uranium-dioxide compacted powder. Each pellet is a right circular cylinder with concave or dished ends. For the first core the pellets in the outer region have a density

of approximately 10.19 g per cc (93% theoretical density) while the pellets in the inner region have a density of approximately 10.30 g per cc (94% theoretical density). The fuel in the outer region is made less dense to accommodate the effects of higher burnup. Sintered, high density uranium dioxide is chemically inert with respect to the cladding and enclosed gases at core operating temperatures and pressures. In the event of cladding defects, the high resistance of uranium dioxide to attack by hot water protects against fuel deterioration or decrease in fuel integrity. Thermal stress in the pellets, while causing some fracture of the bulk material during temperature cycling, does not result in pulverization or gross void formation in the fuel matrix. As shown by operating experience and extensive experimental work in the industry, the thermal design parameters conservatively account for any changes in the thermal performance of the fuel element due to pellet fracture.

The consequences of a breach of cladding are greatly reduced by the ability of uranium dioxide to retain fission products including those which are gaseous or highly volatile. This retentiveness decreases with increasing temperature or fuel burnup, but remains a significant factor even at full power operating temperatures in the maximum burnup element.

A survey of fuel element behavior in high burnup uranium dioxide⁽¹⁾ indicates that for an initial uranium dioxide void volume, which is a function of the fuel density, it is possible to define conservatively the fuel swelling as a function of burnup. Since Region 3 will be retained through three cycles of reactor operation, the pellet density has been reduced to 93% to accommodate the effects of increased burnup.

3.2.3.3 Control System

a) Rod Cluster Control Assembly

Fifty-three individually driven rod cluster control rods are provided to control the reactivity of the core under operating conditions. The rod cluster control assembly is shown in Figure 3-43.

The rod cluster control assembly consists of a cluster of twenty individual absorber rods grouped by fastening to a common hub called the spider. The control rods are inserted directly into the fuel assembly where guide thimbles are provided to assure free passage.

The absorber material used in the control rods is silver-indium-cadmium alloy which is essentially "black" to thermal neutrons and has sufficient additional resonance to significantly increase its worth. The absorber alloy is first extruded into single lengths and inserted into stainless steel tubes to prevent the absorber material from coming in direct contact with the coolant.

The overall control rod length is such that when the rod has been withdrawn through its full travel, the tip remains engaged in the guide thimble so that alignment between rod and thimble is always maintained. Since the rods are long and slender, they are relatively free to conform to any small misalignments between the rod and the guide thimble. Prototype tests have shown that the RCC assemblies are very easily inserted and not subject to binding even under conditions of severe misalignment.

1. Absorber Rod

The absorber rods are constructed by inserting silver-indium-cadmium rods into cold worked stainless steel tubing. The rods are sealed at the bottom and the top by welded end plugs. Sufficient diametral and end clearance are provided to accommodate relative thermal expansions and to limit the internal pressure to acceptable levels.

The bottom plug is made bullet-nosed both to reduce the hydraulic drag during a reactor trip and to guide smoothly into the dashpot section of the guide thimble. The upper plug is threaded for assembly to the spider and has a reduced end section to make the joint more flexible.

Stainless steel clad silver-indium-cadmium alloy absorber rods are resistant to radiation and thermal damage thereby ensuring their effectiveness under all operating conditions. Rods of similar design have been successfully used in the Saxton and SELNI reactors.

2. Spider Assembly

The spider assembly is the center hub with radial vanes from which the absorber rods are suspended. Handling details, and details for connection to the drive shaft, are machined into the upper end of the hub. A spring-loaded piston is assembled into the bottom of the hub to stop the RCC assembly at the end of a trip insertion and to absorb the remaining minimal energy after the rod has traversed the dashpot. The radial vanes are joined to the hub, and the rod mounting adapters are joined to the vanes by furnace brazing. The centerpost which holds the snubber piston and spring stack is threaded into the hub and welded to prevent loosening in service. All components of the spider assembly are made from Type 304 stainless steel except for the springs which are Inconel X-750 alloy.

3. Final Assembly

The absorber rods are secured to the spider so as to assure trouble-free service. The rods are first threaded into the mounting adapters and then pinned to maintain joint tightness, after which the pins are welded in place. The end plug below the pin position, is designed to permit flexing.

b) Control Rod Guide Thimbles

The control rod guide thimbles provide guided channels for the insertion and withdrawal of the control rods. They are fabricated from Type 304 stainless steel tubing, which has been drawn to two different diameters. The larger inside diameter at the top provides a

relatively large annular area for rapid insertion during a reactor trip and to accommodate a small amount of cooling flow during normal operations. The bottom approximately 20 in. of the guide thimble is of reduced diameter, resulting in a reduced clearance with the control rod to perform a dashpot action when the rods are dropped into the guide thimbles upon a reactor trip. The transition zone is conical in shape so that there are no rapid changes in diameter in the tube.

Flow holes are provided just above the transition of the two diameters to permit the entrance of cooling water during normal operation, and to accommodate the outflow of water from the dashpot during reactor trip.

The dashpot is closed at the bottom by means of a welded plug which has a bayonet extension which in turn is fastened to the bottom nozzle during fuel assembly fabrication.

c) Control Rod Drive Mechanism

The control rod drive mechanisms are used for withdrawal and insertion of the rod cluster control assemblies into the reactor core and to provide sufficient holding power for stationary support.

Fast total insertion (reactor trip) is obtained by simply removing the electrical power allowing the RCC assemblies to fall by gravity.

The complete drive mechanism, shown in Figure 3-44, consists of the internal (latch) assembly, the pressure vessel, the operating coil stack, the drive shaft assembly, and the position indicator coil stack.

Each assembly is an independent unit which can be dismantled or assembled separately.

Each drive is threaded to an adaptor on top of the reactor pressure vessel and is connected to the control rod (directly below) by means of a grooved drive shaft. The upper section of the drive shaft is suspended from the working components of the drive mechanism. The drive shaft and control rod remain connected during reactor operation, including tripping of the rods.

Main coolant fills the pressure containing parts of the drive mechanism. All working components and the shaft are immersed in the main coolant.

Three magnetic coils, which form a removable electrical unit and surround the rod drive pressure housing induce magnetic flux through the housing wall to operate the working components. They move two sets of latches which lift or lower the grooved drive shaft.

The three magnets are turned on and off in a fixed sequence by switches which are operated by a rotating cam shaft. One rotation of the cam shaft moves the control rod one step length.

The sequencing of the magnets produces step motion over the 143 inches of normal control rod travel.

The mechanism develops a lifting force of approximately 900 lbs. The total load on the mechanism is approximately 450 lbs. Therefore, extra lift capacity is available for overcoming mechanical friction between the moving and the stationary parts of the mechanism. Gravity provides the drive force for rod insertion and the weight of the whole rod assembly is available to overcome any resistance.

The mechanisms are designed to operate in water at 650°F and 2485 psig. The temperature at the mechanism head adaptor will be much less than 650°F because it is located in a region where there is limited flow of water from the reactor core, while the pressure is the same as in the reactor pressure vessel.

A multi-conductor cable connects the mechanism operating coils to the 125 volt d-c power supply. The power supply includes the necessary switchgear to provide power to each coil in the proper sequence.

1. Latch Assembly

The latch assembly contains the working components which withdraw and insert the drive shaft and attached control rod. It is located within the pressure housing and consists of the pole pieces for three electromagnets. They actuate two sets of latches which engage the grooved section of the drive shaft.

The upper set of latches move up or down to raise or lower the drive rod one step length. The lower set of latches have a 1/32 inch axial movement to shift the weight of the control rod from the upper to the lower latches.

2. Pressure Vessel

The pressure vessel consists of the pressure housing and rod travel housing. The pressure housing is the lower portion of the vessel and contains the latch assembly. The rod travel housing is the upper portion of the vessel. It provides space for the drive shaft during its upward movement as the control rod is withdrawn from the core.

3. Operating Coil Stack

The operating coil stack is an independent unit which is installed on the drive mechanism by sliding it over the outside of the pressure housing. It rests on a pressure housing flange without any mechanical attachment and can be removed and installed while the reactor is pressurized.

The operator coils are made of round copper wire which is insulated with a double layer of filament type glass yarn.

The operating temperature of the coils is approximately 400°F as determined by resistance measurement. Forced air cooling along the outside of the coil stack maintains the coil temperature at an acceptable value.

4. Drive Shaft Assembly

The main function of the drive shaft is to connect the RCC assembly to the mechanism latches. Grooves for engagement and lifting by the latches are located throughout the 143 in. of control rod travel. The grooves are spaced to coincide with the mechanism step length and have 45° angle sides.

The drive shaft is attached to the control rod by the coupling. The coupling has two flexible arms which engage the grooves in the spider assembly.

A small diameter disconnect rod runs down the inside of the drive shaft. It utilizes a locking button at its lower end to lock the coupling and control rod. At its upper end, there is a disconnect assembly for remote disconnection of the drive shaft assembly from the control rod.

During plant operation, the drive shaft assembly remains connected to the RCC assembly at all times. It can be attached to or removed from the RCC assembly when the reactor vessel head is removed.

5. Position Indicator Coil Stack

The position indicator coil stack slides over the rod travel housing section of the pressure vessel. It detects drive rod position by means of cylindrically wound differential transformer which span the normal length of the rod travel.

6. Drive Mechanism Materials

All parts exposed to reactor coolant, such as the pressure vessel, latch assembly and drive rod, are made of metals which resist the corrosive action of the water.

Three types of metals are used exclusively: stainless steels, Inconel X, and cobalt based alloys. Wherever magnetic flux is carried by parts exposed to the main coolant, stainless steel is used. Cobalt based alloys are used for the pins and latch tips. Inconel X is used for the springs of both latch assemblies and 304 stainless steel is used for all pressure containment. Hard chrome plating provides wear surfaces on the sliding parts and prevents galling between mating parts (such as threads) during assembly.

Outside of the pressure vessel, where the metals are exposed only to the reactor plant container environment and cannot contaminate the main coolant, carbon and stainless steels are used. Carbon steel, because of its high permeability, is used for flux return paths around the operating coils. It is zinc-plated 0.001 inch thick to prevent corrosion.

7. Principles of Operation

The drive mechanisms shown schematically in Figure 3-45 withdraw and insert their respective control rods as electrical pulses are received by the operator coils.

On and OFF sequence, repeated by cam operated switches in the power supply, causes either withdrawal or insertion of the control rod. Position of the control rod is indicated by the differential transformer action of the position indicator coil stack surrounding the rod travel housing. The differential transformer output changes as the top of the ferromagnetic drive shaft assembly moves up the rod travel housing.

Generally, during plant operation, the drive mechanisms hold the control rods withdrawn from the core in a static position, and only one coil, either the stationary or movable gripper coil, is energized on each mechanism.

Control Rod Withdrawal:

The control rod is withdrawn by repeating the following sequence:

- (1) Movable Gripper Coil - ON
- (2) Stationary Gripper Coil - OFF
- (3) Lift Coil - ON

The gap between the lift armature and the lift magnet pole closes and the drive rod raises one step length.

- (4) Stationary Gripper Coil - ON

The stationary gripper armature raises and closes the gap below the stationary gripper magnet pole. The three links, pinned to the stationary gripper armature, swing the stationary gripper latches into a drive shaft groove. The latches contact the shaft and lift it 1/32 inch. The load is so transferred from the movable to the stationary gripper latches. (5)

- (5) Movable Gripper Coil - OFF

The movable gripper armature separates from the lift armature under the force of a spring and gravity. Three links, pinned to the movable gripper armature, swing the three movable gripper latches out of the groove.

- (6) Lift Coil - OFF

The gap between the lift armature and the lift magnet pole opens. The movable gripper latches drop to a position adjacent to the next groove.

- (7) Movable Gripper Coil - ON

The movable gripper armature raises and swings the movable gripper latches into the drive shaft groove.

- (8) Stationary Gripper Coil - OFF

Gravity causes the stationary gripper latches and armature to move downward until the load of the drive shaft is transferred to the movable gripper latches. Simultaneously, the stationary gripper latches swing out of the shaft groove.

Control Rod Insertion:

The sequence for control rod insertion is similar to that for control rod withdrawal:

(1) Stationary Gripper Coil - ON

(2) Movable Gripper Coil - OFF

(3) Lift Coil - ON

The movable gripper latches are raised to a position adjacent to a shaft groove.

(4) Movable Gripper Coil - ON

The movable gripper armature raises and swings the movable gripper latches into a groove.

(5) Stationary Gripper Coil - OFF

The stationary gripper armature moves downward and swings the stationary gripper latches out of the groove.

(6) Lift Coil - OFF

Gravity separates the lift armature from the lift magnet pole and the control rod drops down one step.

The sequences described above are termed as one step or one cycle and the control rod thus moves one step for each cycle.

Control Rod Tripping:

If power to the movable gripper coil is cut off, as for tripping, the combined weight of the drive shaft and the rod cluster control assembly is sufficient to move the latches out of the shaft groove. The control rod falls by gravity into the core. The tripping occurs as the magnetic field, holding the movable gripper armature against the lift magnet, collapses and the movable gripper armature is forced down by the weight acting upon the latches.

d) Prototype Testing

To prove the mechanical adequacy of the fuel assembly and RCC assembly, functional test programs were conducted on full scale San Onofre mock-up versions of the fuel assembly and control rods.⁽²⁾

1. Reactor Evaluation Channel (REC) Tests

The prototype assemblies were tested under simulated reactor operating conditions (1900 psig, 575°F, 14 fps flow velocity) in the Westinghouse Reactor Evaluation Channel (REC).

The components were subjected to a total environmental exposure of 4132 hours during which the rod cluster control assembly experienced a total travel of 38,927 lineal feet. The travel was made up of 27,217 ft of normal driven travel and 11,710 ft of reactor trip travel, resulting from 1461 trips, which is equivalent to over two plant service lifetimes.

The fuel assembly remained in excellent mechanical condition. No measurable signs of wear on the fuel tubes or control rod guide tubes were found.

The control rod was also found to be in excellent condition, having maximum wear measured on absorber cladding of approximately 0.001 in.

2. Loading and Handling Tests

Tests simulating the loading of the prototype fuel assembly into a core location were also successfully conducted to determine that the proper provisions had been made for guidance of the fuel assembly during refueling operation.

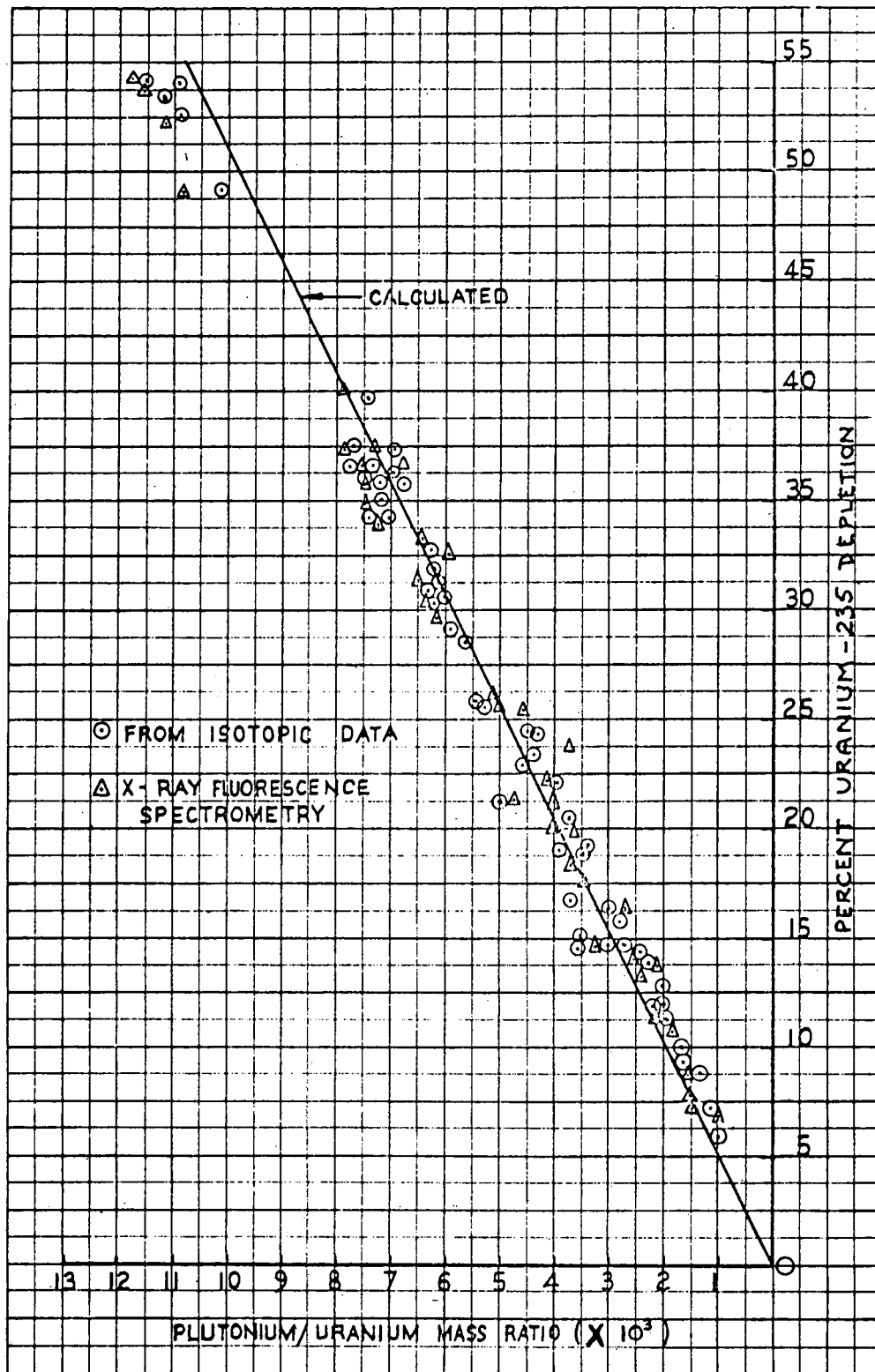
3. Axial and Lateral Bending Tests

In addition, axial and lateral bending tests were performed in order to simulate mechanical loading of the assembly during refueling operation.

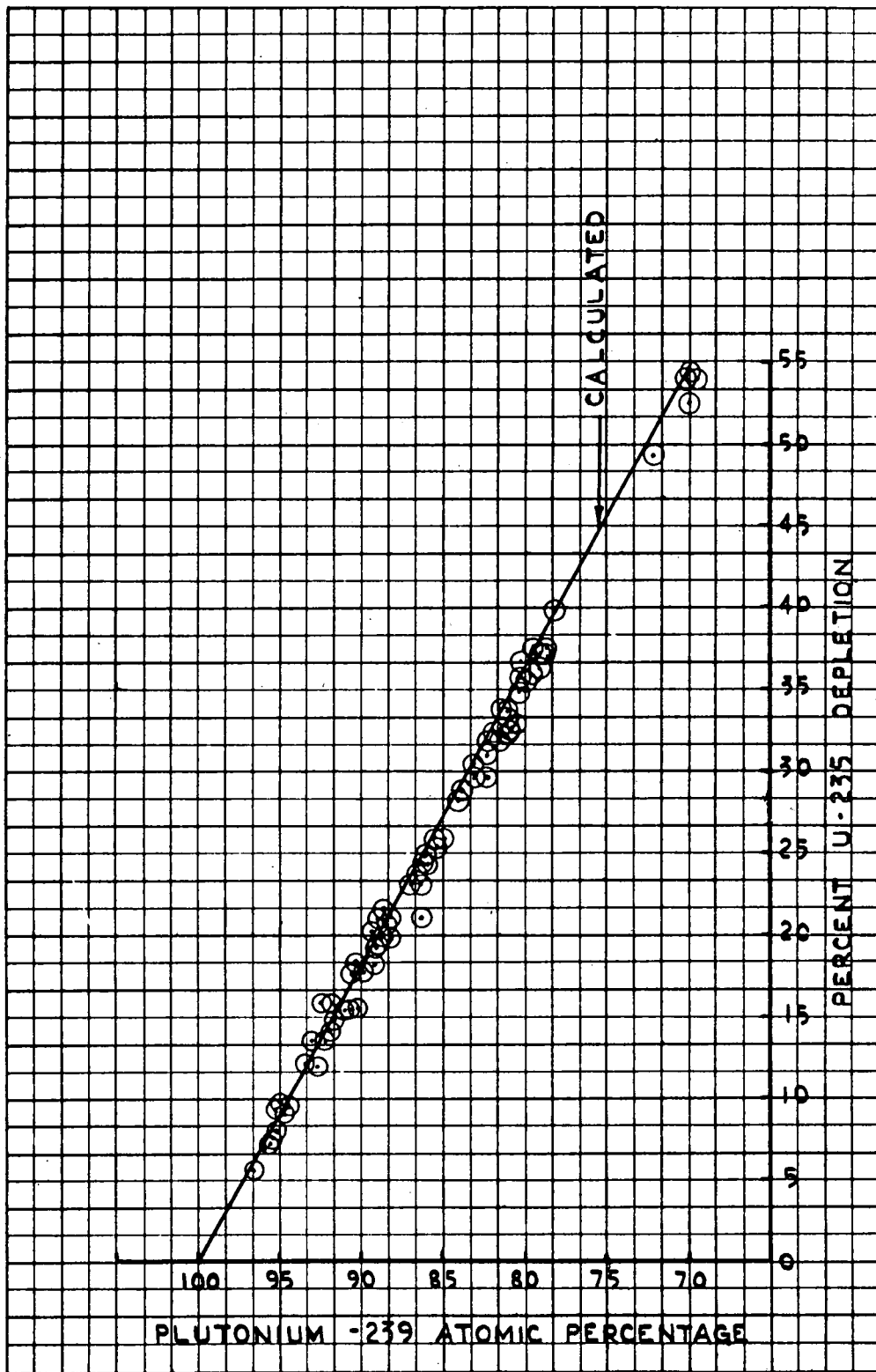
Although the maximum column load expected to be experienced in service is approximately 1000 lb. the fuel assembly was successfully loaded to 2200 lb. axially with no damage resulting. This information was also used in the design of fuel handling equipment to establish the limits for inadvertent axial loads during refueling.

REFERENCES, Section 3.2.3

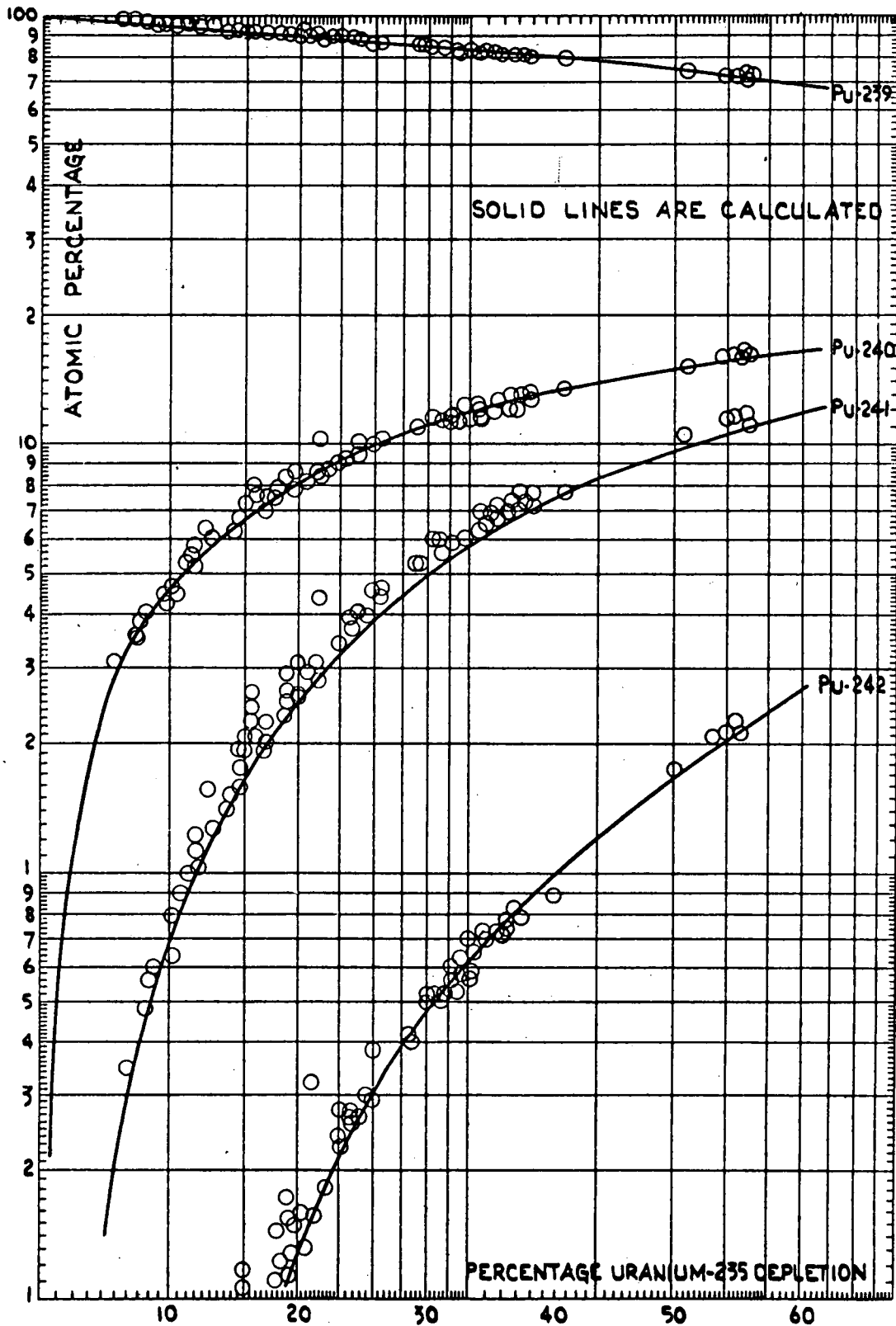
1. Daniel, R. C., et al, "Effects of High Burnup on Zircaloy-Clad Bulk UO_2 , Plate Fuel Element Samples," WAPD-263, (September, 1962).
2. Large Closed Cycle Water Reactor Research and Development Program Quarterly Progress Reports for the period January 1963 through June 1965 (WCAP-3738, 3739, 3743, 3750, 3269-2, 3269-3, 3269-5, 3269-6, 3269-12 and 3269-13).



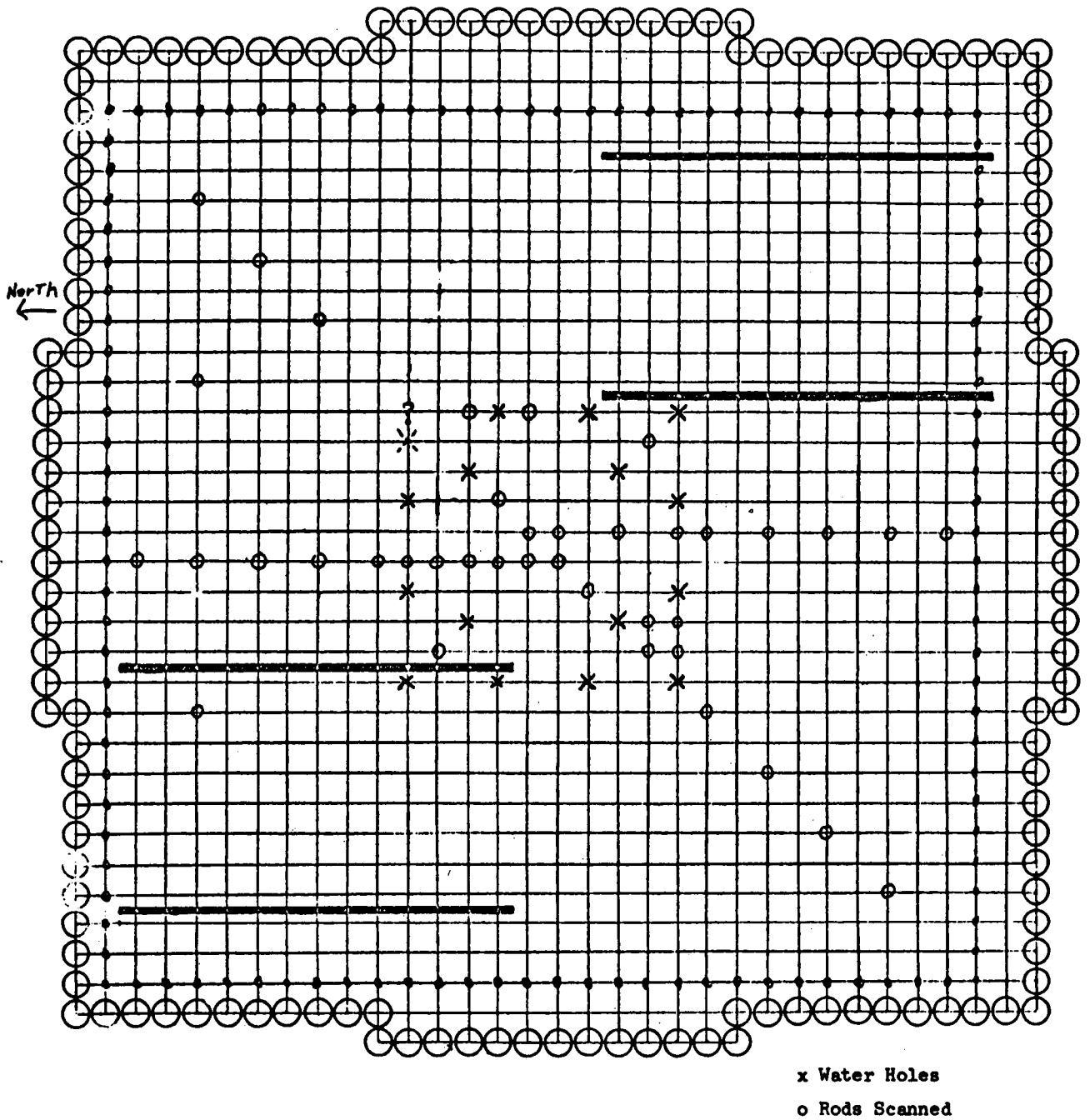
PLUTONIUM / URANIUM MASS RATIO AS A FUNCTION OF URANIUM - 235 DEPLETION



FRACTION OF PLUTONIUM - 239 IN PLUTONIUM
AS A FUNCTION OF URANIUM-235 DEPLETION.

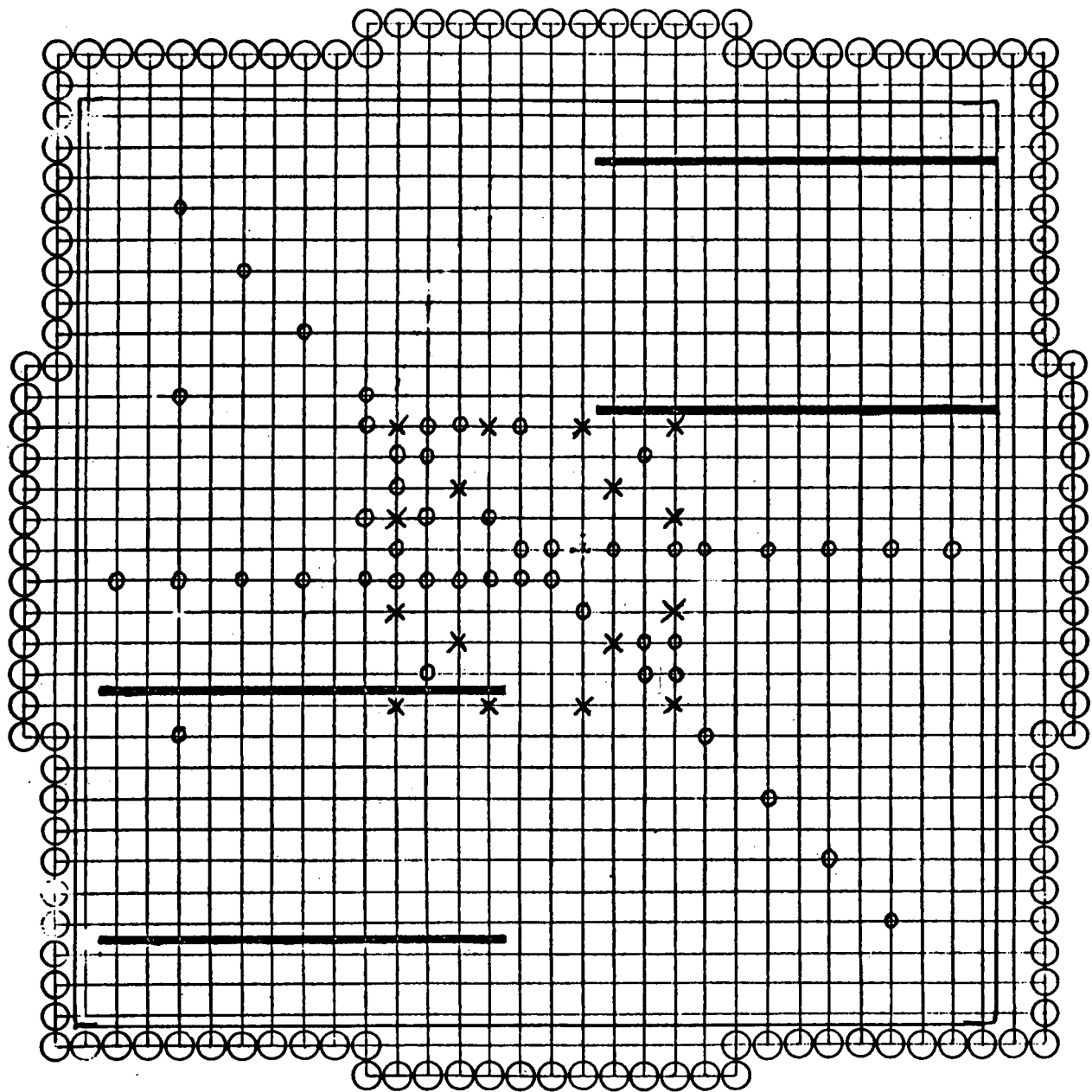


COMPOSITION OF PLUTONIUM AS A FUNCTION OF URANIUM - 235 DEPLETION



0.484 " Diameter , 0.6 " Pitch

PLAN OF CRITICAL EXPERIMENT (UNBORATED CASE)
FIG. 3-4



X - Water Hole
 O - Rod Scanned
 Core: 30 x 30

0.484 " Diameter , 0.6 " Pitch

PLAN OF CRITICAL EXPERIMENT (BORATED CASE)
 FIG. 3-5

(1.525) 1.5056 1.549 1.528 1.521	(1.548) 1.542	(1.586) 1.610 1.574	(1.651) 1.657	(1.717) 1.703 1.669 1.673	(1.515) 1.488 1.472	(1.336)	(1.230) 1.233 1.228	(1.145)	(1.062) 1.0625 1.055	(.984)	(.897) .911 .902	(.833)	(.8460) .8675 .858	
	(1.637) 1.646 1.635		(1.829)	Water Hole	(1.601)									
		Water Hole	(1.842) 1.791	(1.722) 1.718 1.686										
			(1.704) 1.686 1.670 1.672	(1.689) 1.663										
				Water Hole	(1.494)									
					(1.330) 1.296						(.811) .803 .818			
						(1.119)								
							(.997) 1.017 .990							
								(.882)						
									(.766) .778 .774					
										(.653)				
											(.550) .559 .559			
												(.476)		
													(.480)	
														(.702)

Case (2) - Comparison of Experimental and Calculated
Power Distribution Using Two Mesh Spacings Per Fuel Rod
(1/8th Core Symmetry - One Block Represents One Fuel Rod)

(xxxx) PDQ Result
xxxx Experimental Value

(1.532) 1.513 1.556 1.532 1.528	(1.5585) 1.549	(1.607) 1.617 1.582	(1.7005) 1.665	(1.732) 1.711 1.677 1.681	(1.549) 1.495 1.478	(1.339)	(1.2265) 1.239 1.234	(1.1395)	(1.057) 1.067 1.060	(.974)	(.894) .915 .906	(.8345)	(.853) .871 .862	(1.1425)
	(1.6425) 1.642 1.653		(1.795)	Water Hole 1.693 1.726	(1.557)									
		Water Hole	(1.826) 1.799	(1.693) 1.693 1.726										
			(1.733) 1.693 1.677 1.680	(1.649) 1.670										
				Water Hole	(1.469)									
					(1.3375) 1.302						(.809) .807 .822			
						(1.115)								
							(.9925) 1.022 .995							
								(.877)						
									(.763) .781 .777					
										(.651)				
											(.551) .562 .562			
												(.480)		
													(.490)	
														(.710)

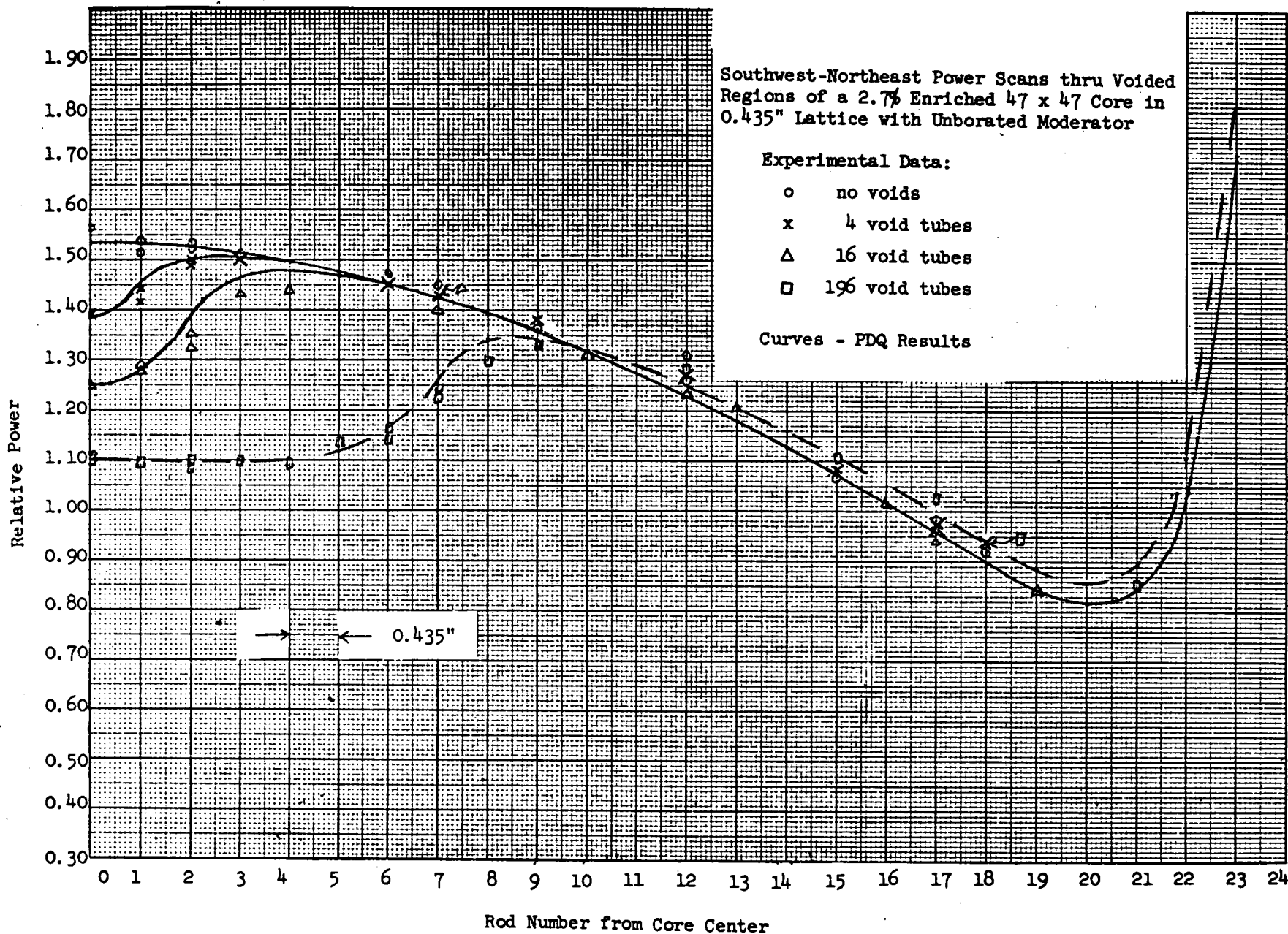
Case (1) - Comparison of Experimental and Calculated
Power Distribution Using One Mesh Spacings Per Fuel Rod

(1/8th Core Symmetry - One Block Represents One Fuel Rod)

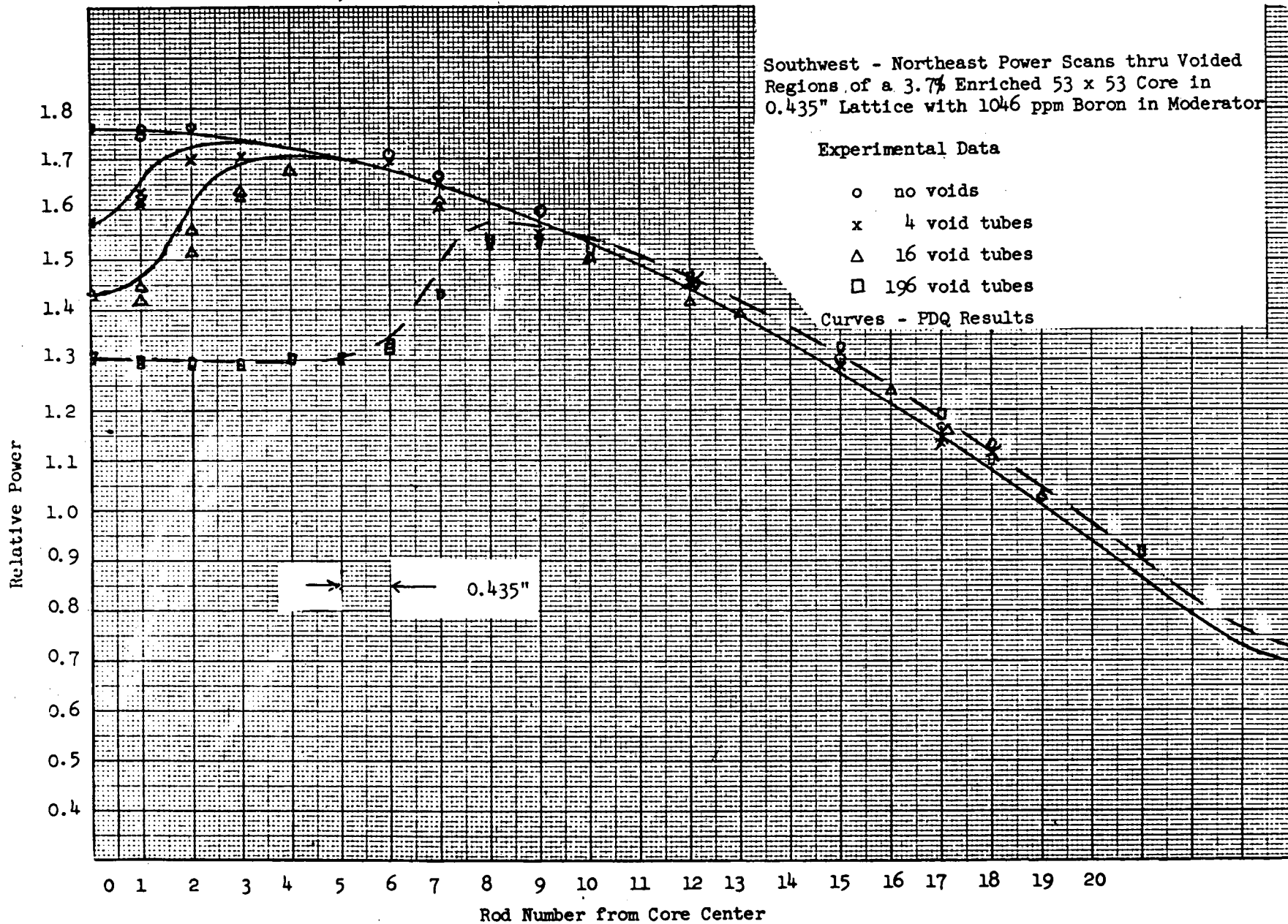
(xxxx) PDQ Result

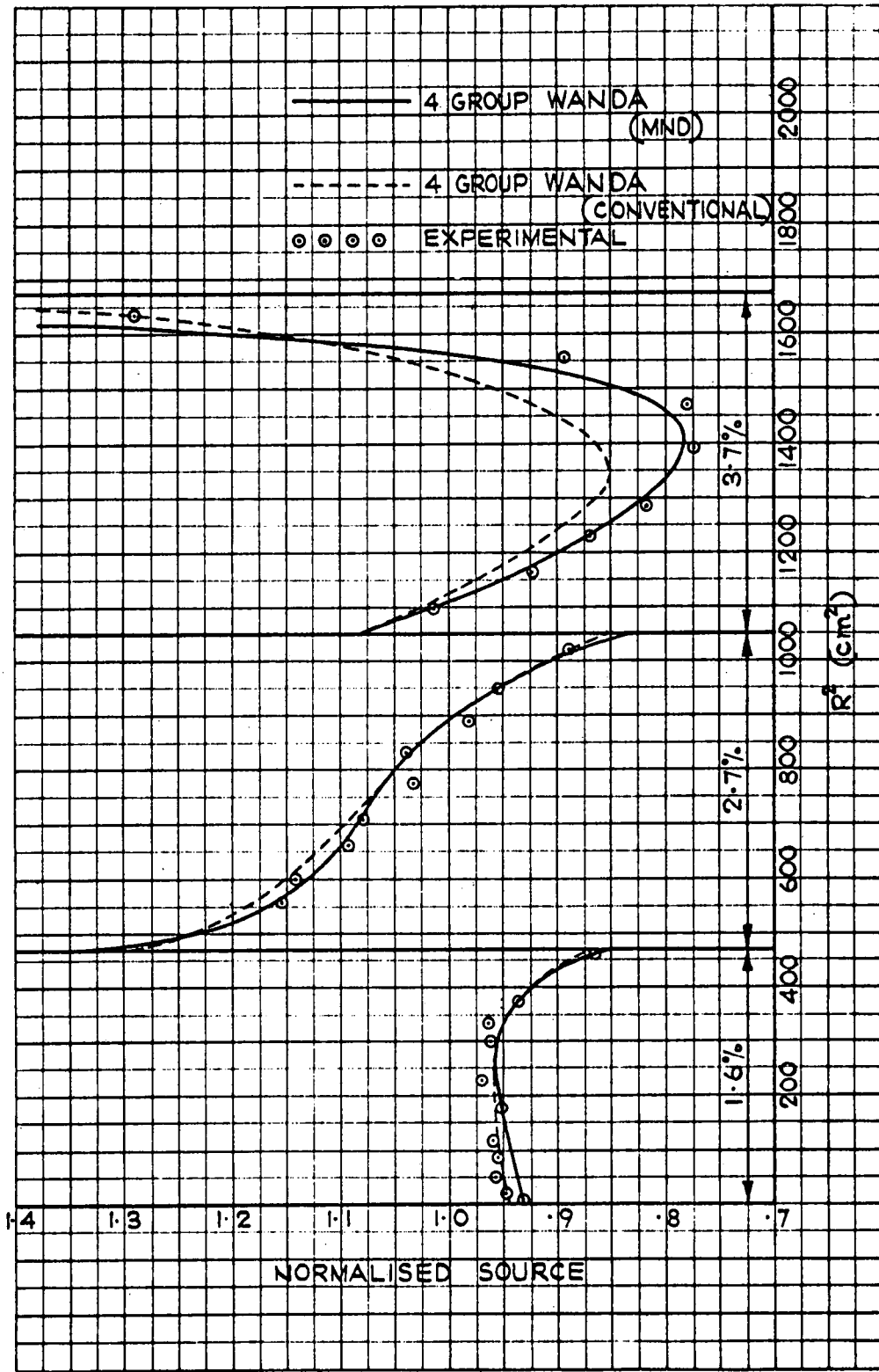
xxxx Experimental Value

POWER SCANS THROUGH VOIDED REGION IN AN UNBORATED CORE
 FIG. 3-9



POWER SCANS THROUGH VOIDED REGION IN A BORATED CORE
FIG. 3-10



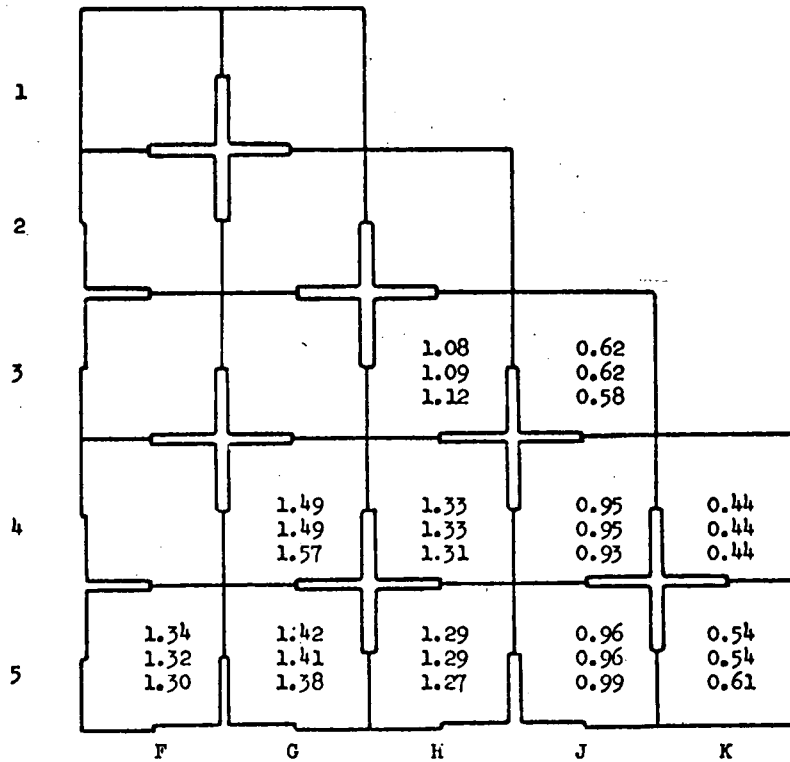


RADIAL FUEL ROD SCAN
 FIG. 3-11

1	0.60 0.59 0.56	0.44 0.43 0.40			
2	1.11 1.10 1.08	0.90 0.89 0.82	0.53 0.53 0.45		
3	1.38 1.38 1.45	1.19 1.18 1.22	0.91 0.91 1.06	0.52 0.52 0.48	
4	1.53 1.60 1.59	1.37 1.37 1.40	1.15 1.15 1.14	0.85 0.86 0.81	0.42 0.42 0.37
5	1.68 1.70 1.69	1.52 1.47 1.52	1.31 1.30 1.37	1.04 1.04 1.03	0.56 0.56 0.55
	F	G	H	J	K

Note: The top value in each assembly is found from the control rod interchange TURBO, the centre value is from the TURBO with no interchange, and the bottom value is experimentally determined.

Analytical and Experimental Power Distribution for YANKEE Core 1. TURBO Time Step 14, 7400 EFPH - $\frac{1}{4}$ core shown.



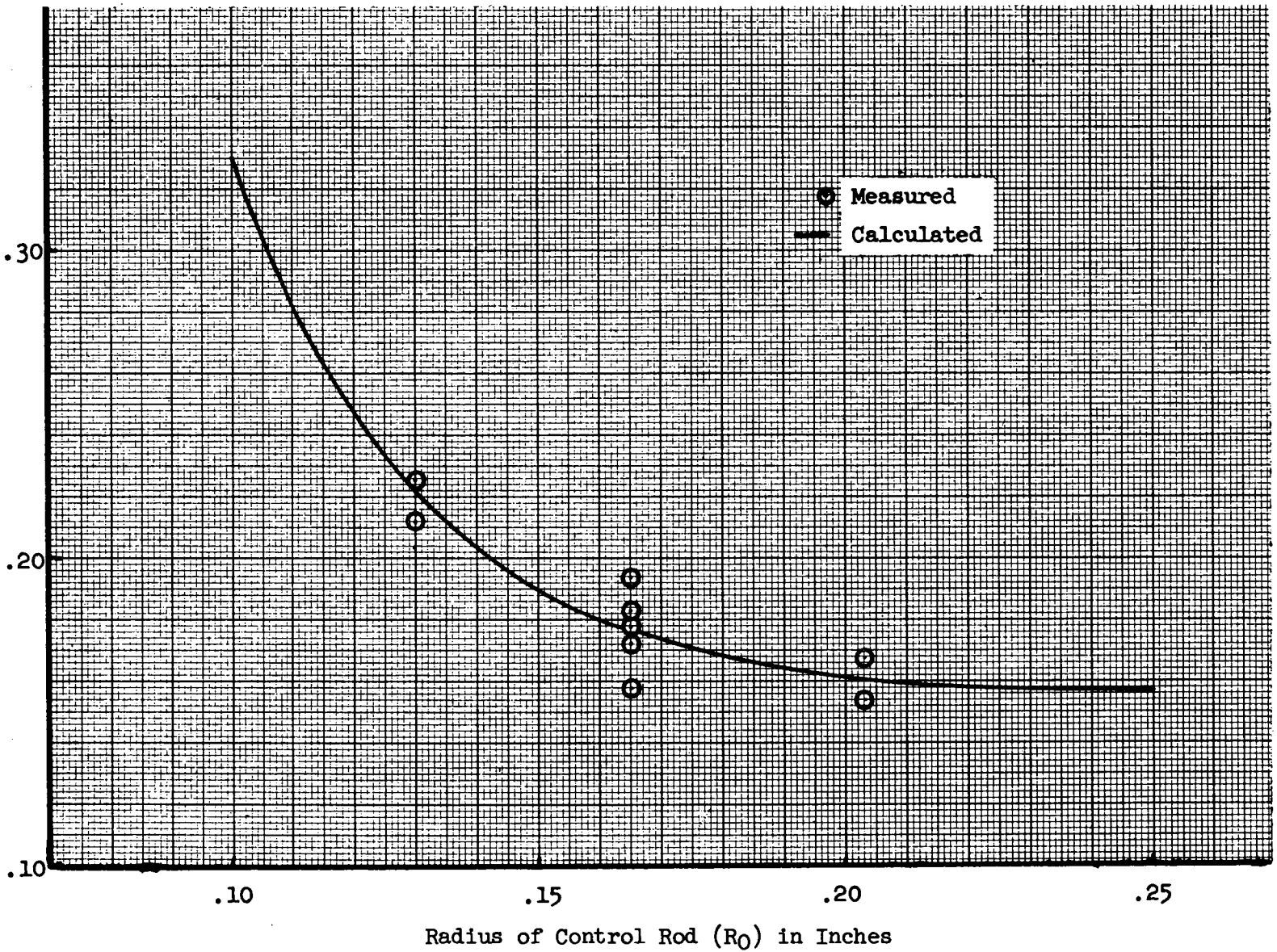
Notes:

1. The top value in each assembly is found from the control rod interchange TURBO, the centre value is from the TURBO with no interchange, and the bottom value is experimentally determined.
2. The burn-up distribution is defined by the ratio of the average burn-up in an assembly to the average in the quadrant. The numbers shown are the average of such values in symmetric assemblies.

Analytical and Experimental Burn-up Distributions for YANKEE Core 1. TURBO Time Step 14, 7400 EFPD - 1/4 core shown, Figures for 1/8 core.

Σ_a^f for Uniformly Distributed Ag-In-Cd Absorbers

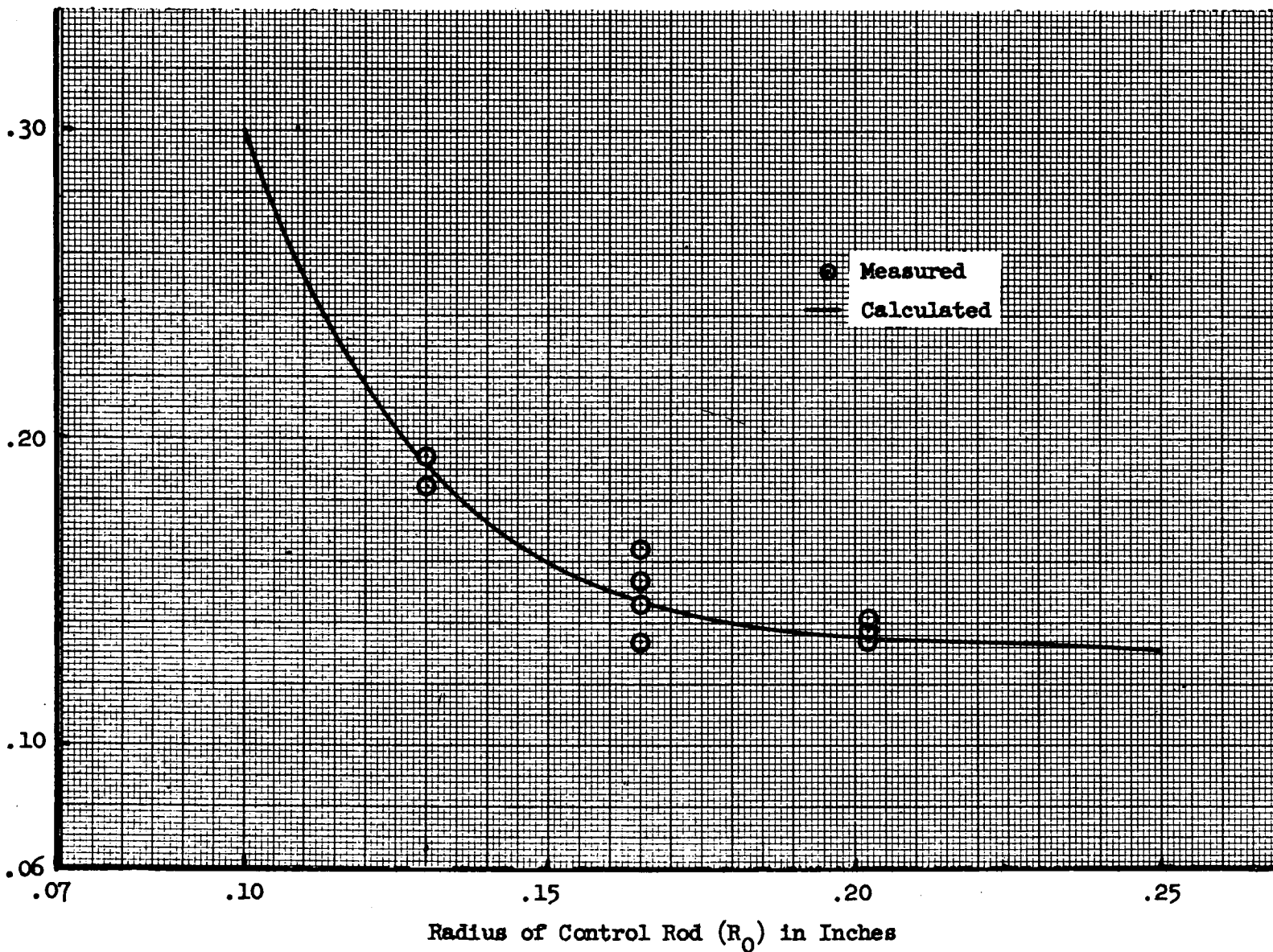
Σ_a^f (Equivalent One Fast Group Macroscopic Absorption)
Cross Section of the Control Rod Region



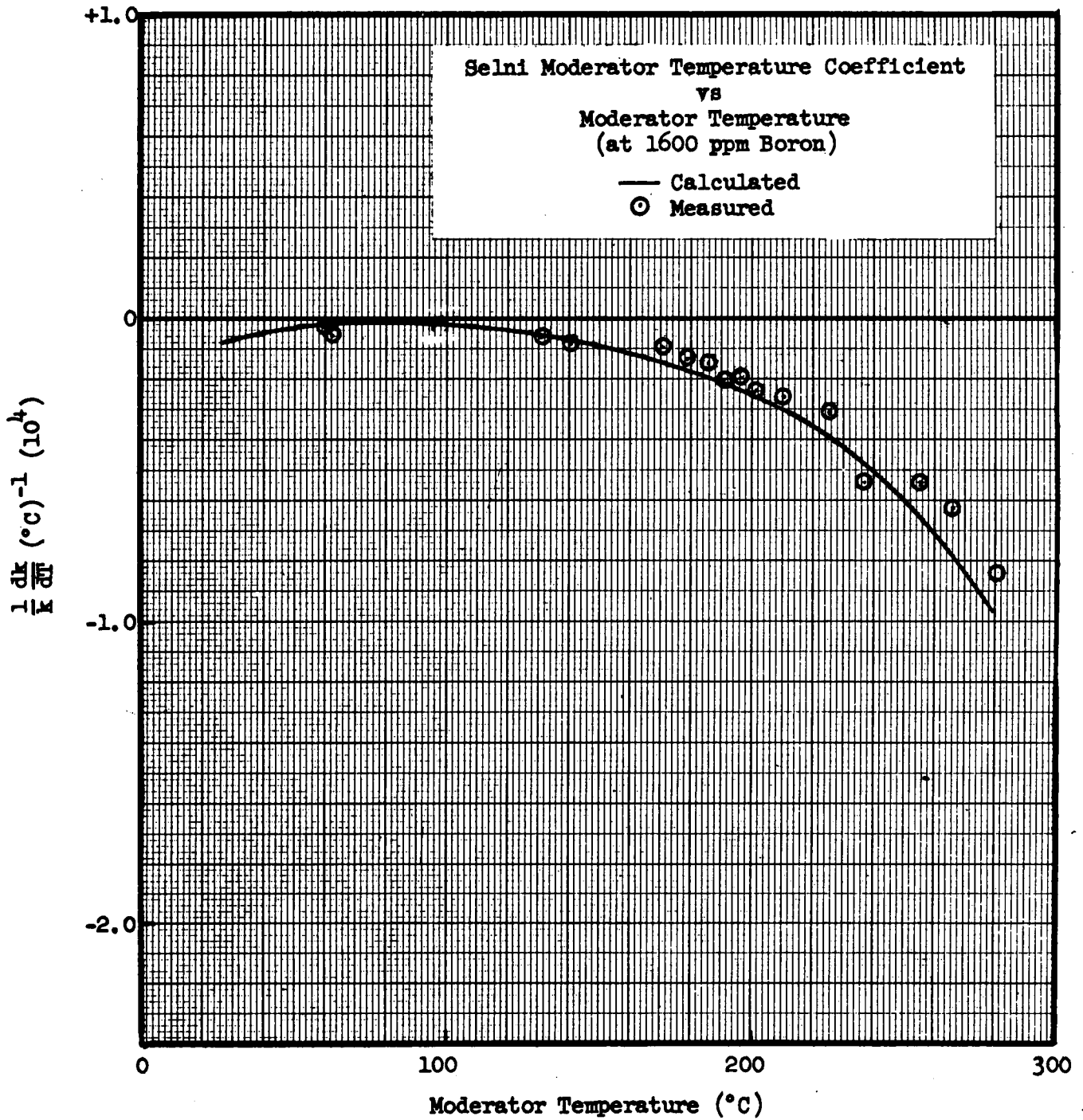
FAST ABSORPTION OF UNIFORMLY DISTRIBUTED ABSORBERS
FIG. 3-14

Σ_a^f for Clustered Ag-In-Cd Cylindrical Absorbers

Σ_a^f (Equivalent One Fast Group Macroscopic Absorption)
Cross Section of the Control Rod Region

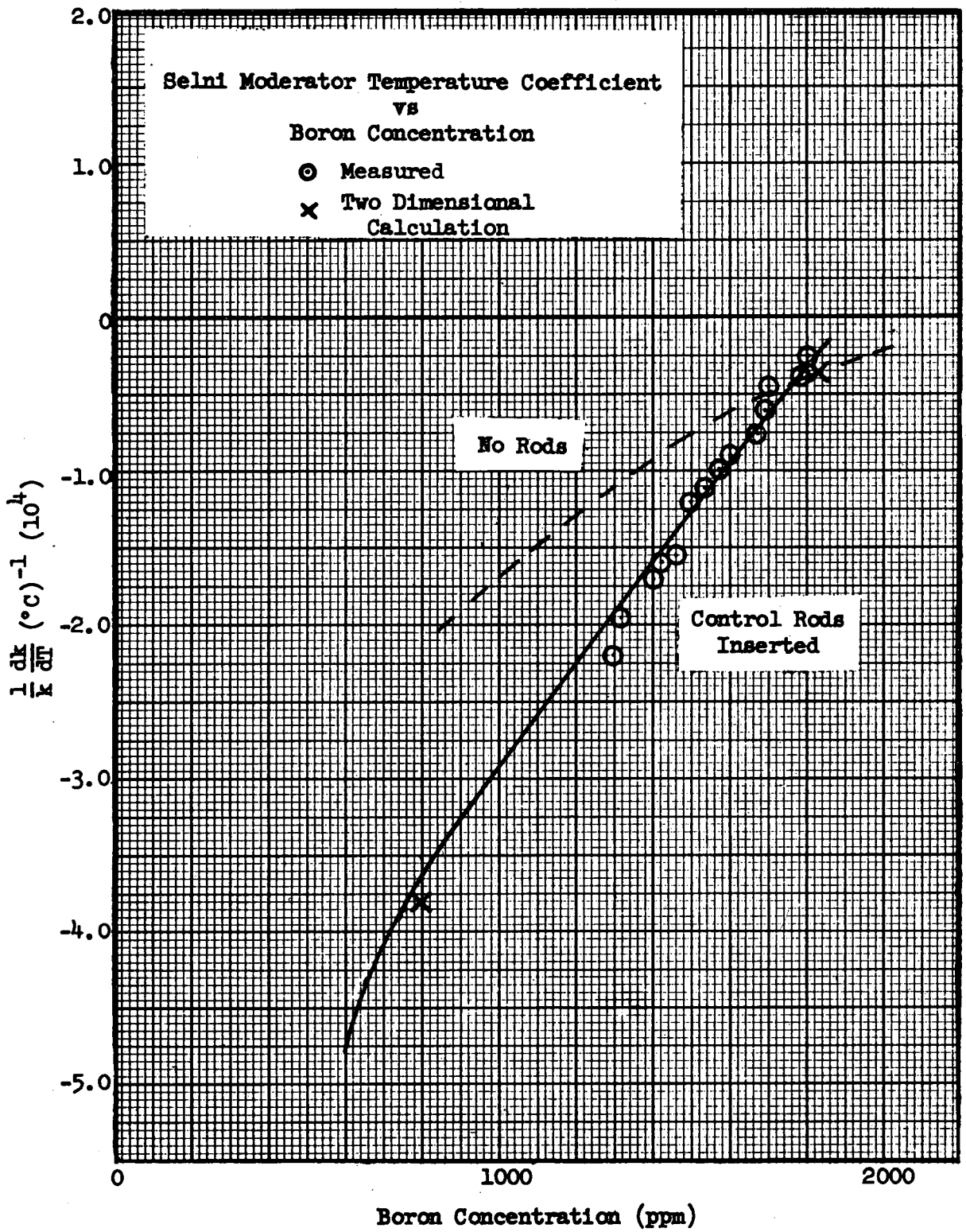


FAST ABSORPTION OF CLUSTERED ABSORBERS
FIG. 3-15

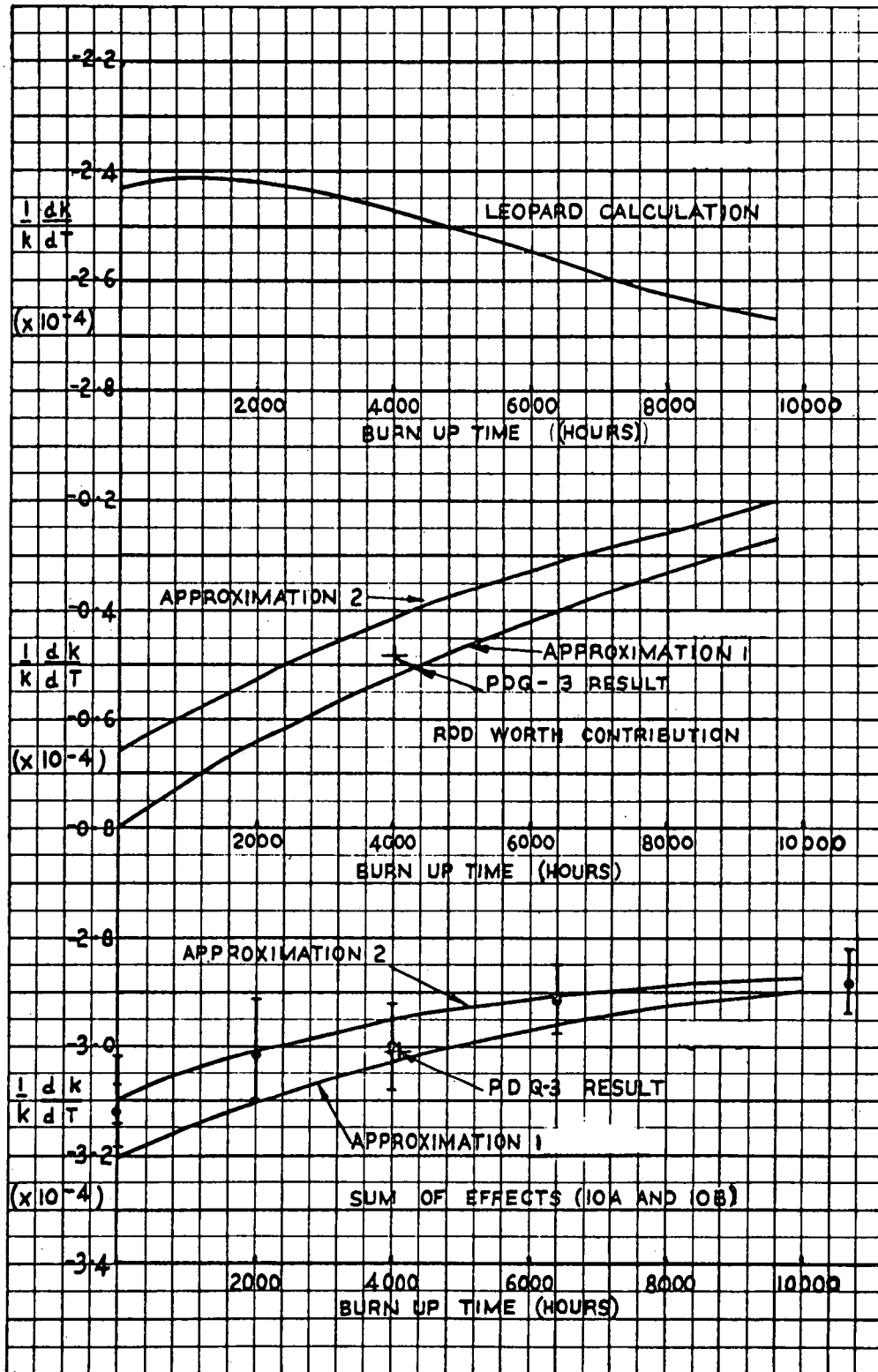


SELNI TEMPERATURE COEFFICIENTS VS MODERATOR TEMPERATURE

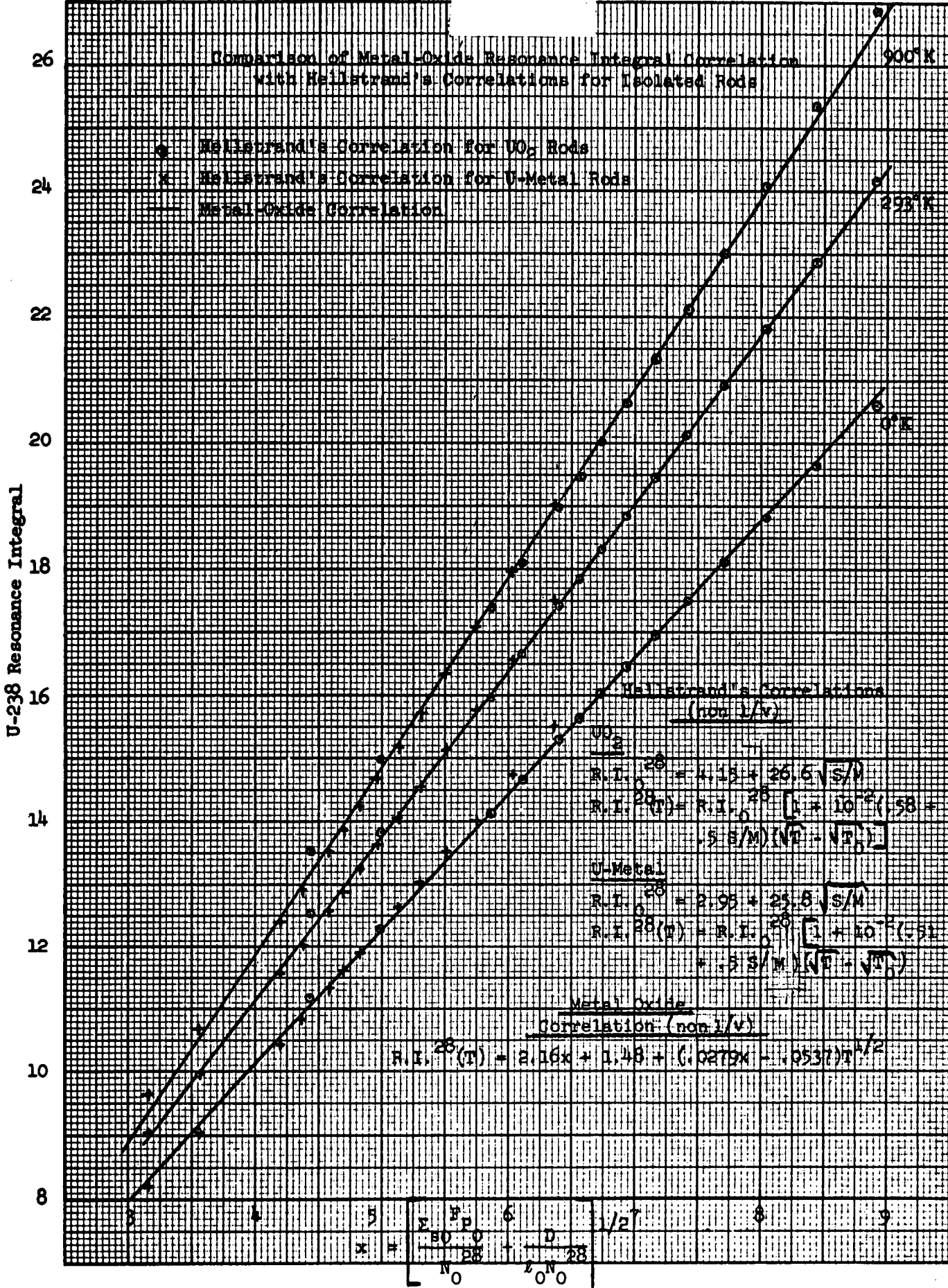
FIG. 3-16



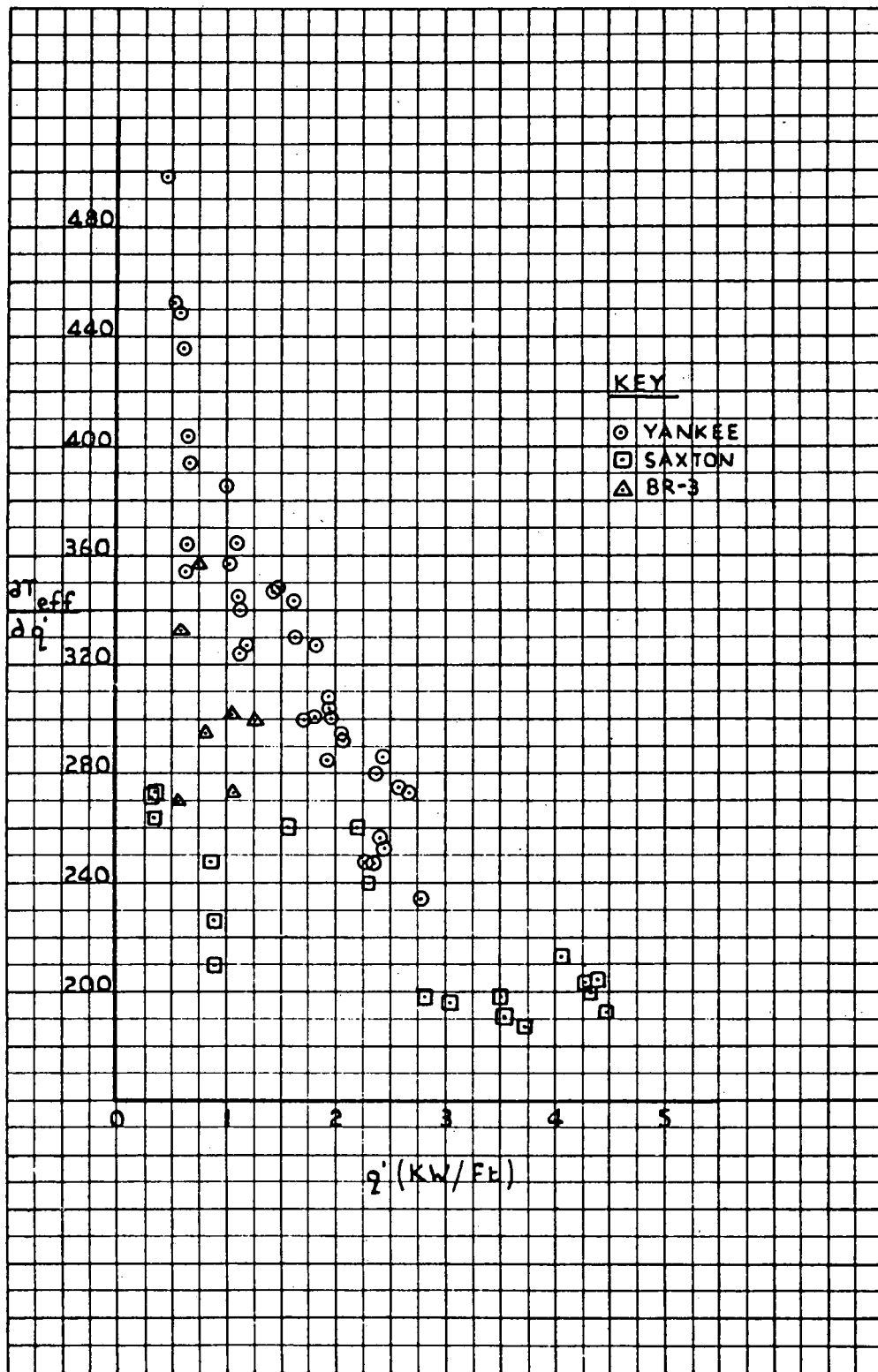
SELNI TEMPERATURE COEFFICIENTS VS BORON
CONCENTRATION



YANKEE TEMPERATURE COEFFICIENTS VS BURNUP
 FIG. 3-18



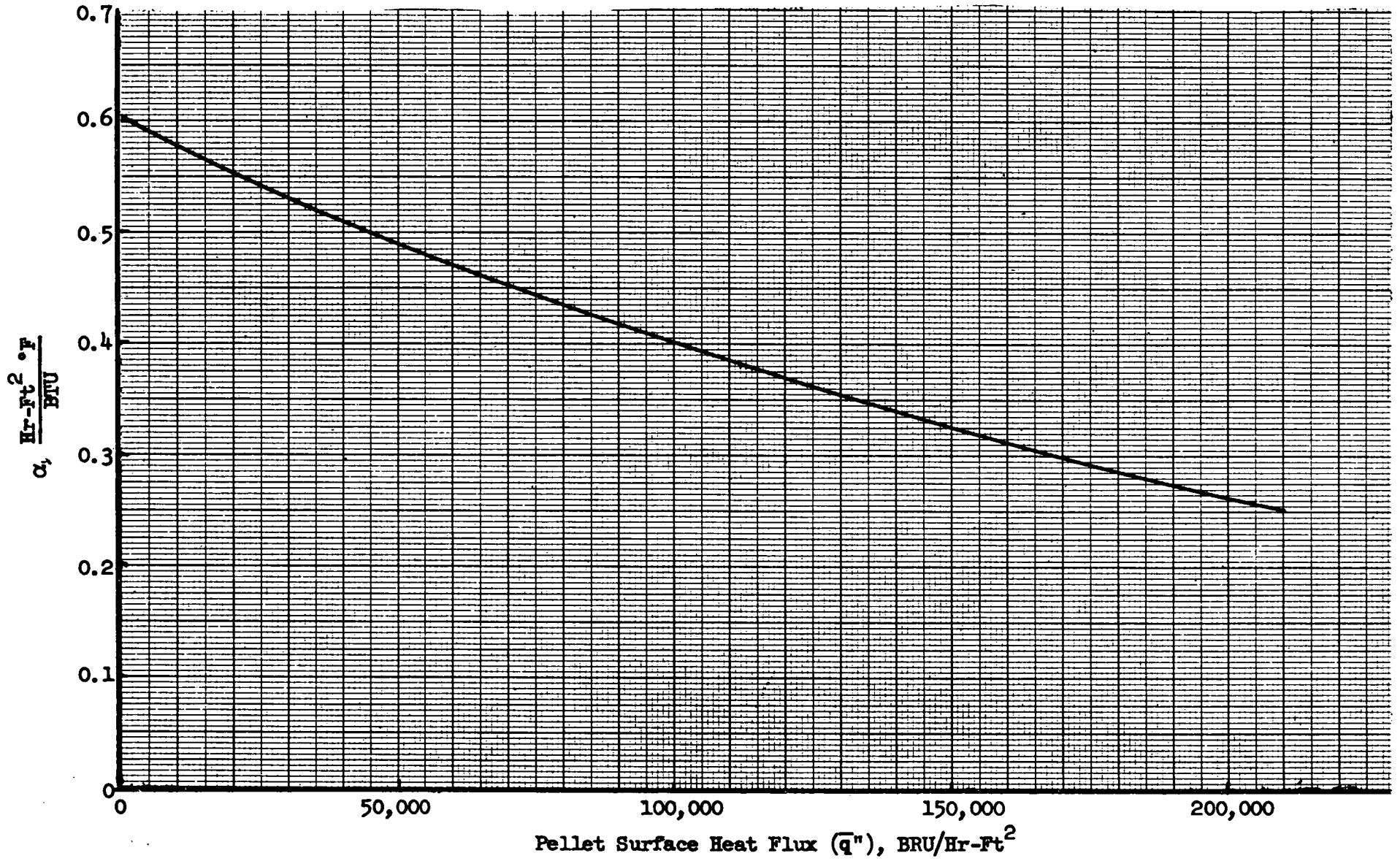
COMPARISON OF RESONANCE INTEGRAL CORRELATIONS
FIG. 3-19



EFFECTIVE FUEL TEMPERATURE CHANGE PER KW/FT vs.

CORE AVERAGE KW/FT

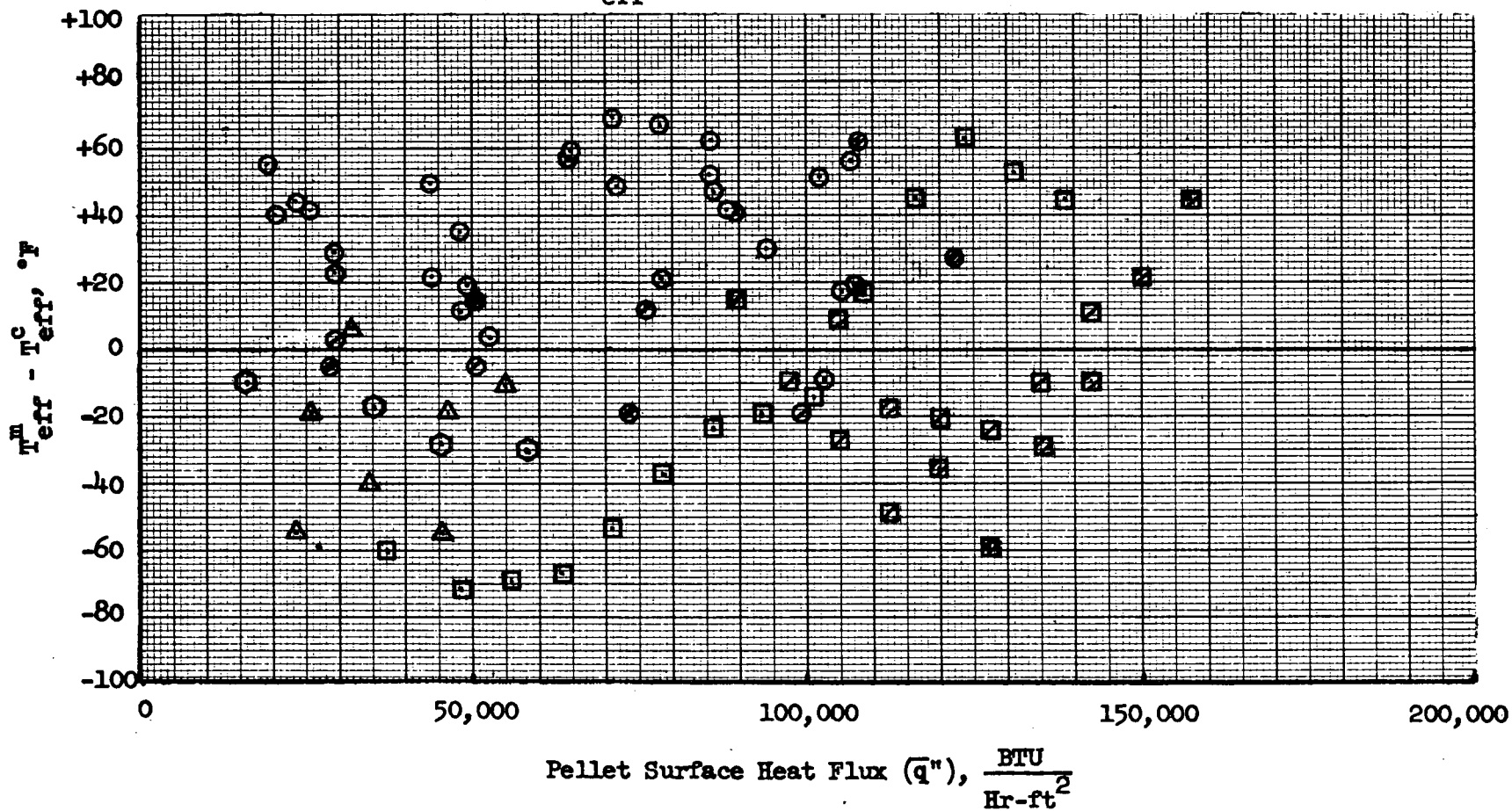
α Versus Pellet Surface Heat Flux



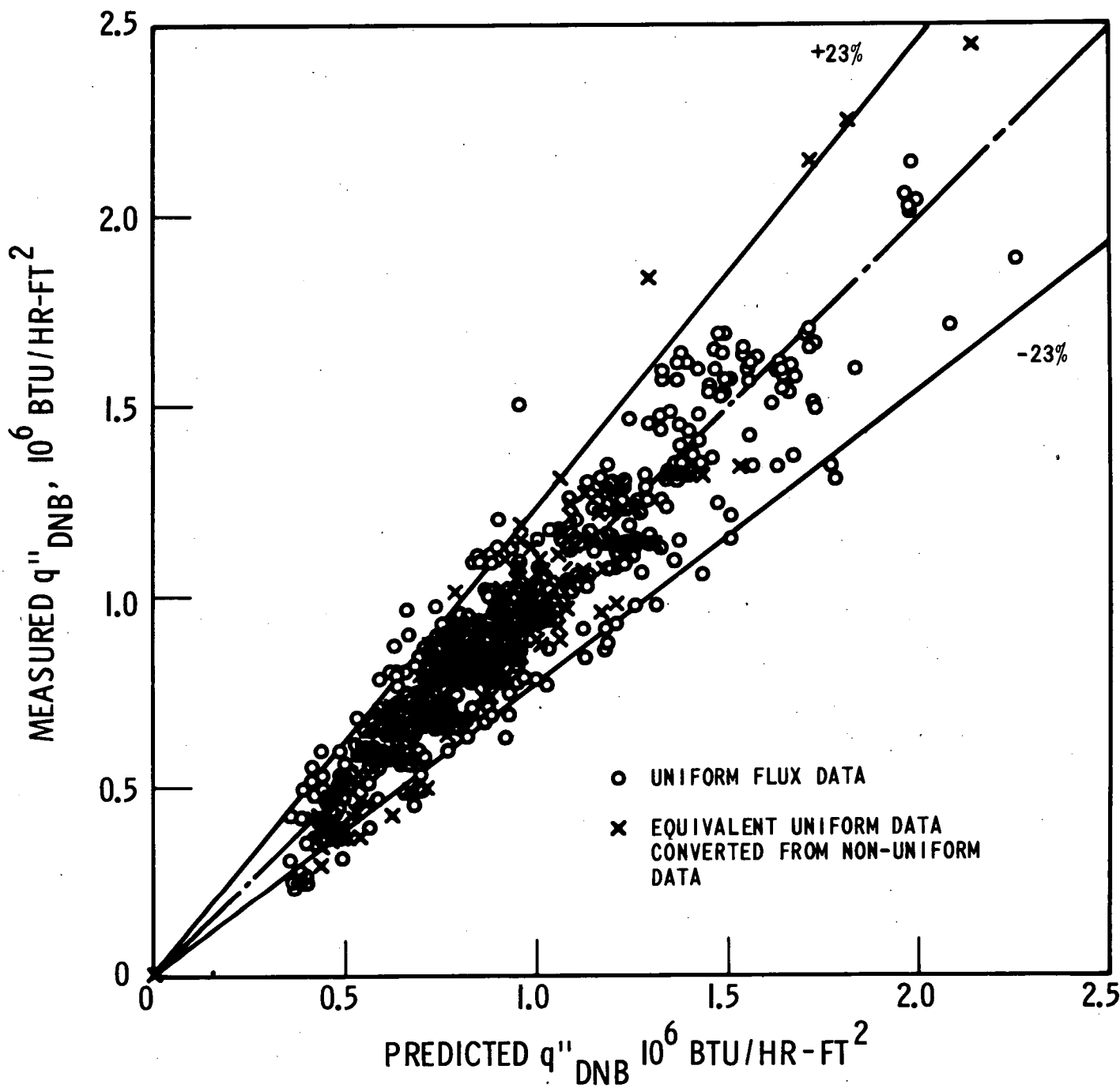
ALPHA VS HEAT FLUX
FIG. 3-21

- - Yankee Core No. 1
- ⊙ - Yankee Core No. 2
- - Yankee Core No. 3
- - Saxton with Crud, With Boron
- ⊠ - Saxton no crud, No Boron
- - Saxton no crud, With Boron
- △ BR-3
- ⊙ SELNI

Difference in T_{eff} Between Measured and Calculated Value

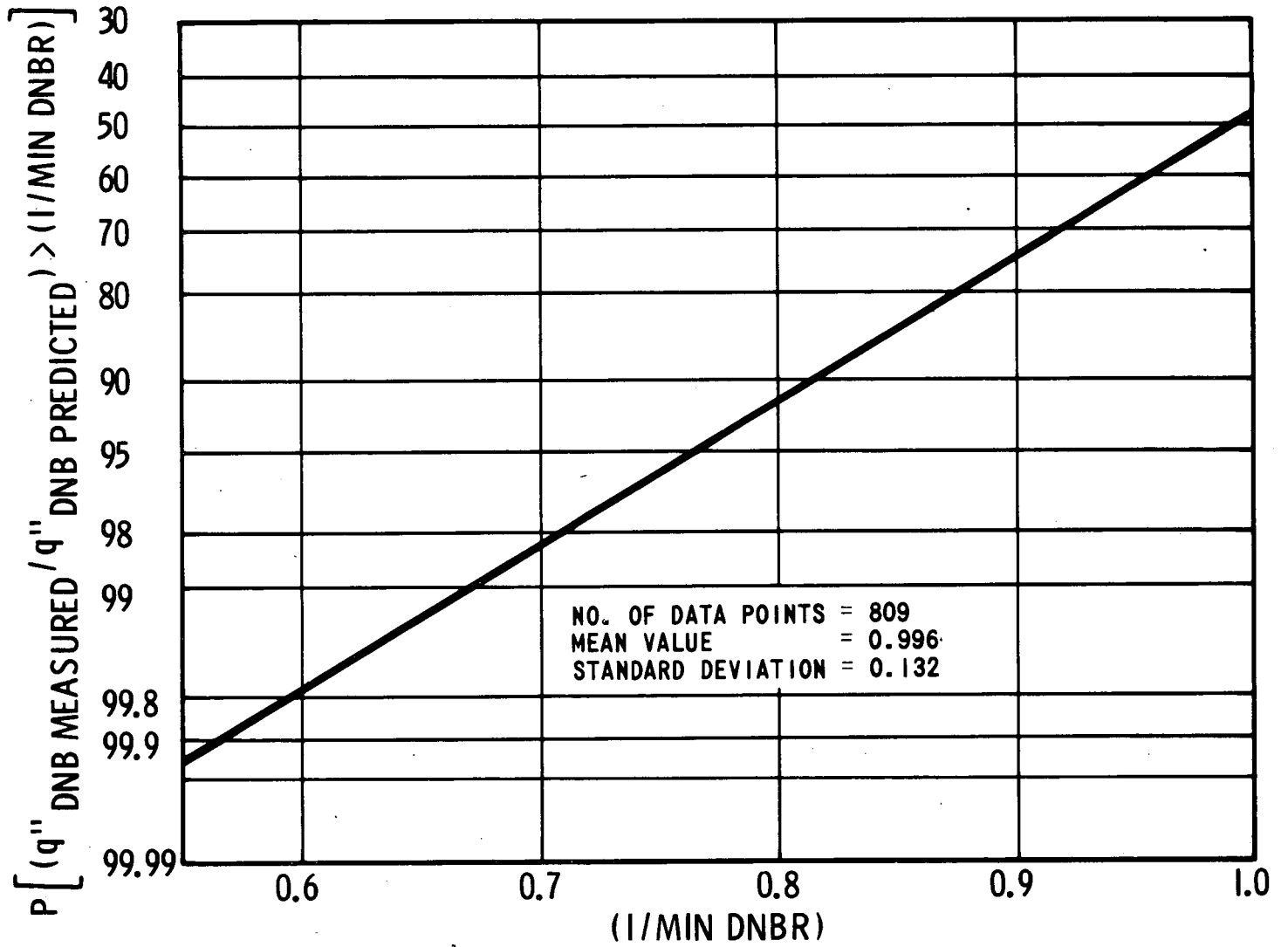


COMPARISON OF EFFECTIVE FUEL TEMPERATURE WITH CHANGING HEAT FLUX
FIG. 3-22



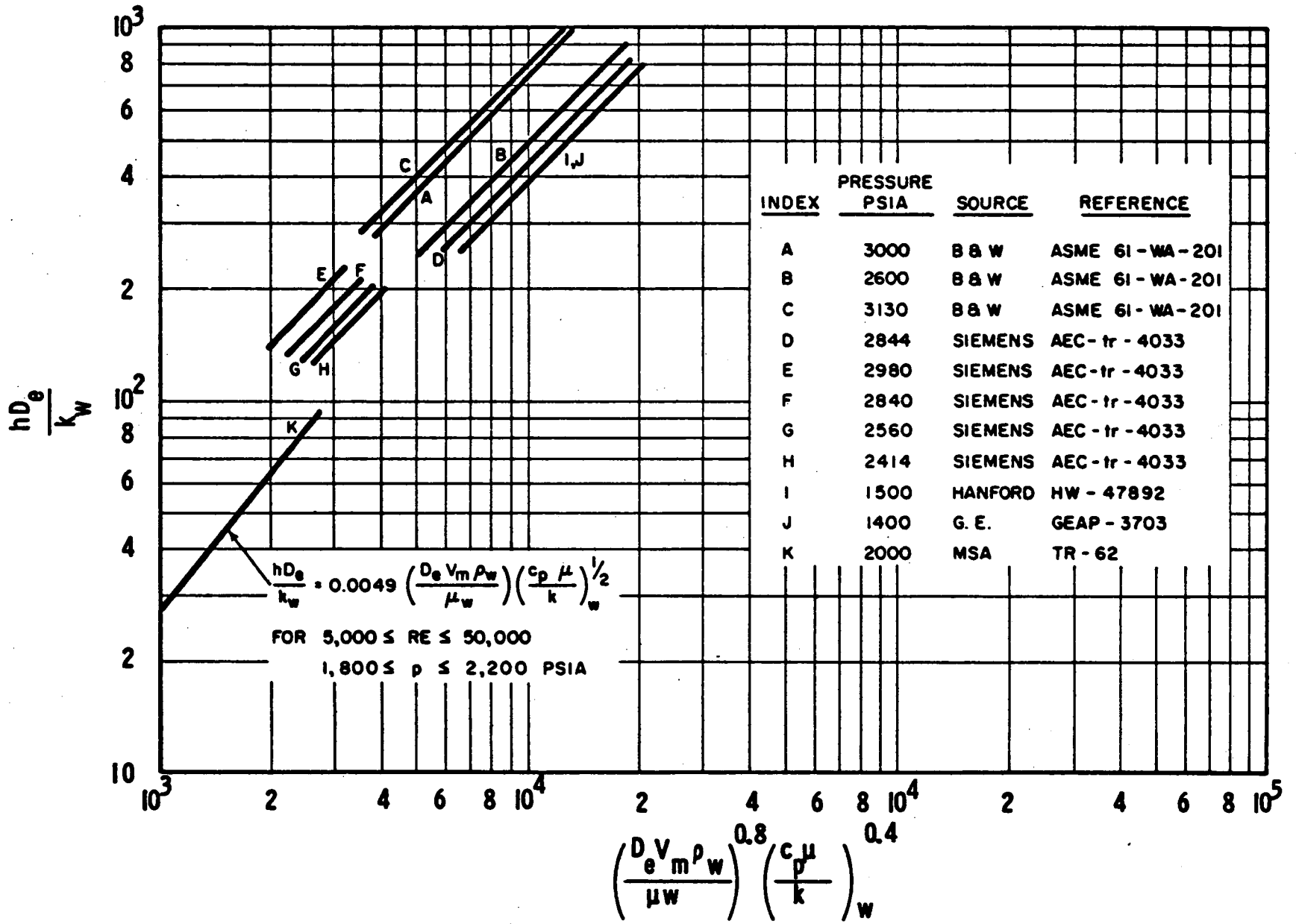
COMPARISON OF W-3 PREDICTION AND UNIFORM FLUX DATA
 ($-0.15 \leq x_{DNB} \leq +0.15$)

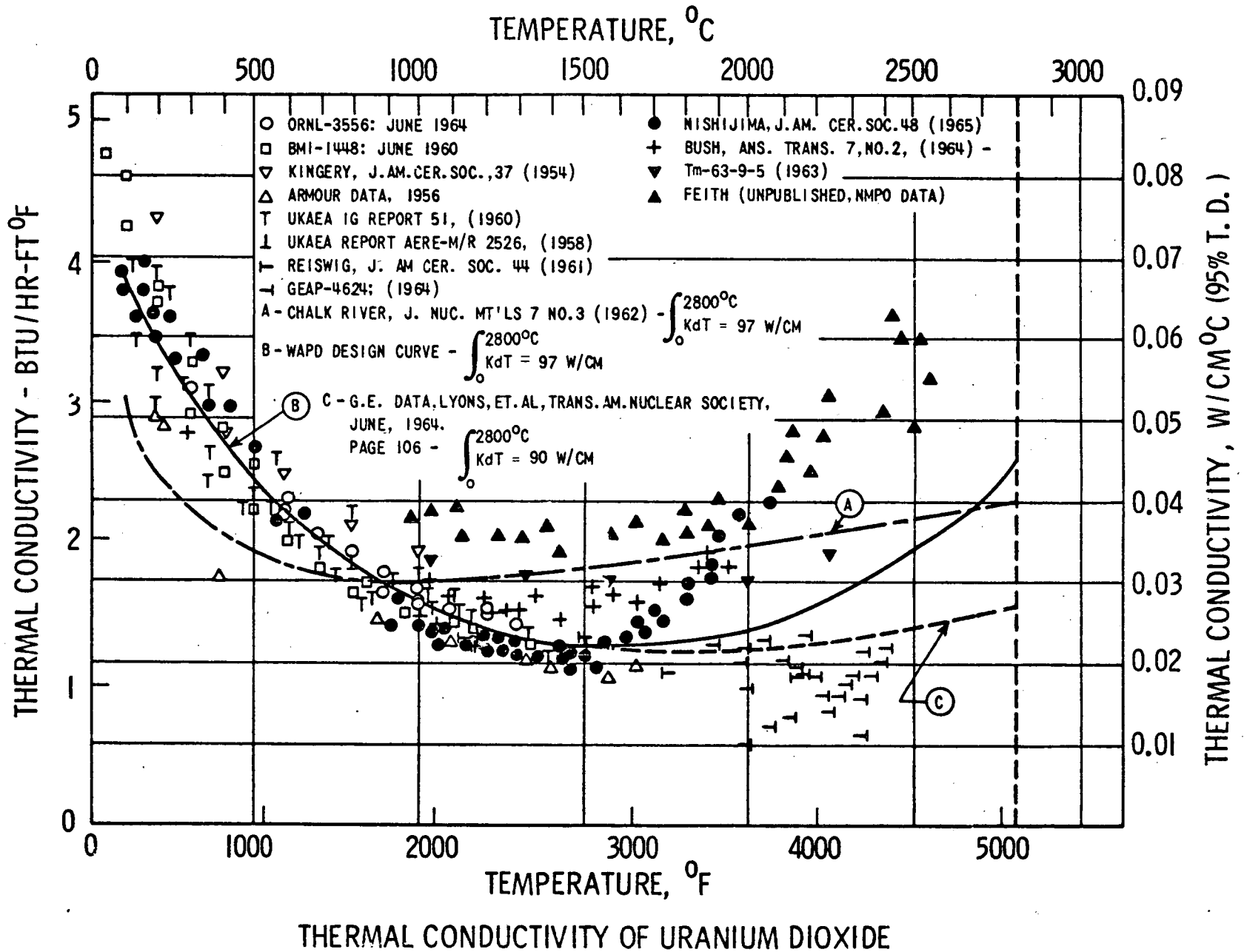
W-3 CORRELATION PROBABILITY DISTRIBUTION CURVE
FIG. 3-24



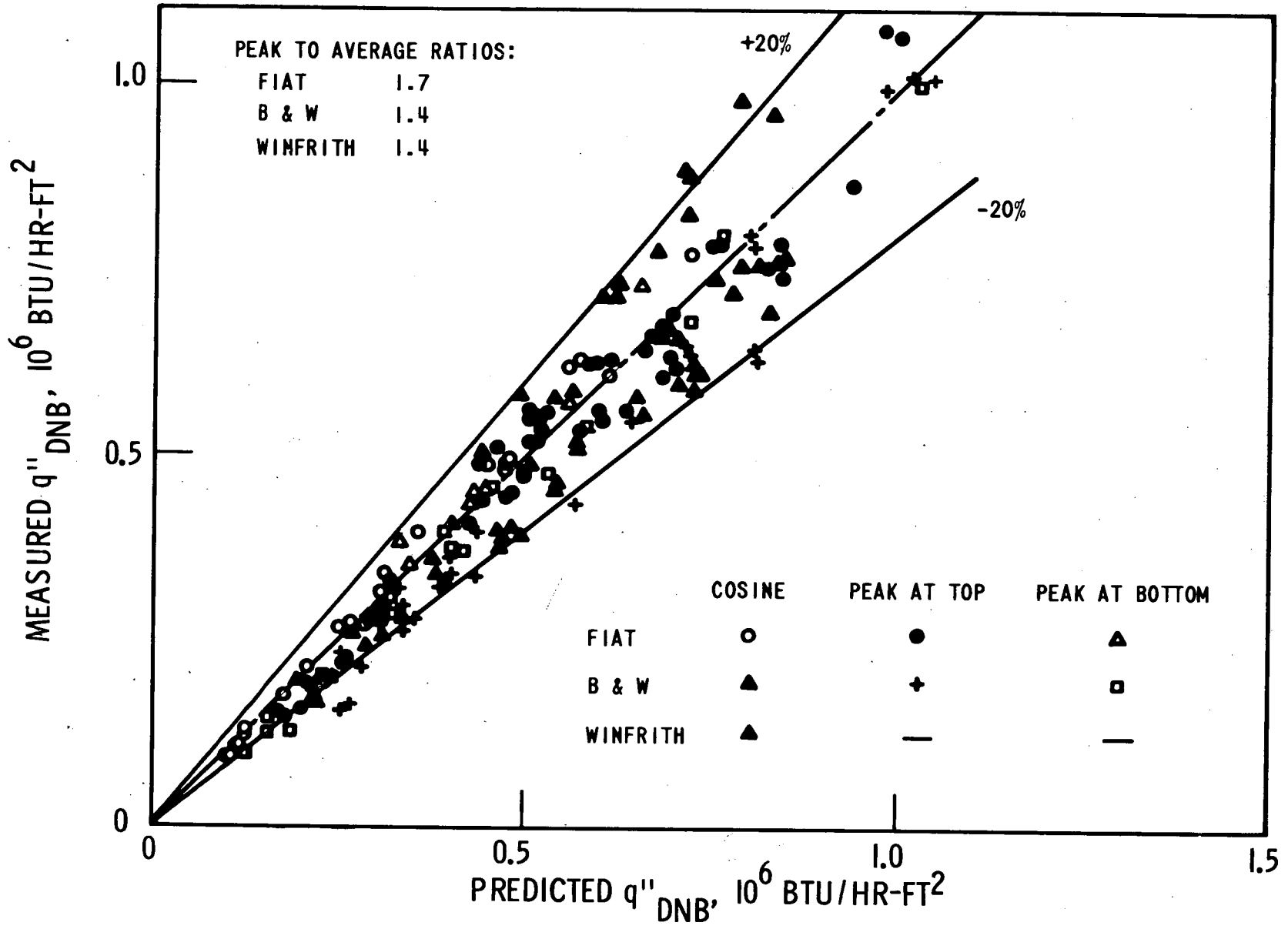
W-3 CORRELATION PROBABILITY DISTRIBUTION CURVE

STABLE FILM BOILING HEAT TRANSFER DATA AND CORRELATION
FIG. 3-25

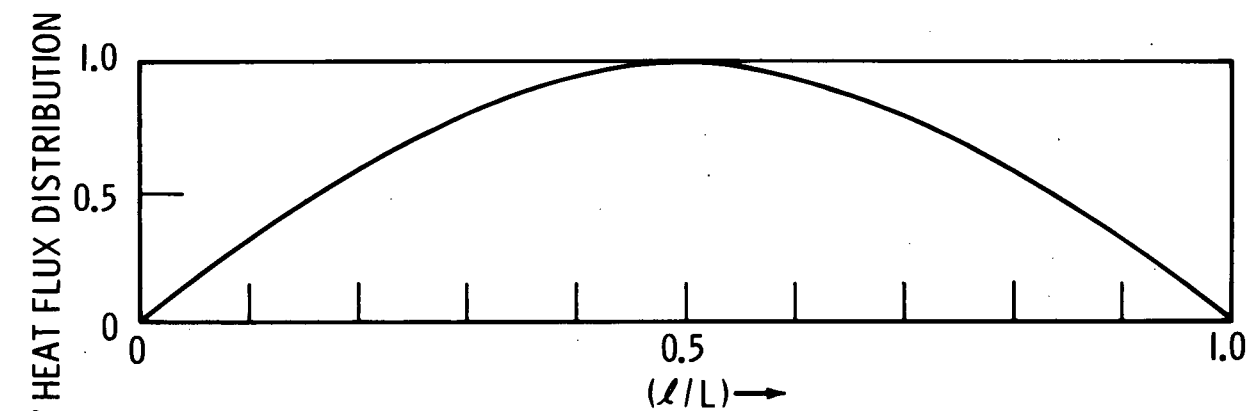
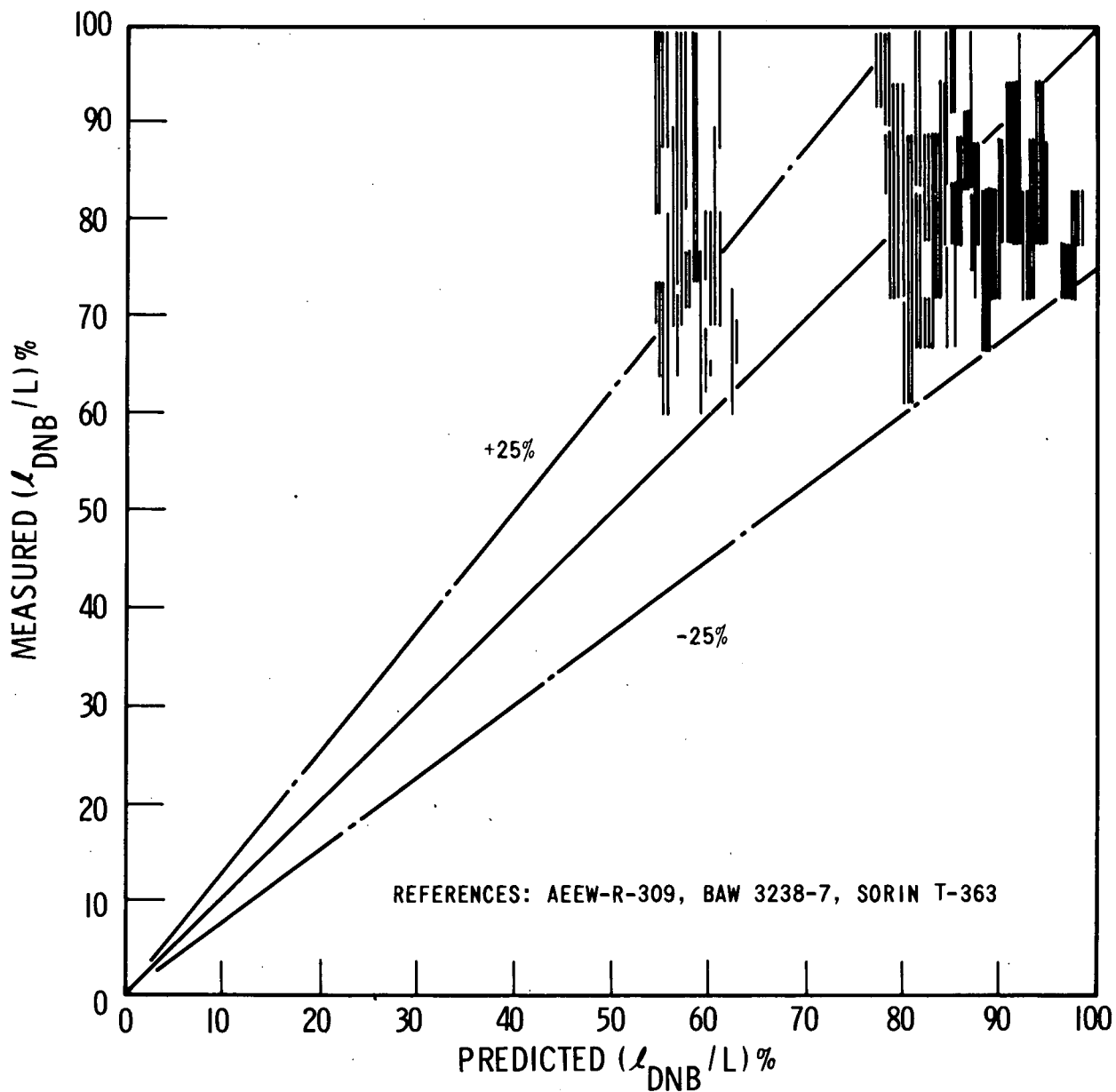




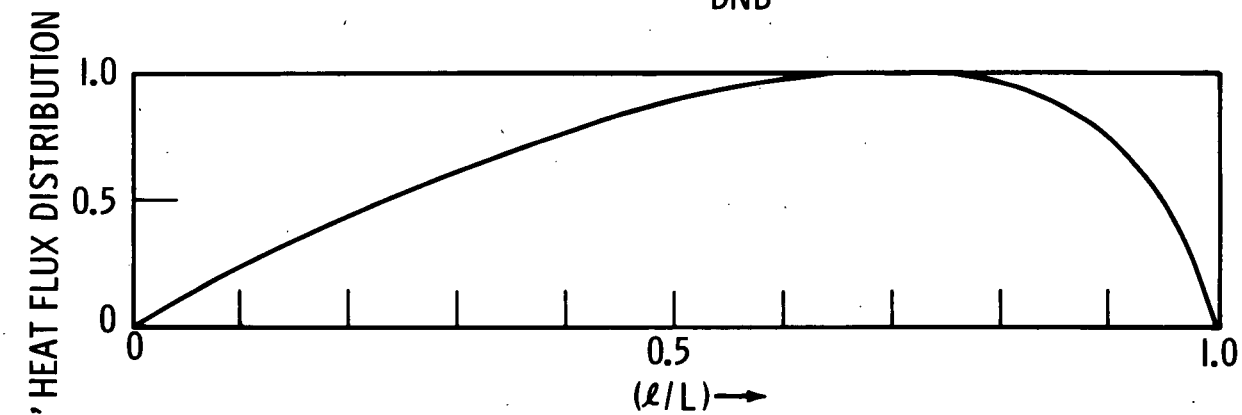
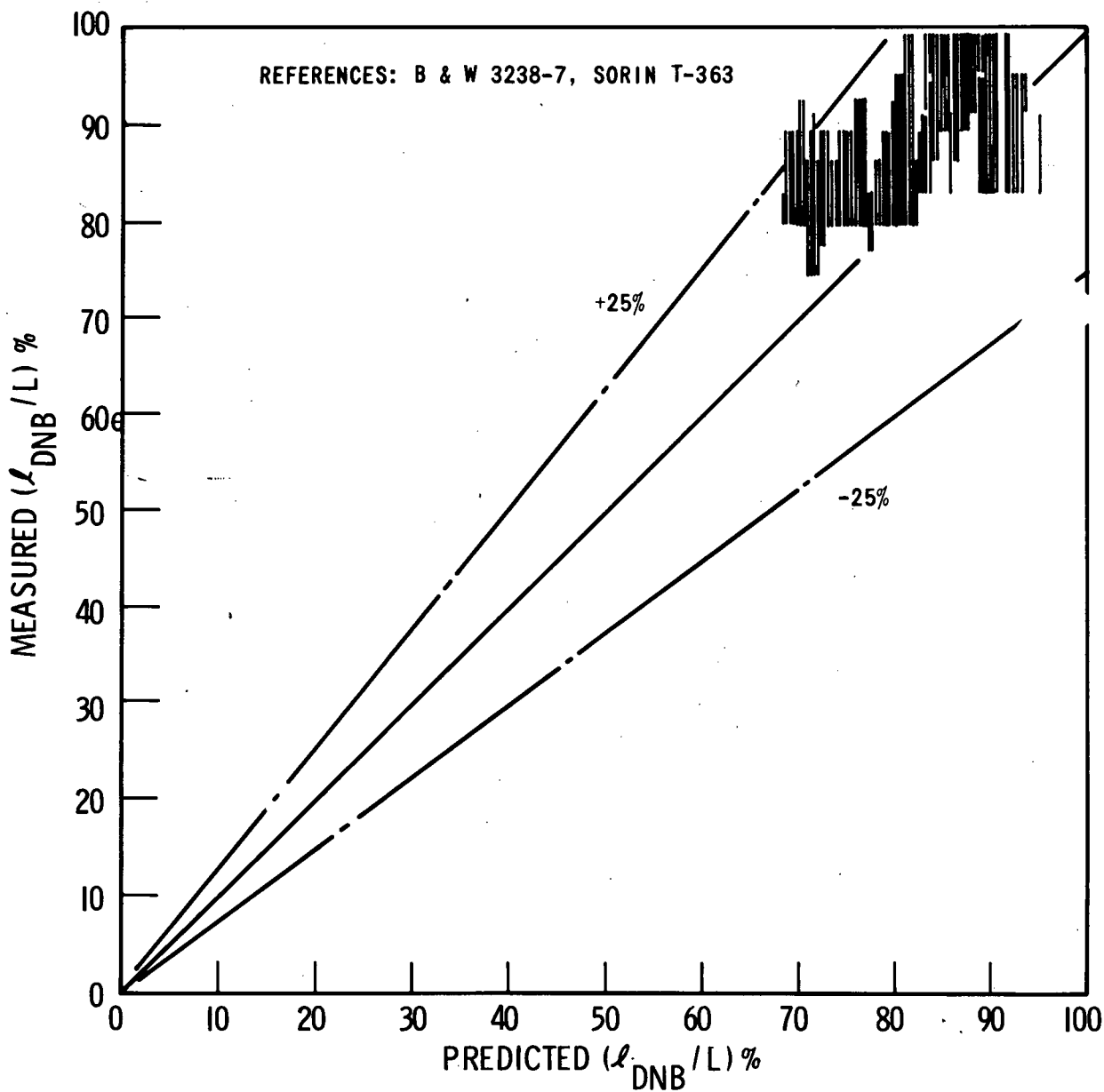
COMPARISON OF W-3 PREDICTION IN THE RANGE OF -0.15 TO $+0.15$ QUALITY, NON-UNIFORM FLUX
 FIG. 3-27



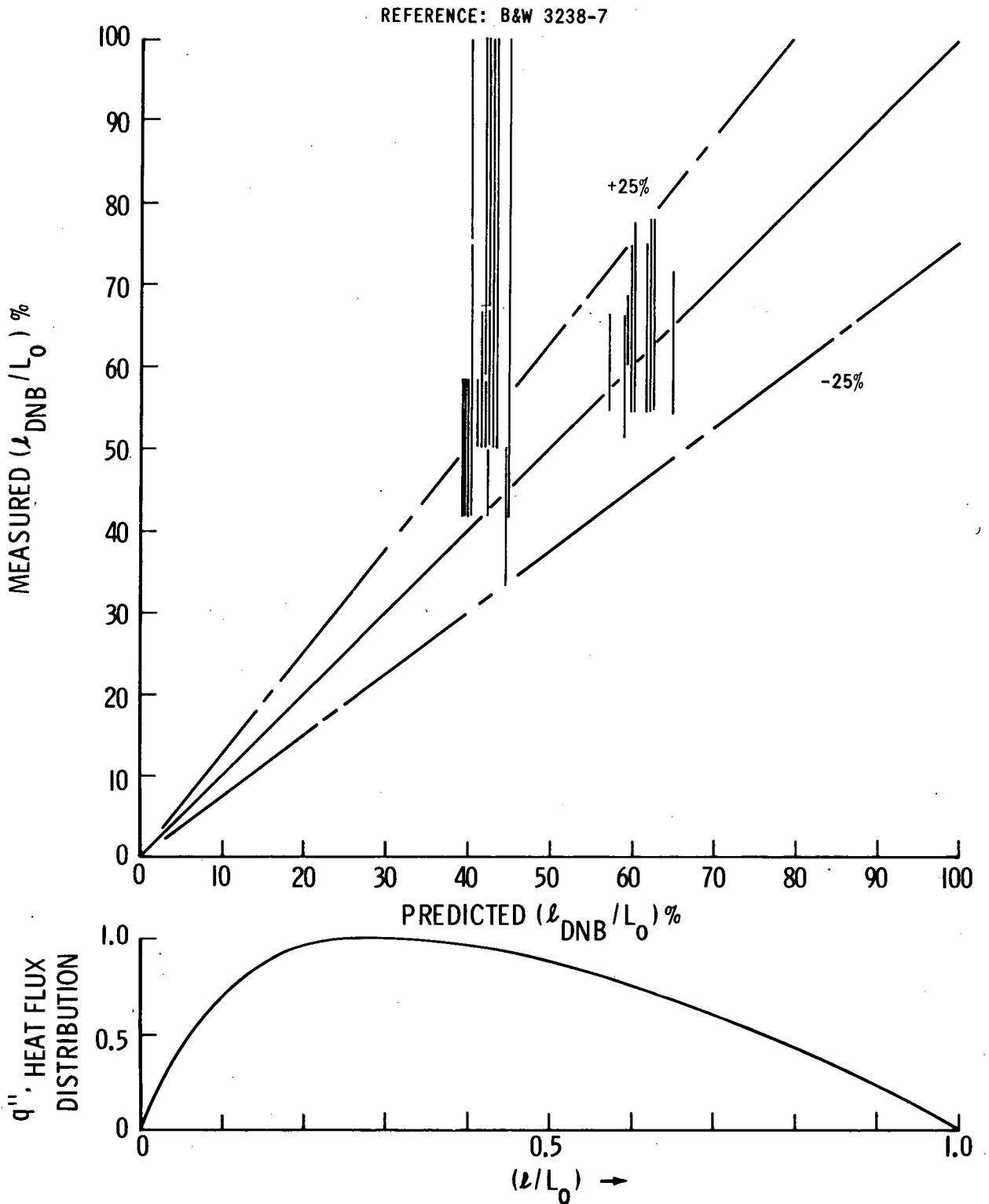
COMPARISON OF W-3 PREDICTION AND NON-UNIFORM FLUX DATA ($-0.15 \leq x_{DNB} \leq +0.15$)



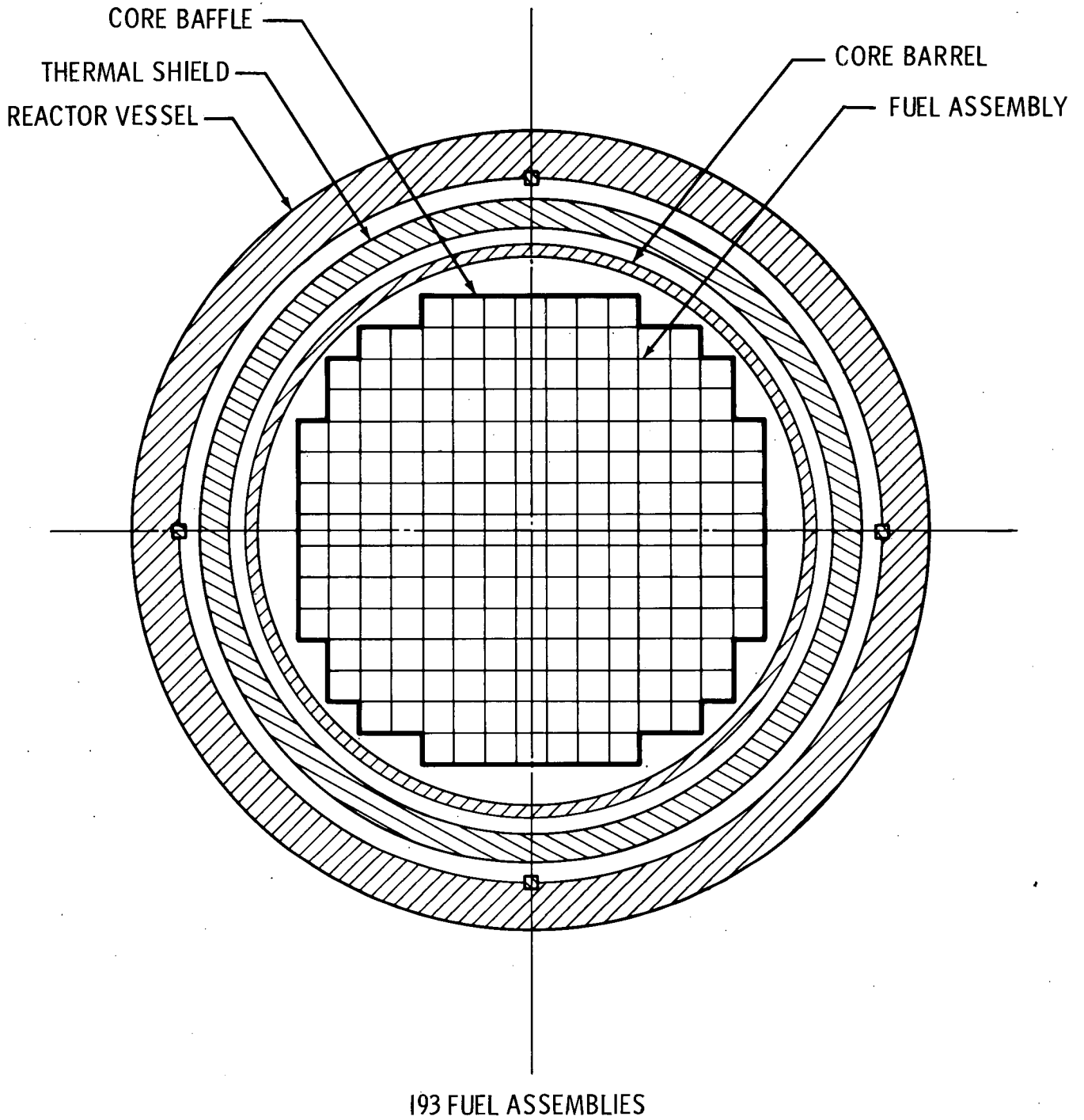
COMPARISON OF THE PREDICTED TO MEASURED DNB LOCATIONS (COSINE)



COMPARISON OF THE PREDICTED TO MEASURED DNB LOCATIONS
(PEAK NEAR EXIT)

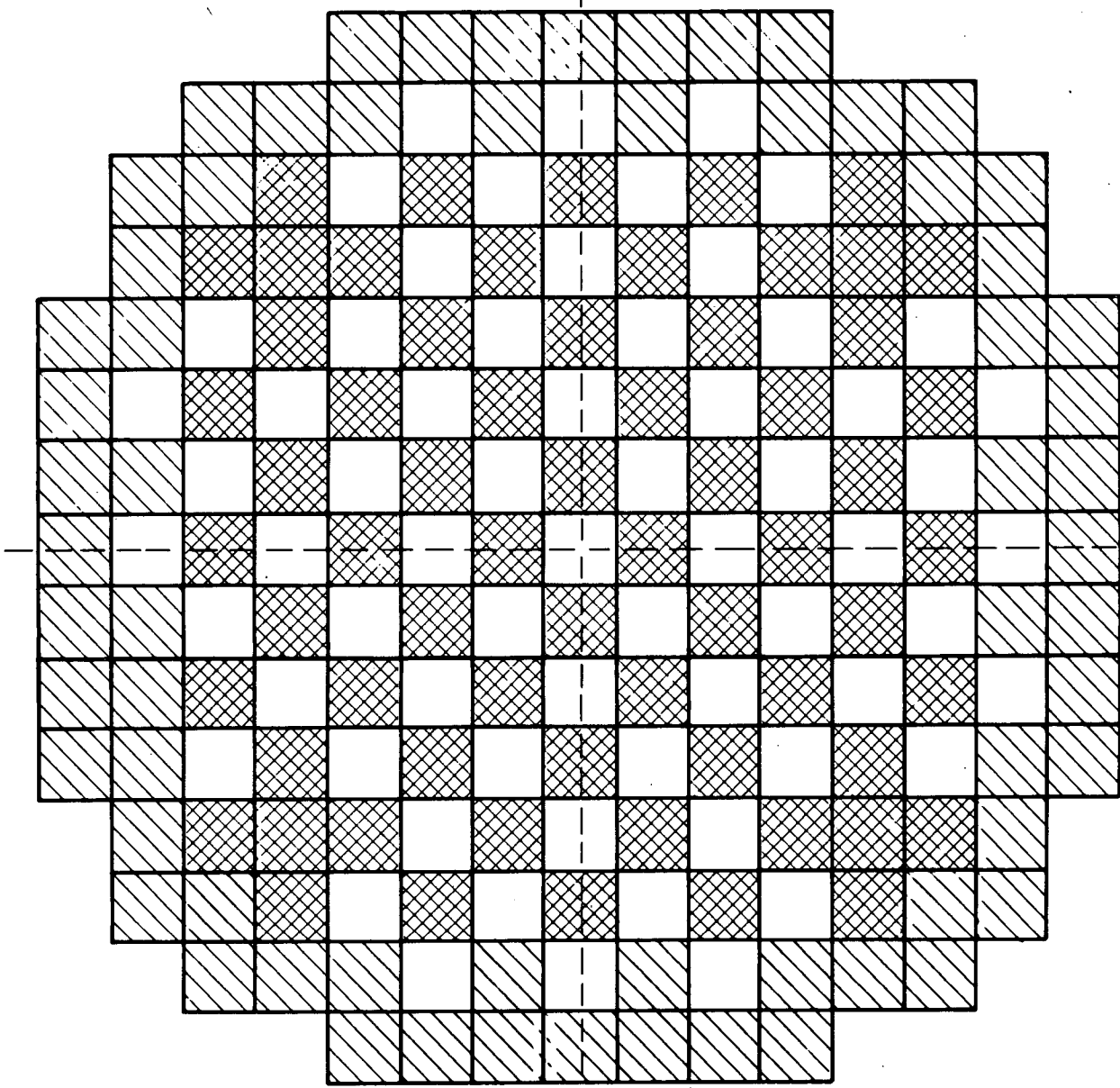


COMPARISON OF PREDICTED TO MEASURED DNB
LOCATIONS (PEAK NEAR INLET) FIG. 3-30

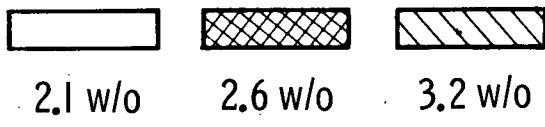


CORE CROSS SECTION
FIG. 3-31

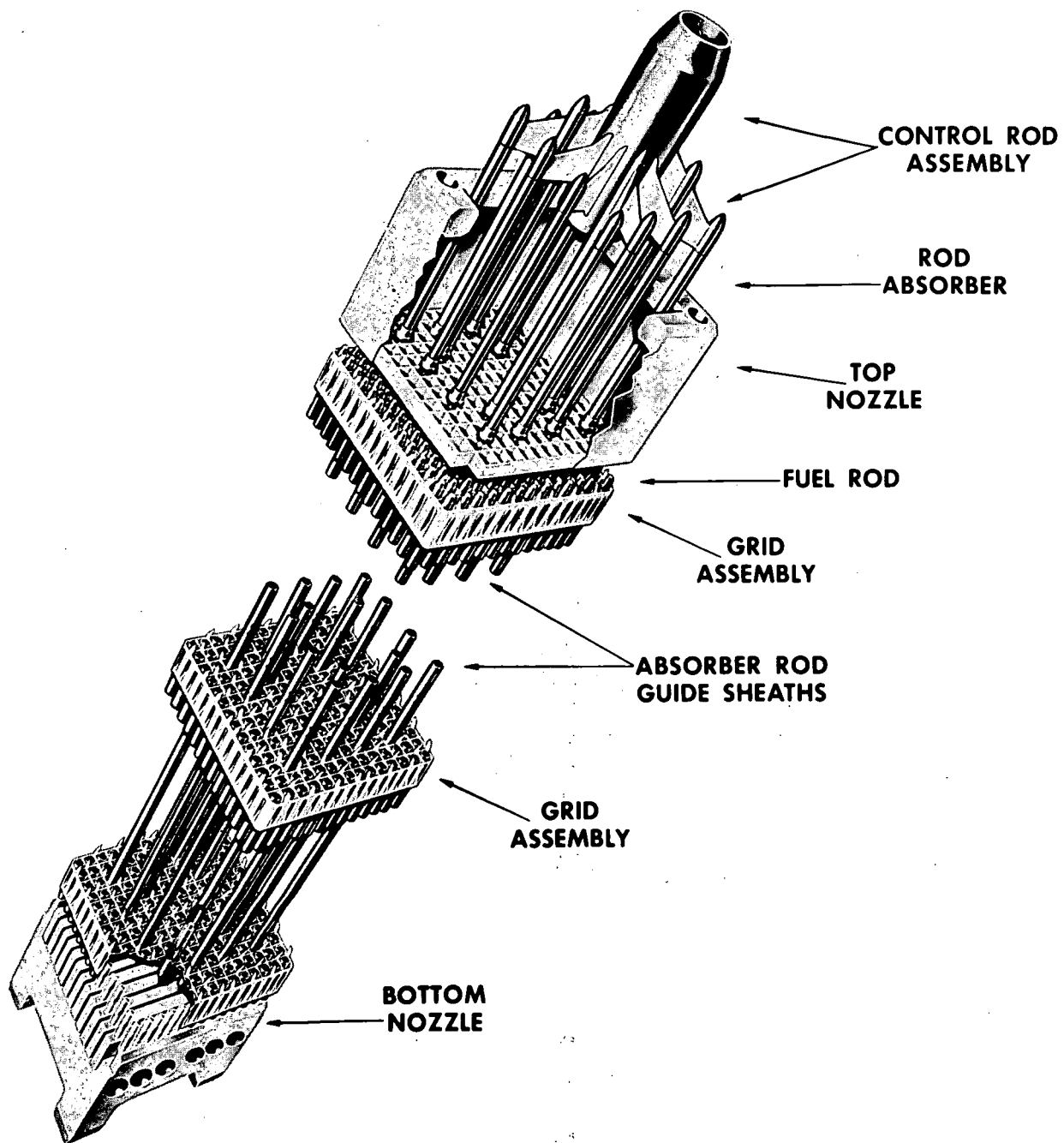
90°



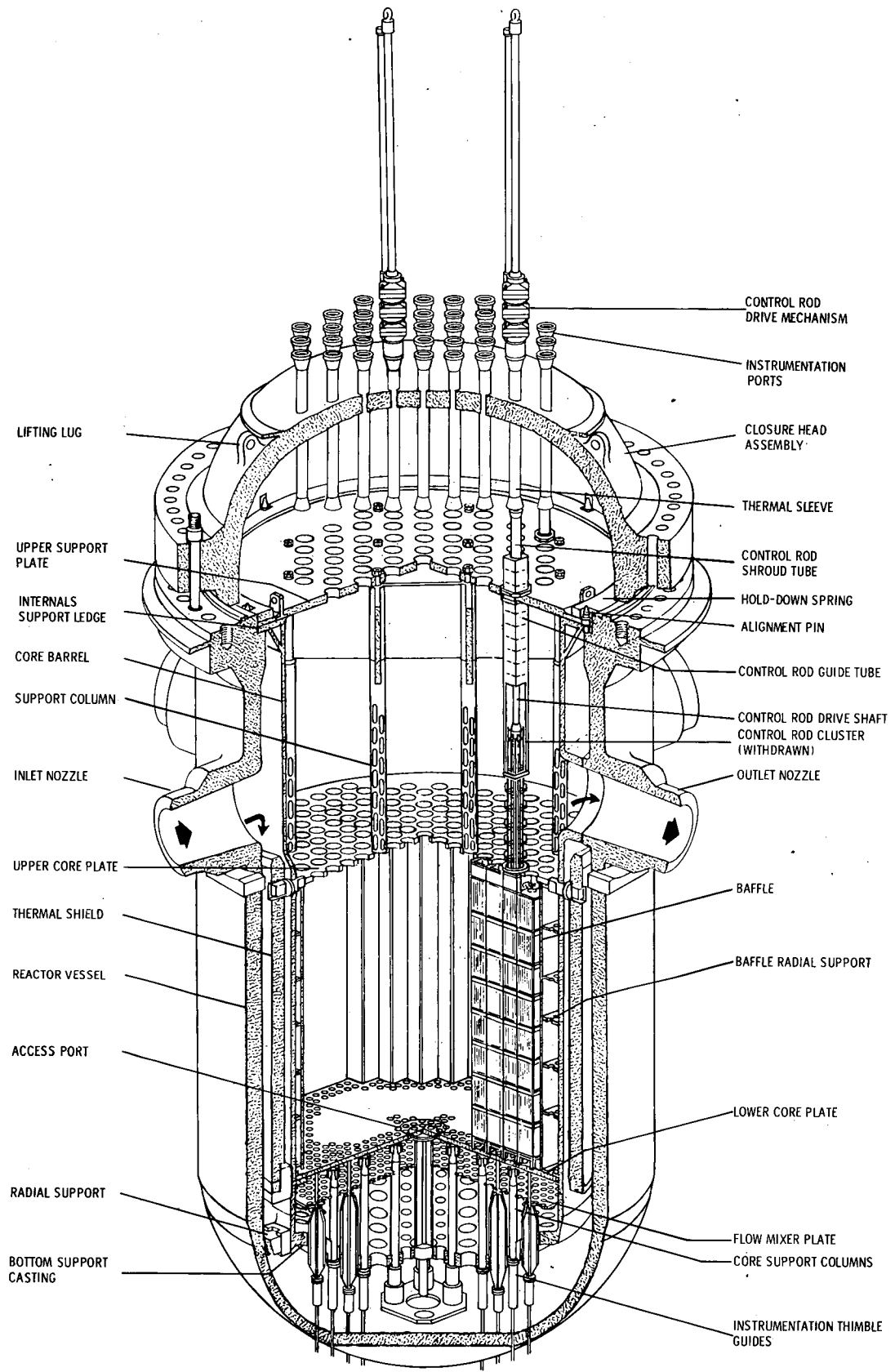
ENRICHMENTS



CORE LOADING ARRANGEMENT
FIG. 3-32

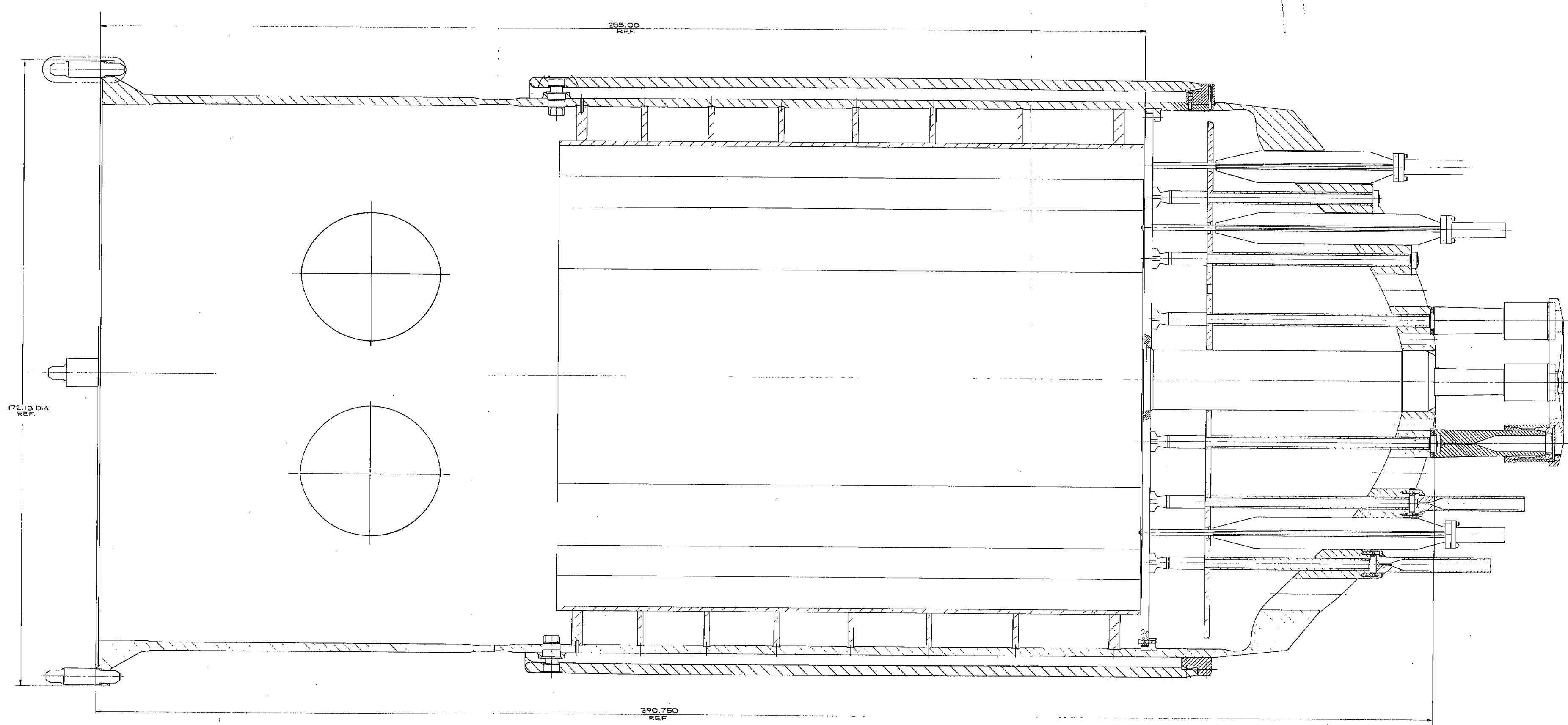


TYPICAL CONTROL CLUSTER ASSEMBLY
FIG. 3-33

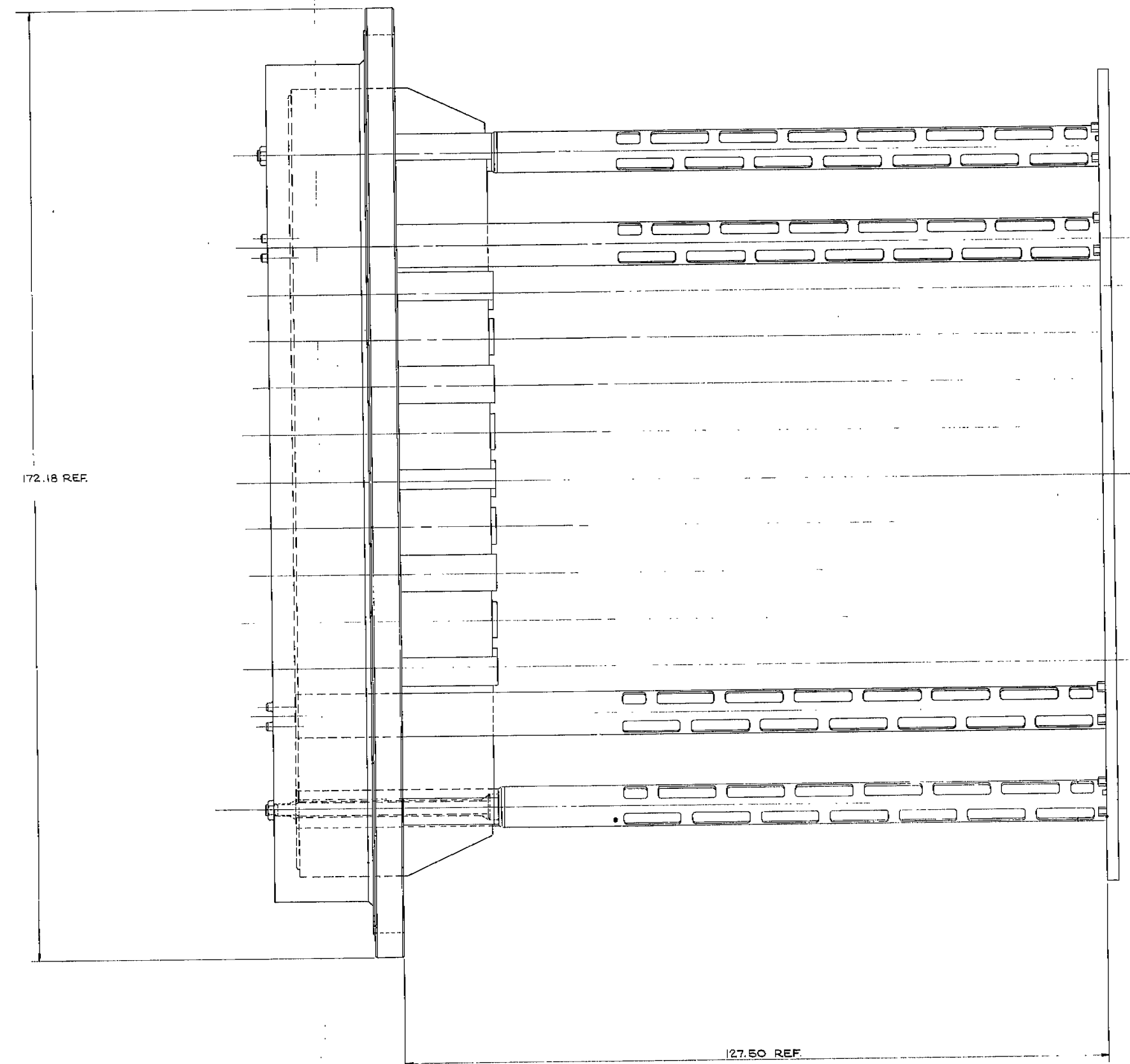
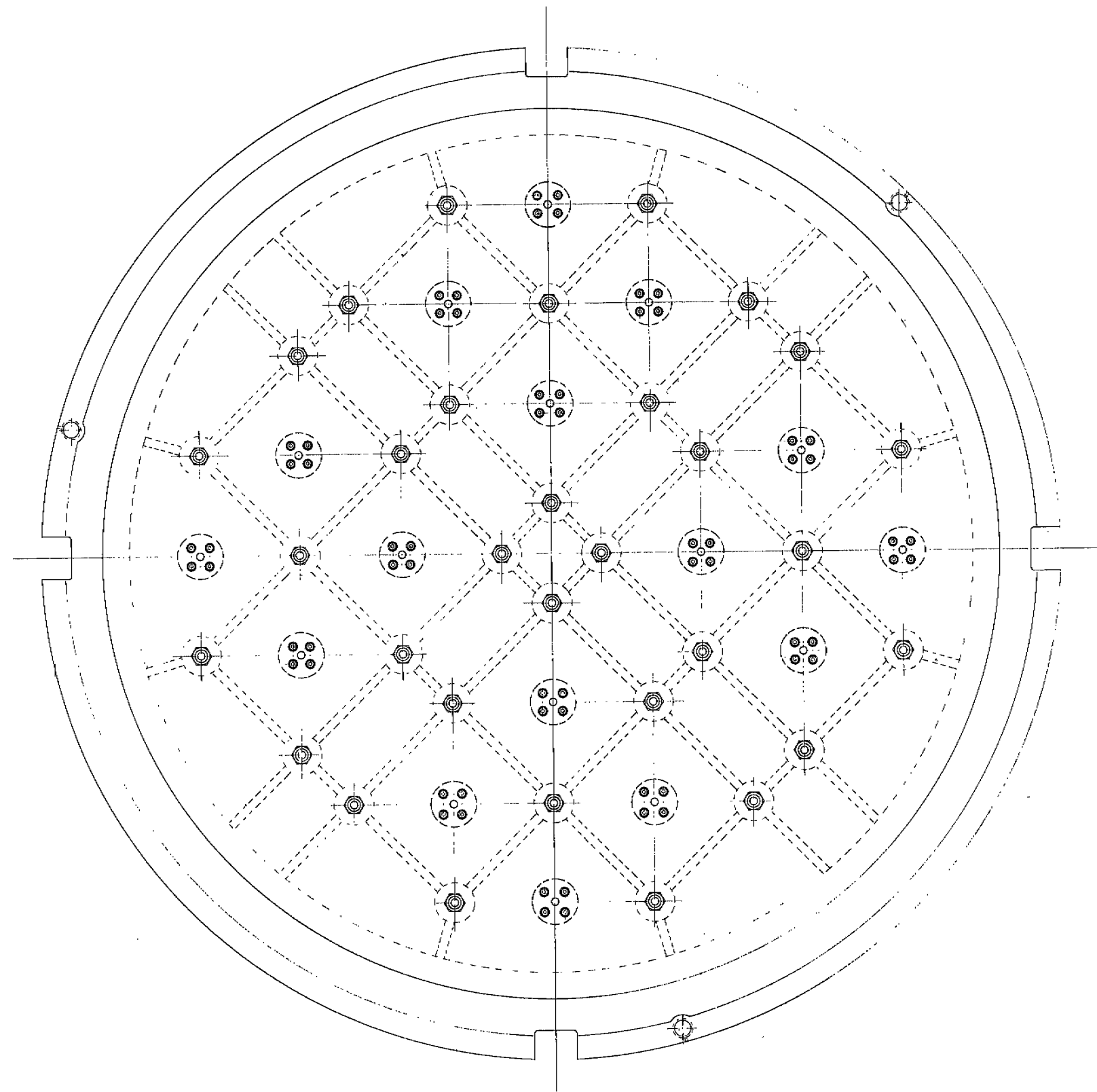


REACTOR VESSEL AND INTERNALS

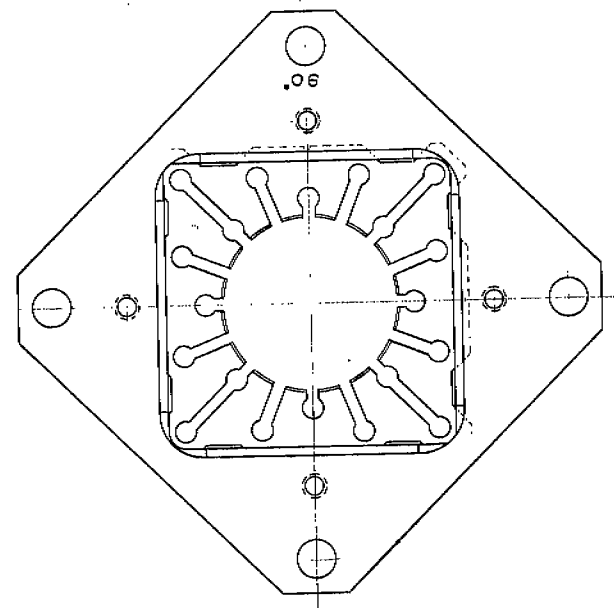
REACTOR VESSEL AND INTERNALS
FIG. 3-34



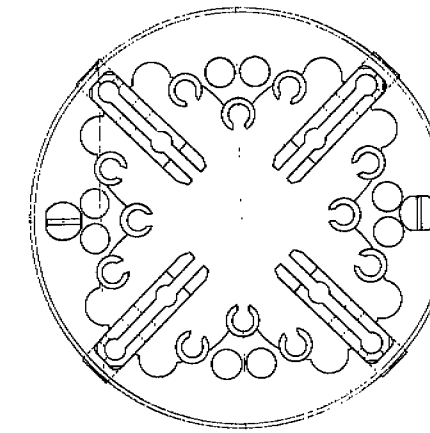
LOWER CORE SUPPORT STRUCTURE
FIG. 3-35



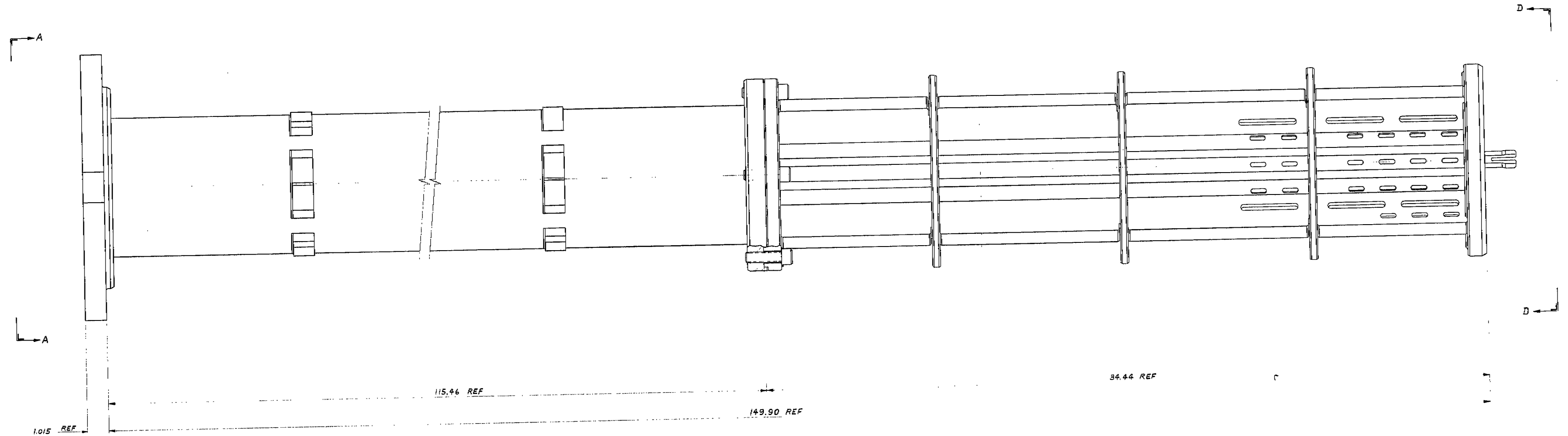
UPPER CORE SUPPORT ASSEMBLY
FIG. 3-36



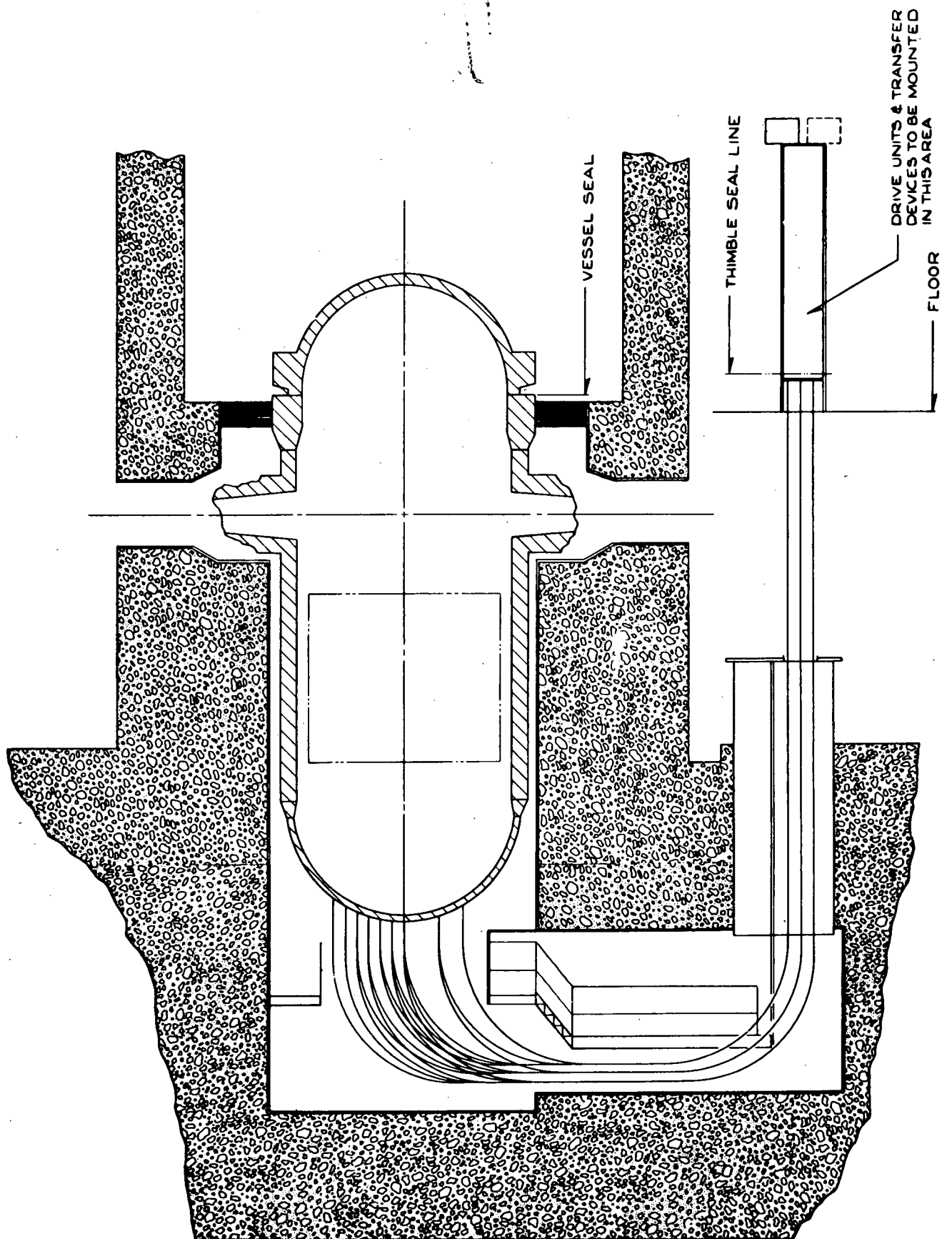
VIEW A-A



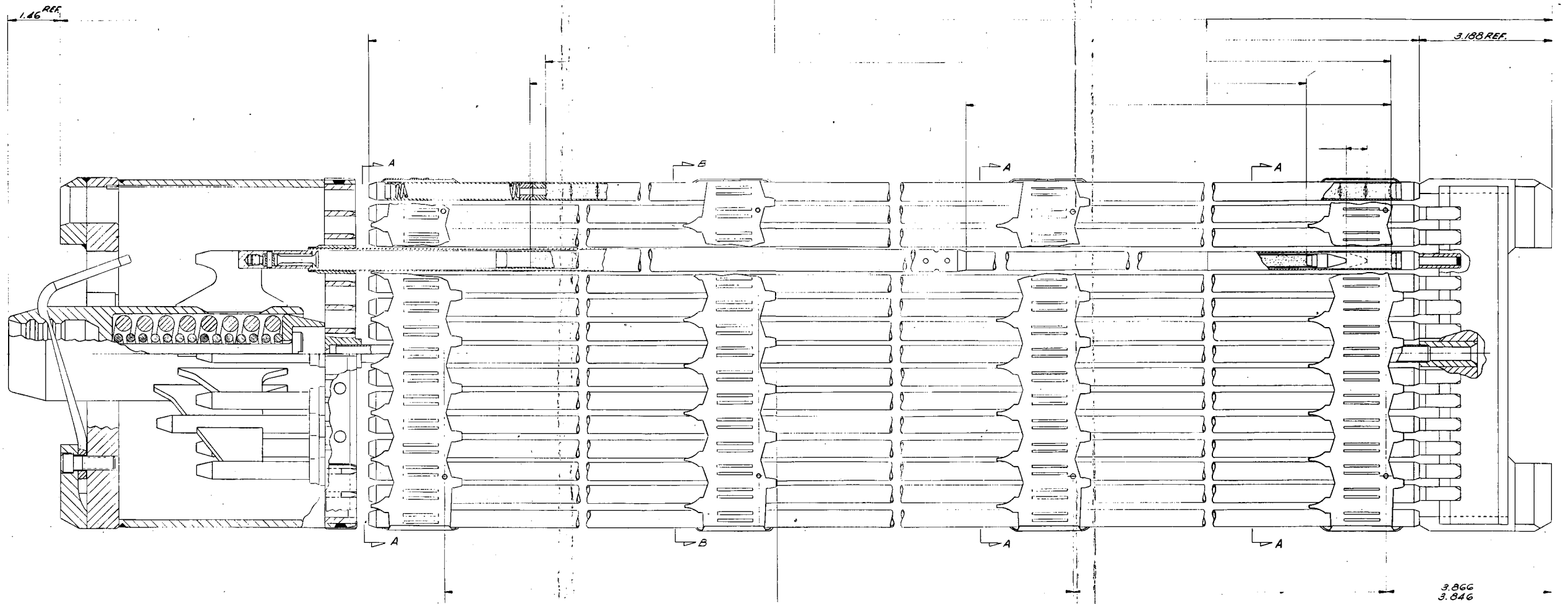
VIEW D-D



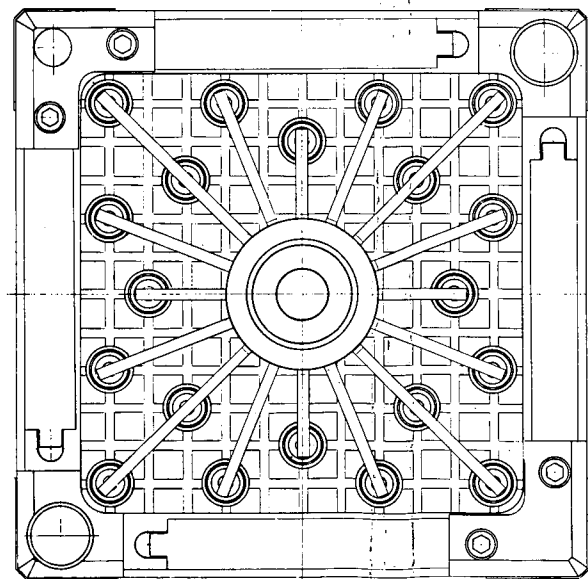
CONTROL CLUSTER GUIDE ASSEMBLY
FIG. 3-37



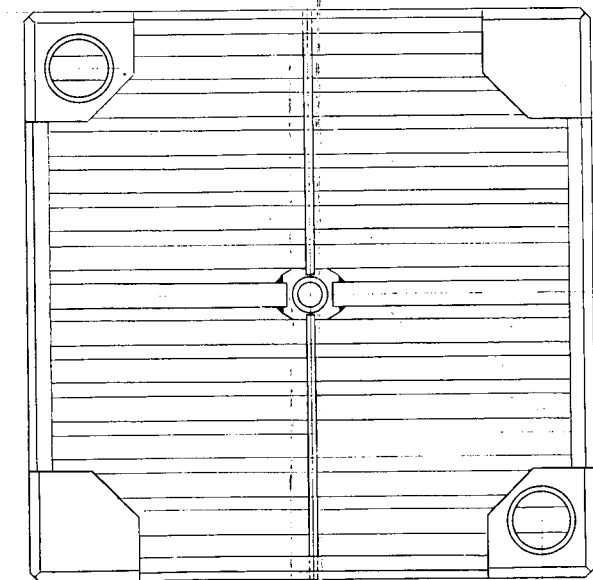
ARRANGEMENT OF IN-CORE FLUX DETECTOR SYSTEM
 FIG. 3-38



3.866
3.846

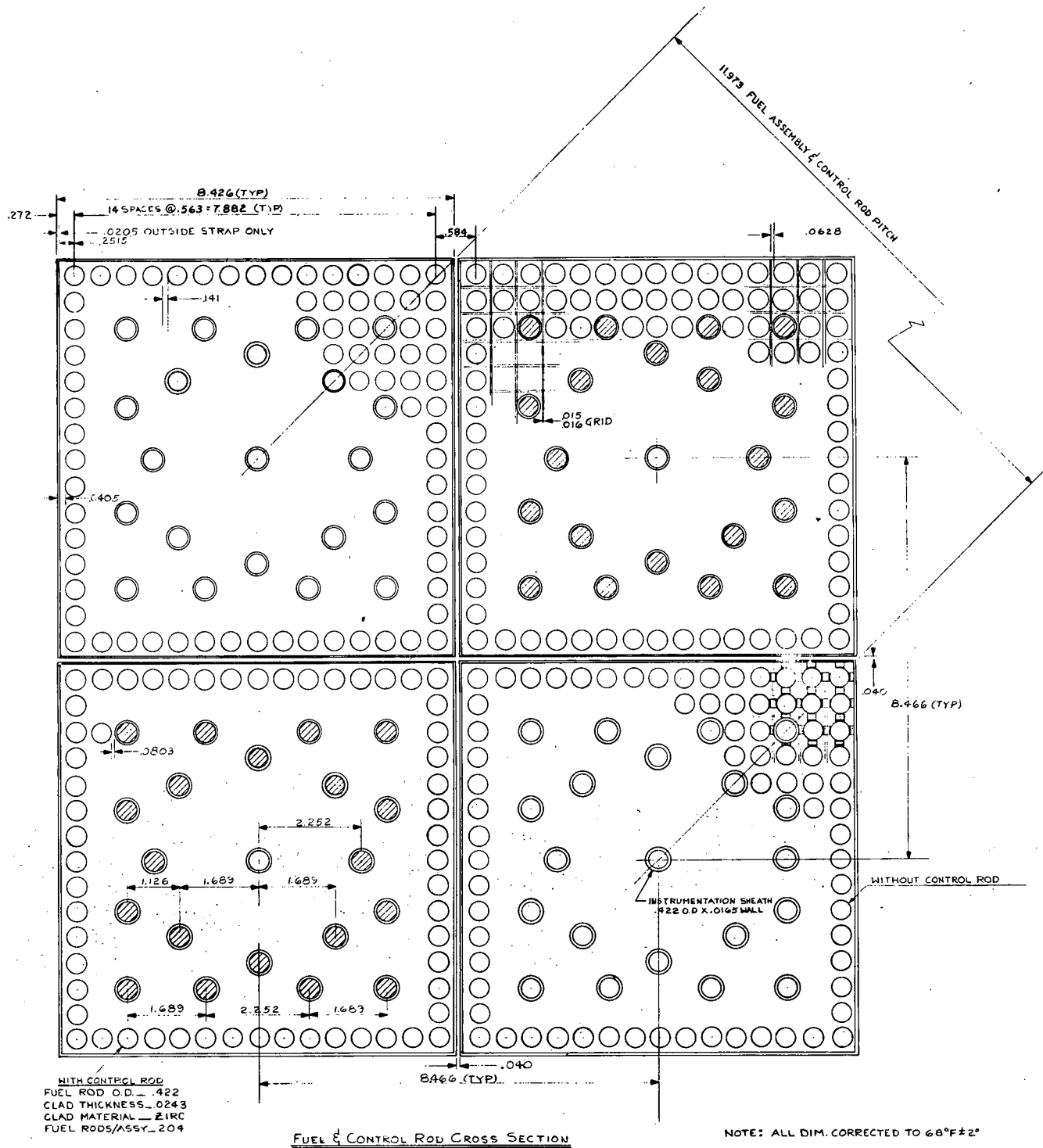


8.426 REF.

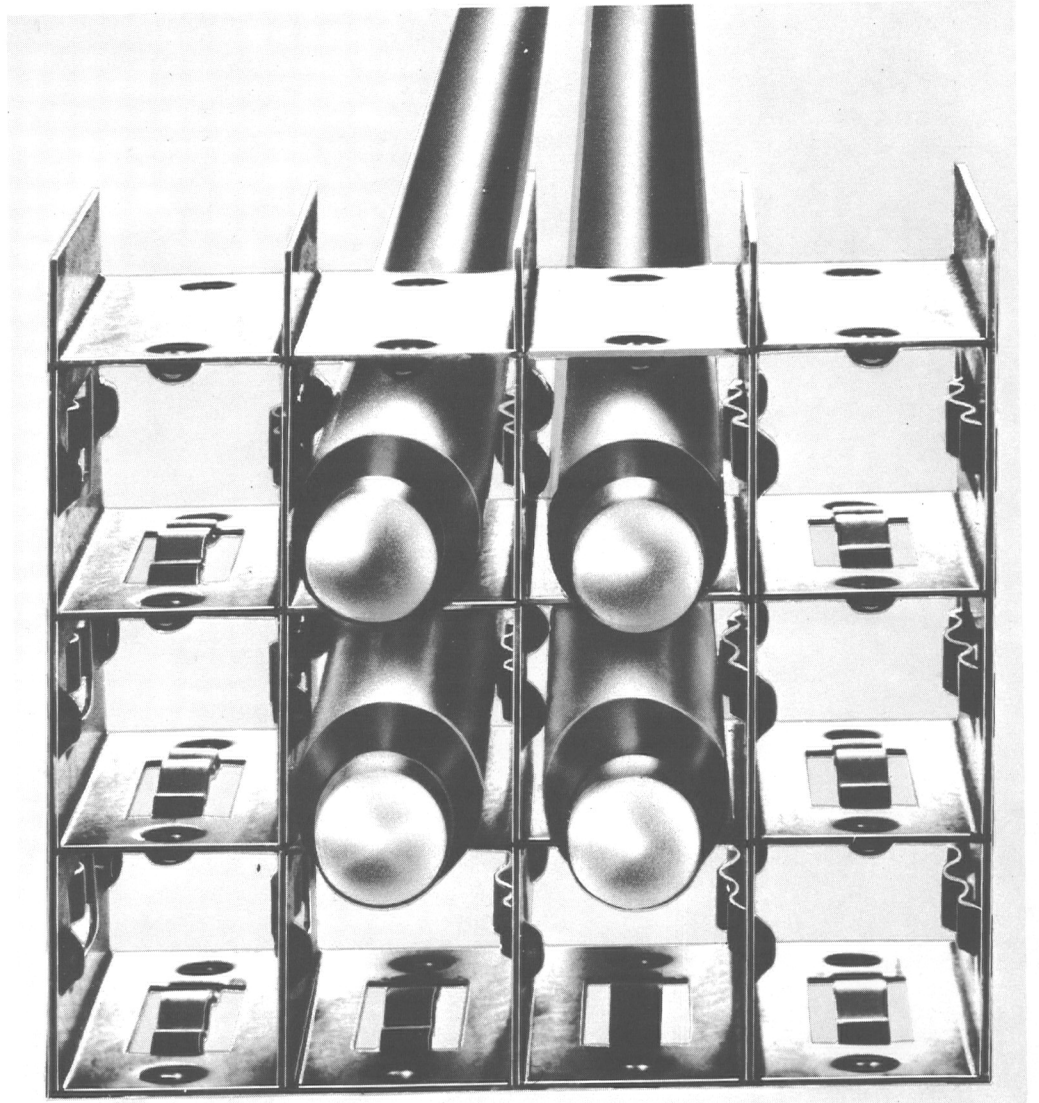


6.750 REF.

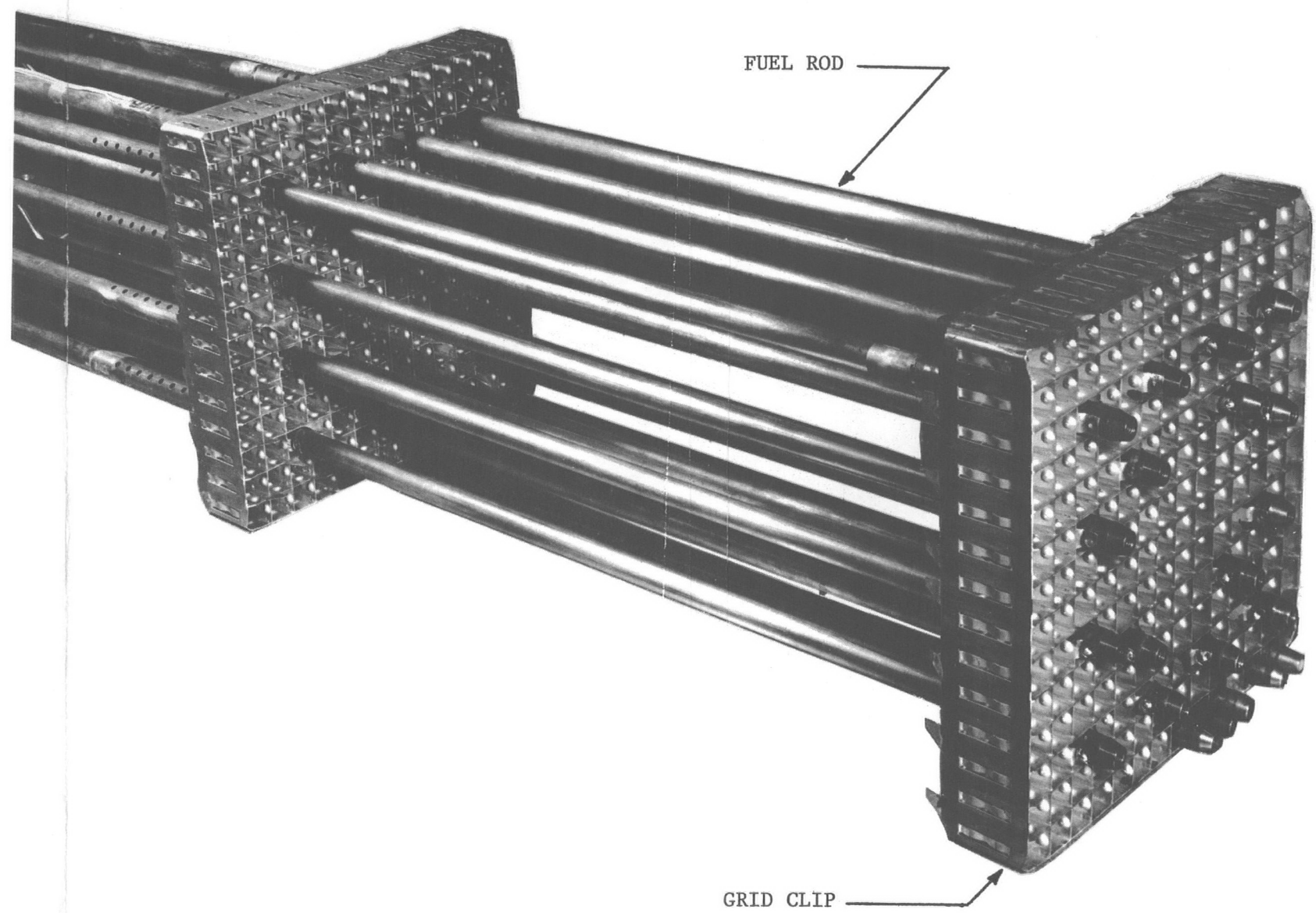
FUEL ASSEMBLY OUTLINE
FIG. 3-39



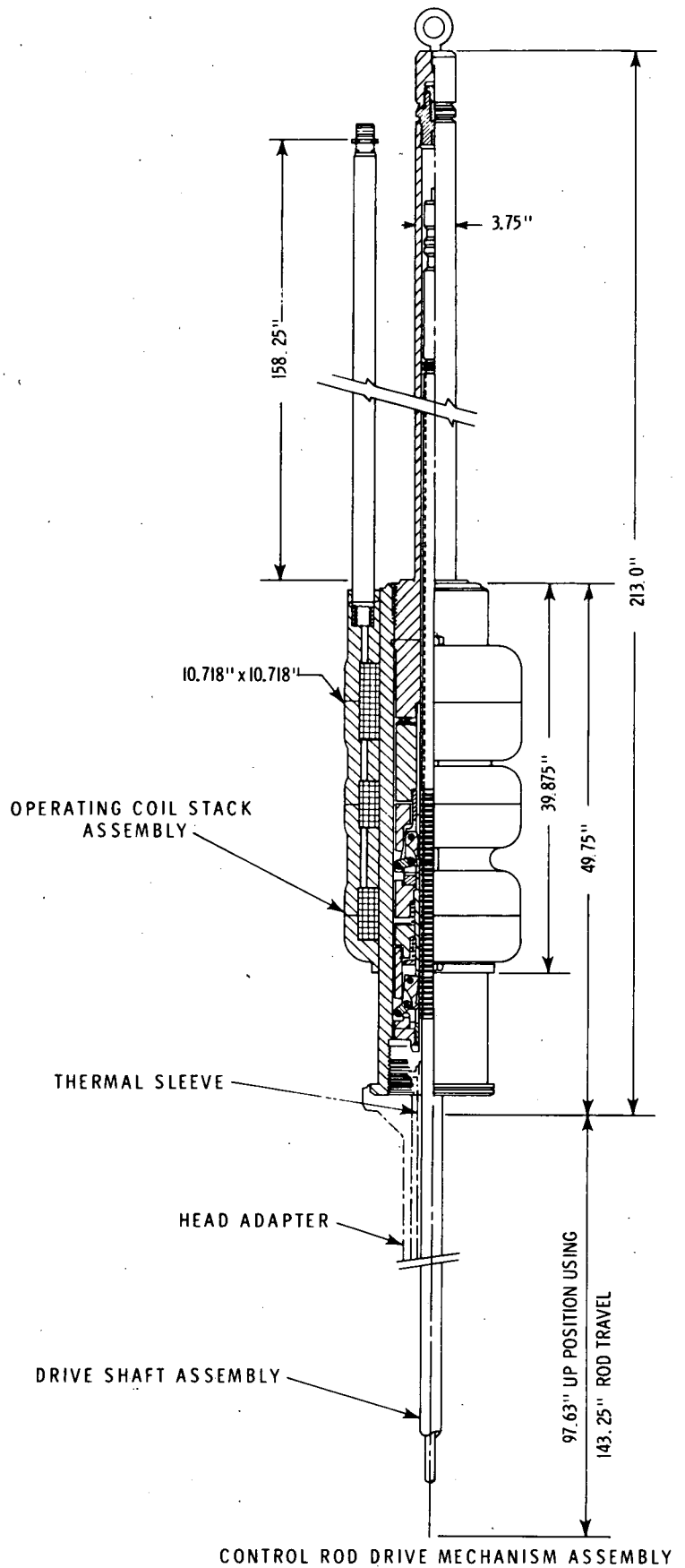
FUEL ASSEMBLY AND CONTROL CLUSTER CROSS SECTION
 FIG. 3-40



TYPICAL SPRING CLIP GRID DETAIL
FIG. 3-41

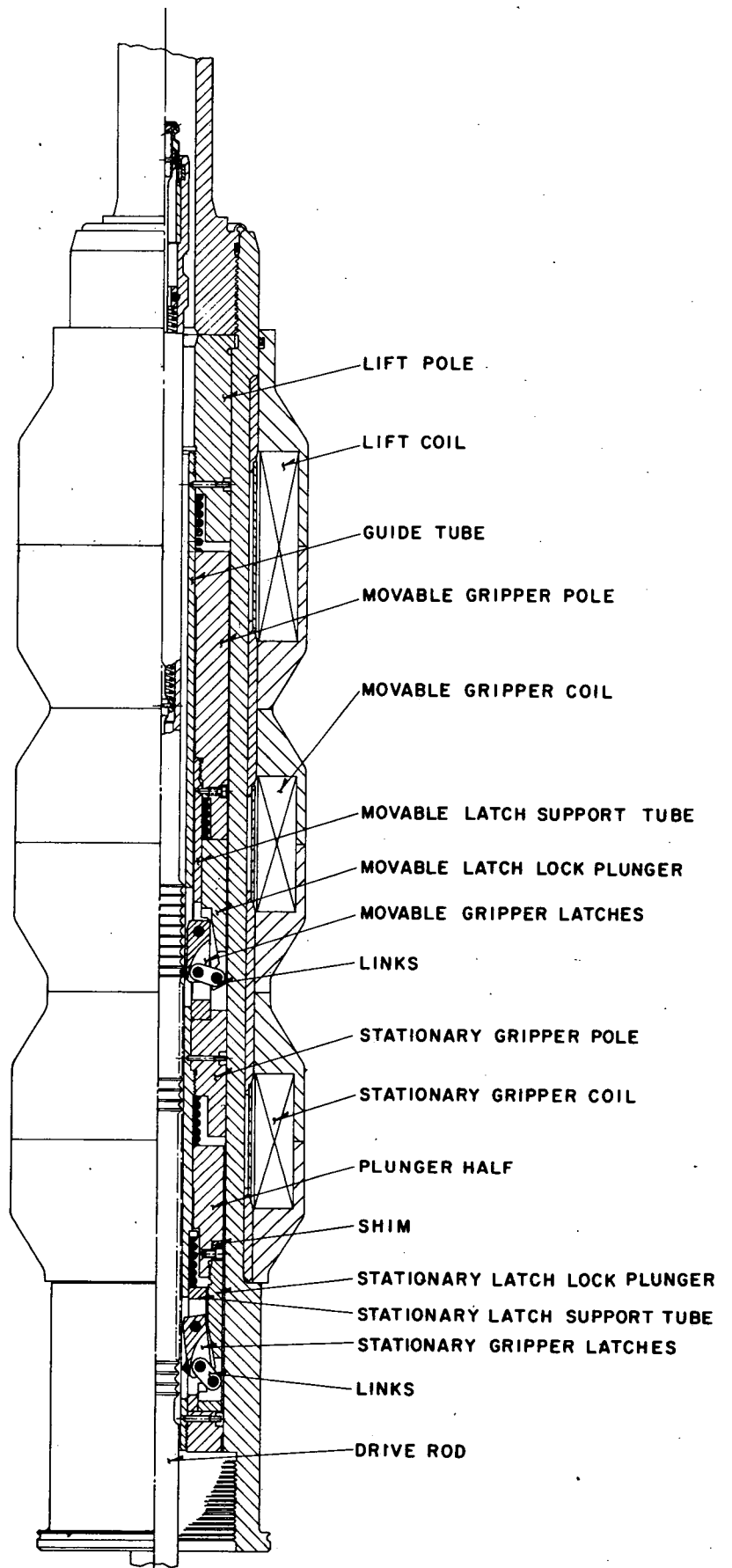
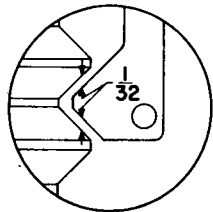


SPRING CLIP GRID ASSEMBLY
FIG. 3-42



CONTROL ROD DRIVE MECHANISM ASSEMBLY
 FIG. 3-44

AXIAL CLEARANCE



CONTROL ROD DRIVE MECHANISM SCHEMATIC
FIG. 3-45

SECTION 4

PSAR

Section	Page	Remarks
4.1	4-3	The last part of Section 4.1 which describes the vessel irradiation exposure has been superseded by the material presented in Item 2 (1 - 3) of Supplement 1, Part a.
4.2.2	4-5	Additional information on the Quality Control/Quality Assurance Program during design, fabrication and installation is found in Supplement 1, Item 2 (1 - 3), pages 20 through 24, Item 5, Item 11 and Supplement 5, Item 4.
4.2.2	4-8	Table 4-3 on the RCS Quality Assurance Program has been superseded by Table 3 (f) - 1 of Item 2, Supplement 1.
4.4.1	4-17	The material on "Reactor Vessel Irradiation Sample Surveillance Program" has been superseded by the write-up in Supplement 1, Item 2 (1 - 3), pages 1 through 19.
4.5	4-25	Additional information on the criterion for inservice inspection for RCS components is given in Supplement 1, Item 1, page 45.
4.6	4-27	Additional information on RCS leakage detection is found in Item 1, page 23 of Supplement 1.